Improved interpretation of stable water isotope signals in snow and ice from northern Greenland

DISSERTATION

Zur Erlangung des Grades Dr. rer. nat.

Vorgelegt dem Fachbereich Geowissenschaften

der Universität Bremen

von

M. Sc. Stefanie Weißbach

Stefanie Weißbach

Alfred-Wegener-Institut

Helmholz-Zentrum für Polar- und Meeresforschung

Am Alten Hafen 26

27568 Bremerhaven

Stefanie.Weissbach@awi.de

Gutachter:

Prof. Dr. Heinrich Miller

Prof. Dr. Gerrit Lohmann

Datum des Kolloquiums:

13. 07. 2016

Das Leben ist wie eine Reise.

Je weniger Gepäck man dabei hat,

desto mehr Eindrücke kann man mitnehmen.

(Hanna Schygulla)

Zusammenfassung

Diese Arbeit befasst sich mit der Analyse und Interpretation von Eiskerndaten aus dem nördlichen Grönland, einem der am wenigsten untersuchten Gebiete der Arktis. Fokus der Arbeit ist dabei das Studium der $\delta^{18}O$-Werte an Schnee- und Eisproben, die als Proxy für die Lufttemperatur genutzt werden.

Bei der Nordgrönland Traverse (NGT 93/95) zwischen den Jahren 1993 und 1995 wurden 13 zwischen 100 und 175 m lange Eiskerne gebohrt. In dieser Arbeit wurden die Eiskerne datiert und die hochaufgelösten $\delta^{18}O$-Werte zu Jahresmittelwerten zusammengefasst, sowie mittlere Schneeakkumulationsraten abgeleitet. Die gewonnenen Zeitreihen umfassen die letzten 500 bis 1000 Jahre.

Als wesentliche Einflussgröße auf die räumliche Verteilung der langjährigen Mittelwerte in $\delta^{18}O$ und Akkumulation bestätigte sich die Topographie des Eisschildes. Die vorherrschenden West/Südwestwinde bewirken, dass der Nordosten Grönlands im Niederschlagsschattengebiet der Haupteisscheide liegt, die das nördliche Grönland in einen östlichen und einen westlichen Bereich teilt. Die geringsten $\delta^{18}O$-Mittelwerte sind östlich der Haupteisscheide zu finden. Weiterhin zeichnen sich die östlich gelegenen Eiskerne durch geringere Variationen in den $\delta^{18}O$- und Akkumulationszeitreihen aus. Die Korrelation der Zeitreihen ist gering auf Grund der großen Distanz zwischen den Kernen und lokal unterschiedlich wirkenden Einflussfaktoren. Durch Mittelung der Zeitreihen aller Kerne konnte das Signal-Rausch-Verhältnis verbessert werden. So wurde eine Zeitreihe erstellt, die repräsentativ für eine große Fläche im nördlichen Grönland ist und Rückschlüsse auf das Klima der letzten tausend Jahre (endend 1994) zulässt. Global bekannte Ereignisse wie die mittelalterliche Klimaanomalie und die darauf folgende Kleine Eiszeit konnten in der gemittelten $\delta^{18}O$-Zeitreihe ausgemacht werden. Die Zeitreihe ist sensitiv für dekadische Schwankungen wie die Wärmeperiode zwischen 1920 und 1930, die bisher nicht in Klimamodellen abgebildet werden kann. Es wurde auch eine Warmphase um 1420 A.D. deutlich, die bislang in keinem anderen Datensatz hervorgehoben wurde. Vermutet wird eine Veränderung der lokalen Klimadynamik im Zusammenhang mit Änderungen in der Meereisbedeckung im Arktischen Raum.

Da sich kein deutlicher Trend in den $\delta^{18}O$-Daten der NGT 93/95 der letzten Jahre abzeichnete, wurden zwischen 2011 und 2012 weitere Firnkerne in Nordgrönland an vergleichbaren Positionen gebohrt, um die aus den Daten der NGT 93/95 gewonnene Zeitreihe zu verlängern. Fünf circa

30 m lange Kerne wurden hierfür am Alfred-Wegener-Institut (AWI) in Bremerhaven bearbeitet. Die Kerne wurden in jährlicher Auflösung datiert. Die Einzelwerte von $\delta^{18}O$ und Schneeakkumulationsraten wurden zu Jahresmittelwerten zusammengefasst. Ein Überlapp von circa 100 Jahren machte es möglich, die Zeitreihe zur Verlängerung der bestehenden NGT 93/95 Zeitreihe zu verwenden. Erstmals war so eine Einschätzung der aktuellsten Temperaturänderungen in Grönland im Vergleich zu den letzten tausend Jahren an einer Zeitreihe aus nur einem Temperaturproxy möglich. Ab 1980 setzt ein anhaltender Erwärmungstrend ein. Der Gradient dieser Erwärmung ist nicht außergewöhnlich, verglichen mit den anderen Werten der letzten tausend Jahre, jedoch die erreichten Absolutwerte.

Abstract

This thesis deals with the analysis and interpretation of ice core data from northern Greenland, one of the least studied areas in the Arctic. The focus of the thesis is the study of $\delta^{18}O$ values which can be used as a proxy for temperature.

The 13 ice cores from the North Greenland Traverse (NGT 93/95) are between 100 and 175 m long and were cored between 1993 and 1995. These cores were dated in this thesis and the high-resolution values of $\delta^{18}O$ and accumulation rate averaged to annual mean values. The time series spans the last 500 – 1000 years.

The topography of the ice sheet is confirmed as the main influencing factor on the long-term annual mean values of $\delta^{18}O$ and snow accumulation rate. The predominant southwest/west winds ensure that the northeast of Greenland is located in the precipitation shadow area of the main ice divide, which divides northern Greenland into east and west regions. The lowest $\delta^{18}O$ ratios are found east of the divide. In addition, the eastern ice cores are characterized by small variations in $\delta^{18}O$ and thickness of accumulation horizons. The correlation between the time series is low due to the large distance between the ice cores and the influence of stratigraphic local noise. By stacking all individual records the signal-to-noise ratio was improved. The stack is representative for a large area in northern Greenland and allows for conclusions regarding the climate during the last thousand years (ending 1994). Globally-known results, such as the Medieval Climate Anomaly that was followed by the Little Ice Age, could be detected in the averaged $\delta^{18}O$ time series. The time series is also sensitive to decadal variations such as the warm signal between 1920 and 1930, which cannot be broken down in climate models. Another warm period around 1420 A.D. was observed, which until now has not been seen in any other data set. It is suspected that changes in the local climate dynamic as a result of changed sea ice coverage in the Arctic Sea are possible reasons.

Because there was no clear trend in the $\delta^{18}O$ NGT 93/95 data in recent years, additional ice cores were drilled in 2011 and 2012 in northern Greenland at comparable positions, in order to extend the series into more recent times. Five cores, each about 30 m long, were analyzed at the AWI Bremerhaven for this purpose. The cores were yearly dated, and the high-resolution $\delta^{18}O$ values were averaged for each year. An overlap of about 100 years made it possible to use the time series as an extension of the NGT 93/95 time series. For the first time, an estimation of the actual air temperatures in Greenland over the last thousand years was possible with only one proxy. Since

1980, there has been a constant warming trend. The gradient of the warming is not unusual when compared with other values from the last thousand years, but the level of the values is unusual high.

Acknowledgment

Contents

List of Figures

List of Tables

List of Abbreviations

AWI ... Alfred-Wegener-Institut, Helmholtz-Zentrum für Polar- und Meeresforschung

A.D. ... Anno Domini. Years since the birth of Jesus Christ

CT ... Computer Tomography

CFA ... Continuous Flow Analysis

CIC ... Center for Ice and Climate (Niels Bohr Institute, University Copenhagen)

CRDS ... Cavity Ring-Down Spectroscopy

D ... Deuterium (^{2}H)

DEP ... Dielectric Property

DMI ... Danish Meteorological Institute, Copenhagen

ECHAM5 ... 5th version of a global climate model by the Max Planck Institute for Meteorology

ECM ... Electric Conductivity Measurement

E.G.I.G. ... Expéditions Glaciologique Internationale au Groenland 1957-1960

EGRIP ... East Greenland Ice Core Project

ERA40 ... ECMWF re-analysis of the global atmosphere and surface conditions (1957-2002)

ESSReS ... Earth System Science Research School

ETCW ... Early Twentieth Century Warming

Excess ... Deuterium Excess

GISP2 ... Greenland Ice Sheet Project 2

GRIP... Greenland Ice Core Project

IC ... Ion Chromatography

LIA ... Little Ice Age

MCA ... Medieval Climate Anomaly

NAO ... North Atlantic Oscillation

NASA ... National Aeronautics and Space Administration

NEEM ... North Greenland Eemian Ice Core Drilling Project

N2E ... North to East (Traverse from NEEM to EGRIP)

NEGIS ... North East Greenland Ice Stream

NGRIP... North Greenland Ice Project

NGT 93/95 ... Nordgrönland-Traverse 1993 -1995

PARCA ... Program for Arctic Regional Climate Assessment

SMOW ... Standard Mean Ocean Water

1 Introduction and Motivation

1.1   Global and Arctic climate change

The climate of the earth has always been subject to natural variations of different duration, intensity and spatial extent. The present warm phase, the Holocene Interglacial (11700 years before 2000 A.D. - modern time), stands out because of its exceptional stability. However, even the small temperature changes of 1-2 °C during the past 2000 years, such as the cold phase called the Little Ice Age (~1500 - 1850 A.D.) or the warmer Medieval Climate Anomaly (~800 - 1450 A.D.), had a huge effect on the environment and social life, especially on the development of human settlements (Dansgaard et al., 1975). More recently, there has been an observable warming trend in the global mean temperature of about 0.85 °C from 1880 to 2012 (Fig. *1-1*) (IPCC, 2013).
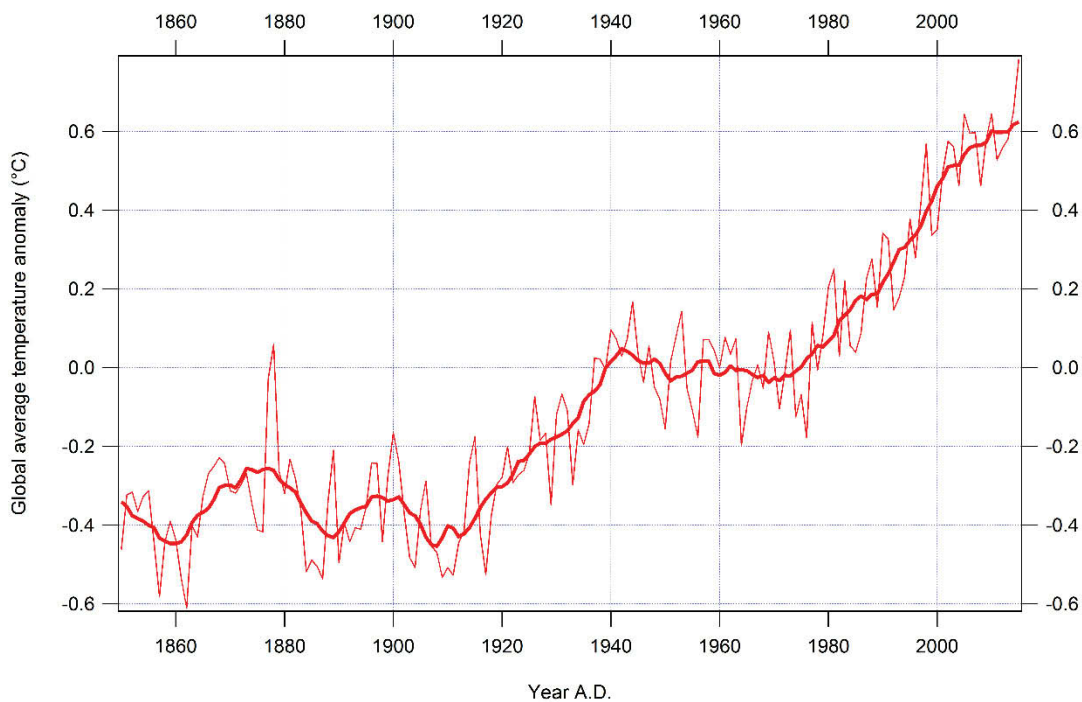
Fig. 1-1 Global annual mean surface temperature over land and ocean relative to the 1951 - 1980 A.D. mean (thin: annual, thick: 11-years running mean; source of data: http://berkeleyearth.lbl.gov/auto/Global/Land_and_Ocean_summary.txt)

Whereas most studies attribute the observed warming to anthropogenic impact on the climate (e.g. emissions of greenhouse gases), skeptics argue that the warming is still within the range of natural climate variability. In the latest report of the *Intergovernmental Panel on Climate Change*, IPCC (2013), steeper linear trends in the global mean temperature were reported for the last 60 and 30 years than for the last 15 years. This slowdown in the global warming is called a *hiatus* (IPCC, 2013). Different reasons for the global warming hiatus were discussed. The main arguments are a) the insufficient quality of some of the meteorological data used to generate the global mean temperature (Karl et al., 2015), b) the role of the deep ocean as a sink of heat, which may connect La-Niña conditions in the Pacific to a slowdown of the global temperature increase (Held, 2013; Meehl et al., 2011), or c) a lack of Arctic temperature data in the global mean (Cowtan and Way, 2014). Figure**Fig. *1-2*** 1-2 shows an example of the distribution of air-temperature records from land-weather stations used in the reconstruction of a global mean temperature record. The lack of direct data from e.g. the Arctic, which is the focus of this thesis, is obvious. Despite that only a few people live in the Arctic, changes in this region are relevant for all of mankind.
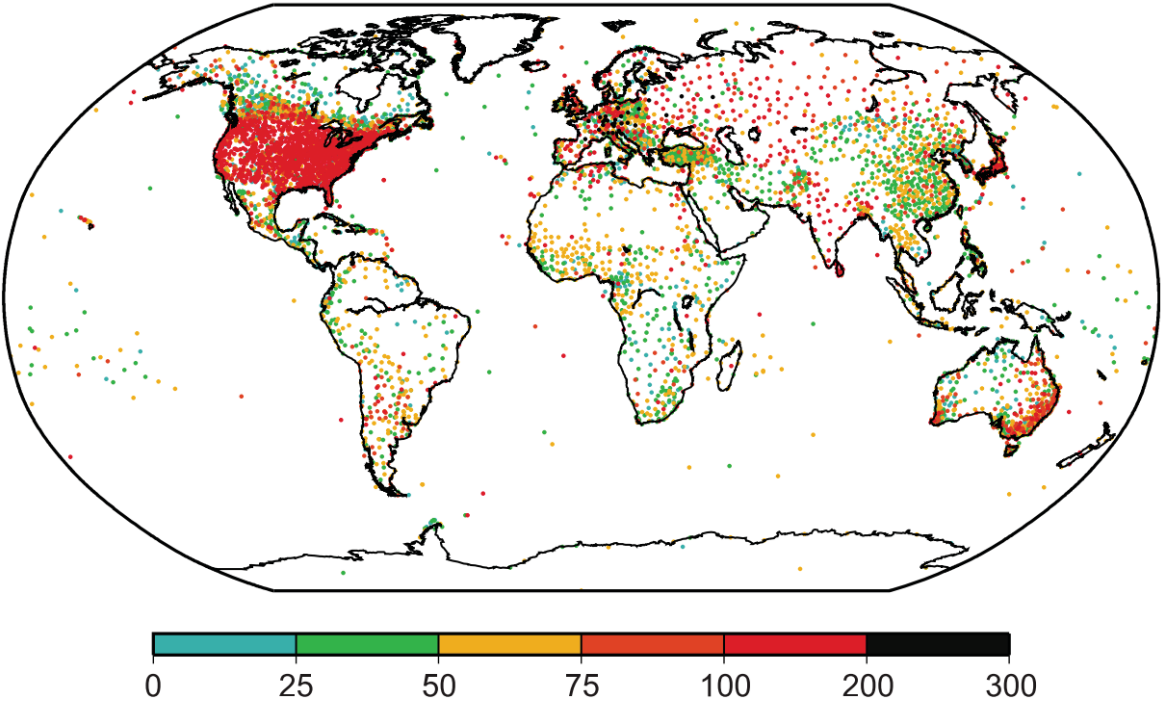
Fig. 1-2 Map of meteorological stations used in the Global Historical Climatology Network (GHCN-M), where surface air temperature was measured on land and on islands. The colors correspond to the number of years of available data for each station (Lawrimore et al., 2011)

A massive temperature rise is expected and has already been observed for the Arctic due to *polar amplification* (Miller et al., 2010). Polar amplification describes the larger change in the mean air temperature in polar areas than in the global mean due to positive feedback mechanisms such as the snow albedo effect and the retreat of sea ice. Recent instrumental records show that during the past few decades, the surface air temperature throughout much of the Arctic has risen about twice as fast as the temperature in lower latitudes (Delworth and Knutson, 2000; Knutson et al., 2006). During the 20th century, air temperature over land in the Arctic rose by up to 5 °C (IPCC, 2007). An insufficient number of Arctic records included in the global mean temperature will therefore result in artificially low mean values and inaccurate future forecasts. This underlines the importance of climate science in the Arctic for a more representative global mean temperature, as well as to show those changes in that region which are of global relevance.

Satellite observations show a great loss in mass for the Greenland Ice Sheet during recent years (Khan et al., 2014; Shepherd et al., 2012) due to rising temperatures. The mass loss can be attributed to increasing melting at the surface of the ice sheet as well as higher flow rates for most of the outlet glaciers. Since 2007, large-scale surface melting has been often observed on the Greenland Ice Sheet, also above the ablation areas. This happened to an extreme in July 2012 (Hanna et al., 2014; Nghiem et al., 2012; Rignot et al., 2011; Tedesco et al., 2013). This melting, which in recent years has been observed earlier in the season (as in 2016) and also in the higher central regions (as happened in 2012), is a consequence of rising temperatures. Whereas the melting is relatively easy to observe and to understand, the reason for the rapid outflow remains largely unknown. The Greenland Ice Sheet accounts for about 83% of the total northern polar land-ice mass and therefore has a strong impact on the global sea level rise, which is hardly predictable due to a large number of unknowns. However, the present Greenland Ice Sheet contains enough water to raise sea level by 7.2 m, so that only a small fractional change in their volume would have a significant effect (IPCC, 2001).

Climate change in the Arctic affects sea ice as well. The extent of sea ice cover at the end of summer and the thickness of sea ice are decreasing (Comiso et al., 2008; Serreze et al., 2007). This offers not only new possibilities to shipping and industry (e.g. exploitation of living and energy resources such as fish, gas and oil), but has also a great impact on the positive feedback mechanism of rising temperatures. Ice-free water is darker than the sea ice-covered surface; thus, the albedo of the Arctic Ocean is reduced. The decline in sea ice is one of the strongest climate signals worldwide and has consequences for the ocean and atmospheric circulation far beyond the Arctic. These consequences are of unknown extent until now.

Understanding the modern changes of the Arctic climate in the context of the natural climate variability is an important and necessary step to better assess the risks and possible consequences of climate change.

1.2   Ice cores as a climate archive

As there is only a small number of direct instrumental meteorological data available from the Arctic, proxy data from climate archives become necessary. Proxy data further opens the possibility of reconstructing longer time records. For instance, temperature was measured at few locations only within about the last 100 years which is not long enough to set the recent values in the context of climate history. However, polar ice sheets are a unique archive for paleo-climate science. Proxy records derived from ice cores offer the possibility to compare recent with paleo values. The idea that ice cores can be used as a climatic archive goes back to the "Deutsche Grönland-Expedition Alfred Wegener" in the 1930s when expedition members studied the annual layers of a 15 m deep snow pit in Greenland. Since that time, ice cores´ contribution to climate science has increased.

Snowflakes accumulate in layers on top of the ice sheet (Fig. 1-3). The snow gradually compacts and sinters under its own weight. It first compacts to firn, then at greater depths to ice. The ice sheet consist of a variety of horizontal layers of different physical and chemical properties. These layers are formed by seasonally varying contents and discontinuities at the surface and survive to great depths. The layers preserve the information of the final deposition and allow the analysis of paleo climate from an ice core. The thickness of a layer is also not constant over time after the final deposition. The effect that layers become smaller with depth is called *thinning*. The rate of thinning depends on temperature and accumulation rate. Unfortunately, annual layers become harder to distinguish in greater depths of the ice sheet due to thinning.

Especially in areas of lower precipitation, the so-called *local noise* (Fisher et al., 1985) is of great importance. Drift can destroy the seasonal layering in the snow. Wind easily erodes the surface snow, removing snow one year old or older. There is a mixing of snow of different types and ages during the snow drift, which may be deposited together at the final deposition. The formation of dunes can more than double the accumulation rate of a single year, while erosion and formation of sastrugis can reduce the accumulation rate at other sites. That is why the accumulation rate is not the same as precipitation. Accumulation is defined as the result of precipitation, drifting and evaporation (Ohmura and Reeh, 1991). The accumulation rate is an important part in mass balance calculations. Glaciers and ice sheets are fed by snow

accumulation rate and loose mass because of melting and glacier ice avalanches. The annual mass balance is defined as the difference of their accumulation rate and ablation. Therefore, accumulation rate is an important parameter to be determined from ice cores.
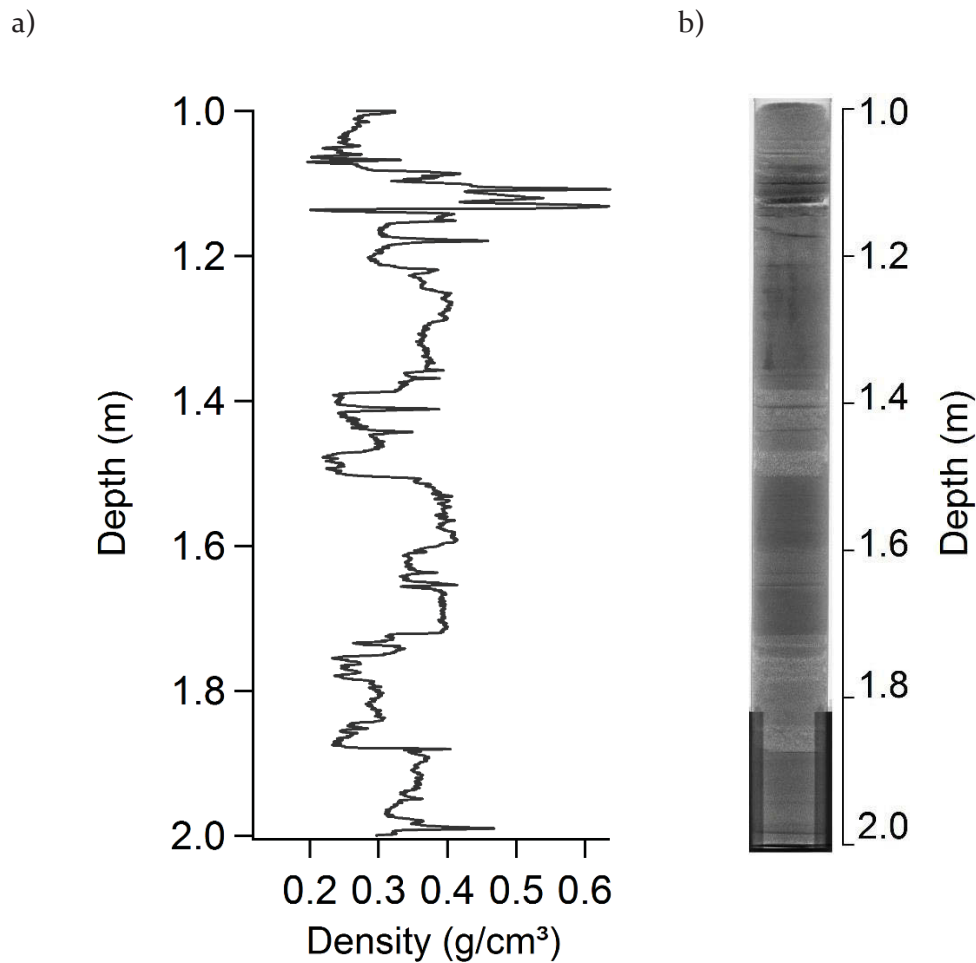
Fig. 1-3 Snow from Greenland in a thin carbon fiber tube (10 cm diameter) as an example of the layering in snow; a) density record b) corresponding 2D-image from CT measurement. The gray values correspond to density. Darker values represent a denser medium. The refrozen melt layer of the 2012 event is visible at a depth of around 1.1 m.

A critical parameter in the reconstruction of the paleo-climate from ice cores is the age of a certain layer. It is common to count layers with seasonal variations to date an ice core record (*annual layer counting*) (e.g. Andersen et al., 2006b; Vinther et al., 2006). Other dating methods include using ash layers or melt layers as tie points for absolute dating (e.g. Rasmussen et al., 2008), or numerical flow models to account for thinning in the deep part of ice cores (e.g. Johnsen et al., 1997), where annual layers are too thin for layer counting.

Paleo-temperature and accumulation rate can be reconstructed from the ice matrix, while air trapped in the bubbles of the ice is directly linked to the paleo-atmospheric composition. In the 1960s, the Dane Willy Dansgaard was the first to observe that the content of the stable water isotopes oxygen [$^{16}O/^{18}O$] and hydrogen [H/D] vary depending on the air temperature during precipitation (Dansgaard, 1953). The differences occur due to fractionation processes. Fractionation can be caused by differences in the distance to the coast or temperature. Gravity causes an earlier rain-out of the heavy isotopes compared to the lighter ones. Therefore, precipitation contains more heavy stable water isotopes in the source areas compared to the precipitation areas and in summer compared to winter. Craig (1961) described that the ratio of heavier to lighter hydrogen stable isotopes (δD) and oxygen stable isotopes ($\delta^{18}O$) of precipitation globally has a linear relationship (*global meteoric water line*). Dansgaard (1964) extended that finding by defining a new parameter, the deuterium excess d ($d=\delta D-8*\delta^{18}O$) that is assumed to provide information on the evaporation conditions. Some years later, Johnsen et al. (1989) found that there is also a linear relationship between the mean $\delta^{18}O$ values of surface snow and the annual mean surface temperature, which is represented by the firn temperature at 10 to 20 m depth. They introduced an alpha-factor (α) for the translation of isotope ratios to temperatures. Since then, the method of using stable water isotope composition as a *paleo-thermometer* has become better established in ice core studies (e.g. Petit et al., 1999). Johnsen et al. (1989) determined the coefficient to translate $\delta^{18}O$ values in Greenland to annual mean air temperatures ($\alpha=0.67$), which is still commonly used, by empirical studies along Greenland's main ice divide. This coefficient is assumed to be only valid for the Holocene, and there are also several situations where the relationship is not applicable. One reason is changes in the seasonality of the precipitation. However, knowledge of the relationship between $\delta^{18}O$ in the snow and temperature offers high potential for paleo-climate studies from ice cores. Even considering all the uncertainties it allows for a direct translation of $\delta^{18}O$ to temperature.

1.3 Greenland

Greenland is the largest island in the world. Greenland spans 2700 km from north to south and 1100 km at its widest point (Funder, 1989). Greenland's northern coast borders the Arctic Ocean; the northeast borders the Greenland Sea; the south borders the North Atlantic Ocean, and the west borders the Labrador Sea and Baffin Bay (Fig. 1-4).

Fig. 1-4 Overview map of Greenland. Drill sites of ice cores (for the NGT cores, see Fig. 3-1) are marked with dots. Their colors indicate the number of years covered by the ice core. Meteorological stations with long temperature records (up to ~100 years) are marked with dark red stars. The names of the surrounding seas are given in blue (modified after Box et al., 2013).

Today, eighty percent of the island is covered by ice. The *summit* in central Greenland is the highest elevation on the ice sheet. Here, the ice reaches 3.2 km above sea level. In this study, the area north of the summit is named "northern Greenland" and the area to the south "southern Greenland." A main ice divide separates northern Greenland into an eastern and a western part (Fig. 1-4 and Fig. 3-1). Cyclones control the weather (Chen et al., 1997). The main wind direction is south/south-west to east/north-east. Therefore, the north-eastern part of Greenland is located in the precipitation shadow of the main divide. Precipitation decreases from south to north from about 2500 mm/a in the southeastern coastal areas to less than 150 mm/a in entire north-east Greenland (Funder, 1989). The coldest place in Greenland is the ice sheet, where temperatures in winter can fall below -70 °C (Cappelen, 2015). Generally, the temperatures hardly rise about 0 °C as a reason of altitude and high albedo effect (Cappelen, 2015). The monthly mean air temperatures in central Greenland show a clear seasonality (Barlow, 1994), which is important to ice core dating approaches. The monthly mean air temperature there ranges from -13 °C in summer to -45 °C in winter (studies at Eismitte 1930/31, Station Centrale 1949/51 and Cathy Site 1987/89) (Barlow, 1994). Temperature measurements of automatic weather stations at Summit also detected about 30 °C difference between monthly mean summer and winter values in the years 1987 to 1999 (Shuman et. al. 2001).

The Greenland Ice Sheet offers the possibility to study the last about 122 000 years. An increasing number of deep ice cores in central and southern Greenland have been drilled since the beginning of ice core studies. To study the paleo-climate variability, deep ice cores have been drilled into the Greenland Ice Sheet (e.g. Dye3, GRIP, GISP2, NGRIP and NEEM see Fig. 1-4). However, little is known about the climatic representativeness of such isolated studies due to local differences in layering. There can be large differences between the individual records. Even long-term, NGRIP shows different results than GRIP or GISP2 (NGRIP members, 2004), which were all drilled in central Greenland close to the summit.

There are first studies on spatial representativeness of ice core data in south (e.g. Andersen et al., 2006a; Vinther et al., 2010) and central Greenland (e.g. White et al., 1997) but there is still little known about northern Greenland.

1.4 Why is so little known from ice core studies in northern Greenland?

There are only few ice-core drilling activities in northern Greenland, and weather stations with direct temperature observations are mainly located in the southern coastal areas (Fig. 1-4). The area of northern Greenland is very remote, being far away from the coast, airports, and bigger settlements. This makes it a logistically difficult area to study. The weather is generally more hostile than in the southern and coastal areas. Temperatures are lower on average (-30 °C annual mean air temperature), and wind is a common occurrence. The mean precipitation in northern Greenland is much lower compared to the south, which hampers ice core studies. Annual layers are already thin at the surface of the ice sheet and get even thinner with increasing depth and age due to layer thinning. Small annual layers make exact dating difficult, and the small sample volume means that a high quality and accuracy of measurements is required. These effects are most important for areas of low mean accumulation rates such as northeast Greenland (~100 mm/a).

Since the beginning of ice core studies in the 1950s, techniques, equipment and logistics have improved and make it now possible to also core in remote places such as northern Greenland. The AWI North Greenland Traverse 1993/1995 (NGT 93/95) was the first expedition team who successfully drill several ice cores in northern Greenland, and covered a large area to study the spatial and temporal variability of $\delta^{18}O$ and accumulation rate of the last 500 to 1000 years in this area of the Greenland Ice Sheet. With the todays laboratory techniques it becomes now, years later, possible to measure the samples with the necessary accuracy, offering new possibilities for reconstructing the paleo-climate.

1.5 Objective and structure of this study

This study deals with the analysis of northern Greenland ice cores collected in the course of the NGT 93/95. It offers a promising dataset, closing a huge gap in paleo-climate information from the Arctic region. For the first time, the entire set of the NGT 93/95 $\delta^{18}O$ records is made available, allowing for more representative mean values and opening the possibility to study the spatial distribution. The NGT 93/95 records are updated by the data of newly drilled firn cores. All records have been stacked to a mean record. This updated stacked record allows for study of the most recent climate trends in the context of climate history for the first time. All records are dated and annual mean values of $\delta^{18}O$ and accumulation rates calculated. The results are interpreted in terms of spatial as well as temporal variability. Besides the climatic interpretation, the study also addresses the problems, limits and possibilities of ice core science in low-accumulation rate areas.

The main topics are:

Topic A

Due to its possible impact on global sea level, the mass balance of the Greenland Ice Sheet is subject of many studies. As the positive part of the mass balance, the accumulation rate is a crucial parameter, which has been obtained from many local pointwise measurements and interpolated over large areas (e.g. Ohmura and Reeh, 1991).

In this study ground-truth data covering a large area in northern Greenland is provided. The spatial and temporal variability of accumulation rate and how it fits to previous accumulation rate maps is discussed. The presented data offer a crucial input for future mass balance studies.

➔ *How can the spatial distribution of accumulation rate be characterized in northern Greenland? What about temporal changes of the accumulation rate over the last millennium?*

Topic B

The relationship between air temperature and $\delta^{18}O$ in snow has been used for paleo-temperature reconstructions. However, this relationship is altered by different circumstances such as changes in the seasonality of the precipitation, differences in altitude or differences in the distance to the coast. Studying the spatial $\delta^{18}O$ distribution of the NGT 93/95 data offers the possibility to extract the effect of altitude, accumulation rate and geographic coordinates on the temperature - $\delta^{18}O$ relationship. With the presented data the spatial distribution of $\delta^{18}O$ and the climatic and topographic reasons for that are studied.

Furthermore, the discussion on recent temperature changes need to be based on the context of natural variability. The provided data sets offer the great possibility to study both, the local and the temporal aspects of natural variability of each of the drilling sites and, because of the amount of data, to separate local variability from climate variability.

➔ *What was the spatial and temporal distribution of $\delta^{18}O$ in northern Greenland over the last millennium?*

Topic C

In the context of the discussion on recent global temperature increase, the observed slow-down of the warming gradient, missing data from the Arctic is cited as one possible reason for that. With this study not only very recent temperature-proxy data is provided by the NGT-updating firn cores from 2011/12, it also can be set into historical context by merging the NGT 93/95 and NGT-updating firn cores and therefore clearly explore the question:

➔ *Is there a recent warming trend in northern Greenland?*

The thesis is divided into an introduction (1) providing the motivation, background information (2), data (3) and used methods (4), data analysis (5), results (6), and a conclusion (7) chapter. The results are briefly summarized followed by the original research papers (Table 1-1), which were designed for publication in international peer-reviewed journals or books. Two papers are already published, while another two are presented here as a draft for publication.

Table 1-1 Overview of publications presented within this thesis

Chapters	Publication
First author	
4. 1 Publication 1	Weißbach, S., Wegner, A., and Kipfstuhl, J.: Snow accumulation in North Greenland over the last millennium. In: Towards an interdisciplinary approach in earth system science, Lohmann, G., Meggers, H., Unnithan, V., Wolf-Gladrow, D., Notholt, J., and Bracher, A. (Eds.), Springer Earth System Science, London, 2015.
4. 2 Publication 2	Weißbach, S., Wegner, A., Opel, T., Oerter, H., Vinther, B. M., and Kipfstuhl, S.: Spatial and temporal oxygen isotope variability in northern Greenland – implications for a new climate record over the past millennium, Clim. Past, 12, 171-188, 2016.
4. 3 Publication 3	Weißbach, S., Kipfstuhl, S., Freitag, J., Hörhold, M., Lohmann, G., and Laepple, T.: The unusual recent warming trend in northern Greenland. In preparation for submission to Nature
Co-author	
4. 4 Publication 4	Faber, A.-K., Vinther, B.M., Weißbach, S., Kipfstuhl, S., Ørum, N.O.: Using ice core and weather station observations to construct a spatial map of $\delta^{18}O$ and temperature for present-day Greenland. In preparation for submission to JGR-Atmospheres

The author´s contribution to the individual publications

Publication 1

I developed the core chronology and calculated the annual mean values. I prepared the relevant literature, analyzed and interpreted the data, and wrote the manuscript. Anna Wegner and Sepp Kipfstuhl advised me during the whole process.

Publication 2

I completed the NGT 93/95 data set by digitalization of lab and field notes, calibrated raw data and also added new data. I prepared the samples for these new $\delta^{18}O$ measurements in the cold laboratory. I did CFA measurements (of 70 m firn), which were used to date the cores. I developed the chronology of the cores, calculated the annual means, and stacked the records. I prepared the relevant literature, analyzed, interpreted the data and drafted the manuscript. All co-authors critically reviewed and discussed interpretations and earlier versions of the manuscript. Anna Wegner and Sepp Kipfstuhl advised me during the whole process.

Publication 3

I was involved in the measurements preparation, the analysis of the raw data, and monitoring of the $\delta^{18}O$ measurements. I annual layer-counted the data and calculated the stacked record. I drafted the manuscript. Thomas Laepple counseled me in the statistical analysis and data interpretation. Sepp Kipfstuhl and Johannes Freitag advised me during the whole process.

Publication 4

I was involved in the data compilation (provide NGT 93/95 data) and writing the final manuscript.

2 Background

This chapter gives an overview about the knowledge of spatial and temporal variability of $\delta^{18}O$ and accumulation rate in northern Greenland without the in this thesis presented full data set of the NGT 93/95.

2.1 Spatial Variability

Few details are known about the distribution of accumulation rates and mean $\delta^{18}O$ values in northern Greenland due to a lack of data. However, a better knowledge of their distribution is important to the mass balance studies of the ice sheet and $\delta^{18}O$ to temperature translations to get more precise forecasts of sea-level rise contribution.

2.1.1 Distribution of $\delta^{18}O$ and accumulation rate- expectations from the ice sheet topography

A difference between southern to northern Greenland, as well as a difference between the eastern to western parts of northern Greenland, is expected for both parameters from the topography of the Greenland Ice Sheet (Fig. 1-4).

The summit in Central Greenland is the highest elevation. For this reason going northward in northern Greenland also means to go downward. At higher altitudes, when temperature drops and air mass lost moisture, lower $\delta^{18}O$ ratios as well as lower accumulation rates are expected (Dansgaard, 1964).

The direction of the main ice divide in Greenland is almost North-South. It is expected that the eastern part of northern Greenland is in the precipitation shadow due to the dominant westerlies, while there are higher accumulation rates on and west of the divide. As the heavier isotopes rain out first, it is further expected that there are lighter isotope ratios in the snow east of the divide. Therefore, additional to the south-north differences an east to west gradient is expected.

2.1.2 Accumulation rate distribution- previous studies and methods

There are different methods used to derive mean accumulation rates for glaciated areas; an important one is the use of ice cores and snow studies. However, there was only little drilling activity in northern Greenland before NGT 93/95. A few glaciological activities in the north were

performed by Wegener and Koch in 1913 (Koch and Wegener, 1930), by Benson in 1952-53 (Benson, 1962) and by the British North Greenland Expedition in 1958 (Bull, 1958) to study accumulation rates in northern Greenland.

Ohmura and Reeh (1991) derived an overview map of Greenland's snow accumulation rates (Fig. 2-1), using data from the 1930s. Most of this old, historical data is connected with high uncertainty as it is only one value of one single year and not a mean over several years. The spatial interpolation is also highly insecure and a higher resolution not possible due to the larger areas where no data is available, like in northern Greenland. The map generally shows lower accumulation rates in the north of Greenland compared to the southern and coastal areas, and an area of very low accumulation rate east of the main ice divide in northern Greenland is expected from the topography of the ice sheet.

Several short cores were drilled along the 2000 m contour line in Greenland to assess accumulation rates during the NASA-Program for Arctic Regional Climate Assessment (PARCA) from 1995 to 1999 (Mosley-Thompson et al., 2001). During this program, there was also little activity north of the Summit.
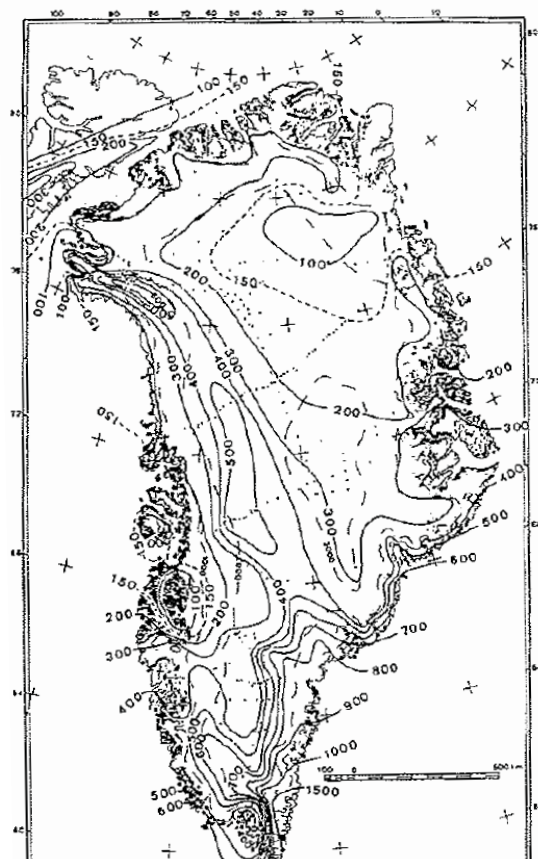
Fig. 2-1 Overview map of snow accumulation rate in kg m^{-2} a^{-1} over the Greenland Ice Sheet compiled by Ohmura and Reeh (1991)

Bales et al. (2001) extended the study of Ohmura and Reeh (1991) by adding data from NASA´s PARCA, coastal meteorological stations, as well as preliminary NGT 93/95 snow-accumulation rate data of shorter time periods (see table 2 in Bales et al. 2001). The map of Bales et al. (2001) shows a smaller area of very low accumulation rates (< 100 mm/a) but supports the general distribution in Greenland found by Ohmura and Reeh (1991). The inaccuracy is, however, still high due to the isolation of ice-core studies and large areas of missing data. Bales et al. (2001) give an error of about 24% (which is about 70 mm/a) for the mean accumulation rate over the ice sheet. Cogley (2004) noticed that the accuracy has to be doubled to achieve a ±1 mm/a accuracy in sea level rise (95% confidence interval). To achieve this accuracy more and reliable data is needed.

Besides the spatial interpolation between the isolated ice core data, there are other methods being developed to derive accumulation rates for maps of possibly higher resolution. High resolution space and airborne radar surveys seem to be a promising avenue for accomplishing this in the nearer future (e.g. Kanagaratnam et al., 2001). Radar-scatterometer images are a powerful tool for investigating changes in accumulation rate over the past 2 decades. However, they still need in situ accumulation rate data from ice core studies to calibrate their depth-time-resolution. Another method to derive accumulation rates is climate modeling. Global circulation models using reanalysis data (e.g. ERA 40) could be used to derive accumulation rates (e.g. Hanna et al., 2006). However, these models still underestimate the accumulation rates in northern Greenland compared to ice core results (Hanna et al., 2006).

2.1.3 The $\delta^{18}O$ distribution– previous studies

In contrast to accumulation rate, there are no available maps of $\delta^{18}O$ values of higher spatial resolution. A general map was produced by Dansgaard and Tauber (1969) (Fig. 2-2). They show that the values in central Greenland are more depleted compared to those at the coast. Additionally, there are maps of mean air temperature (e.g. Ohmura, 1987). These maps should be of comparable distribution features, as $\delta^{18}O$ values in snow are a proxy for air temperature. Models (e.g. ECHAM5-wiso) using reanalysis data can give an overview of the distribution of $\delta^{18}O$ values of lower spatial resolution but still need in situ measurements to be calibrated. The $\delta^{18}O$ mean values derived from ice core studies are usually isolated values (e.g. NGRIP and NEEM). It was not possible to make distinct distribution statements before the NGT 93/95 data became available, as the drilling activity in northern Greenland was low. However, a detailed knowledge of the spatial distribution would allow for studying the influencing factors on $\delta^{18}O$ besides temperature and result in a more definitely translation of the $\delta^{18}O$ values to temperature in northern Greenland.
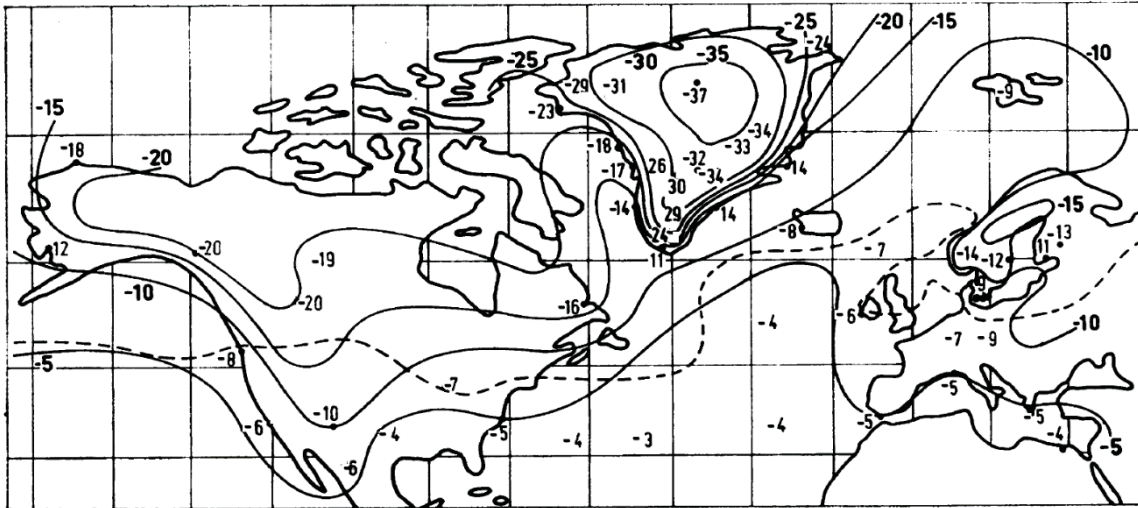
Fig. 2-2 General map of the distribution of δ¹⁸O values of annual precipitation and approximate δ -isolines over the Northern hemisphere (between 165°W and 45°E longitude) (modified after Dansgaard and Tauber (1969)).

2.2 Temporal variability

To understand the recent climate and maybe be able to make forecasts with the help of appropriate climate models it is necessary to study the paleo climate and its natural variability. Greenland is a key area in the discussions about global warming due to its impact on global sea level rise and polar amplification. However, there is only little known about the decadal temperature variability of the last millennium in northern Greenland.

2.2.1 The temperature history of the last 1000 years

The climate of the Holocene interglacial is characterized by fairly stable temperature conditions compared to that of the previous glacial period. However, temperature changes of about 1-2 °C during the Holocene are also reconstructed from different sources of archives (e.g. tree rings, lake sediments and ice cores). These changes could be pronounced with unequal strength in different areas. Some events are prominent and can be observed globally. We know from temperature proxy data of different sources and areas that periods of warmer and colder conditions occurred during the last 1000 years (e.g. Mann et al., 2009). There were slightly warmer conditions around the 10th to 14th century (Medieval Climate Anomaly, MCA) followed by a period of colder temperatures from the 15th to the mid-19th century (Little Ice Age, LIA). The LIA ended with a warming trend that is ongoing. Besides insolation, changes of solar radiation and volcanic activity are important external drivers of the overall Holocene climate (e.g. Mayewski et al., 2004; Sigl et al., 2013). Higher solar radiation causes warmer temperatures, while

higher volcanic activity with explosive eruptions and a higher emission of sulfur is mostly followed by cooler temperatures (e.g. Zielinski, 2000).

2.3 Recent temperature evolution in a historical context

Recently, rising global mean temperatures and changes in the Arctic environment have been observable. However, there are fewer possibilities to study the recent Arctic temperature changes in an historical context. Instrumental temperature data is too short and sparse, especially in northern Greenland. Therefore, proxy data has to be used to reconstruct the paleo-temperature. However, available Arctic proxy data is mostly summer-biased (e.g. tree rings) or difficult to calibrate as a stack of different types of proxies (e.g. Consortium Pages2k, 2013). Records of $\delta^{18}O$ in ice cores offer the possibility of longer one-proxy records and are directly correlated to temperature for an easier calibration.

However, most of the ice core studies are performed in isolation from each other and therefore show a high level of local noise. The differences in the $\delta^{18}O$ records of GRIP and NGRIP which were drilled only about 30 km apart, illustrate the evidence of regional variability in Greenland (NGRIP members, 2004). Especially in the low-accumulation area of northern Greenland, local noise is extremely important because annual layers are thin and often altered. The wider climate representativeness of single-spot studies becomes questionable. Derived from annual layer thickness and $\delta^{18}O$ values the signal-to-noise-ratio in southern Greenland were calculated with about 4 while central Greenland has only 1-2, which means that to obtain records representative for a larger area time series have to be smoothed by a low pass filter (Dansgaard et al., 1985). Vinther et al. (2010) present a study using a stacked record of twenty ice-core records from southern Greenland. They were able to study the prominent globally known climate events during the Holocene from the $\delta^{18}O$ values of the stacked record. They make clear that stacking of multiple records becomes necessary to obtain data with a reasonable signal-to-noise ratio to study also decadal climate variability, especially in low-accumulation-rate areas. Information is needed from stacked $\delta^{18}O$ data with that noise ratio to achieve a representative picture of the climatic evolution also in northern Greenland.

The ice cores from the NGT 93/95 offer for the first time the possibility of a representative one-proxy record over the necessary time interval (last millennium). First results from NGT 93/95 with climatic interpretation were published by Fischer et al. (1998c). They found a distinct cold event during the 17th and first half of 19th century, which was attributed to the LIA in northern Greenland from a stacked $\delta^{18}O$ record of four NGT 93/95 cores (B16, B18, B21, and B29). This was the first hint that by stacking northern Greenlandic $\delta^{18}O$ data, a climatic interpretation of $\delta^{18}O$

becomes possible for this low-accumulation-rate area as well. However, the whole set of NGT 93/95 $\delta^{18}O$ data has to be stacked and interpreted for more precise and regionally-representative results. A stack of more records will be more accurate and more representative for a larger area.

Since the NGT 93/95 cores were drilled during the 1990s, the stacked record does not cover the most recent years. That is why updated ice cores are necessary to unambiguously assess the modern Greenlandic temperature trends in the context of natural variability.

3 Data and Measurements

The following chapter gives a brief historical overview of the projects, which provide the ice-core records for this thesis and a summary of the available data. The measurements of the stable water isotopes are explained in detail.

3.1 Northern Greenland ice core records - a brief history

Central North Greenland was probably the least-investigated region of the northern hemisphere until about 25 years ago due to its relative inaccessibility. In 1992 and 1993, two deep drilling projects (GRIP and GISP2) successfully penetrated the ice sheet at the Summit. Both deep drilling projects created the logistical prerequisites for initiating following-up projects during the 1990s such as the NGT 93/95 or PARCA (Mosley-Thompson et al., 2001).
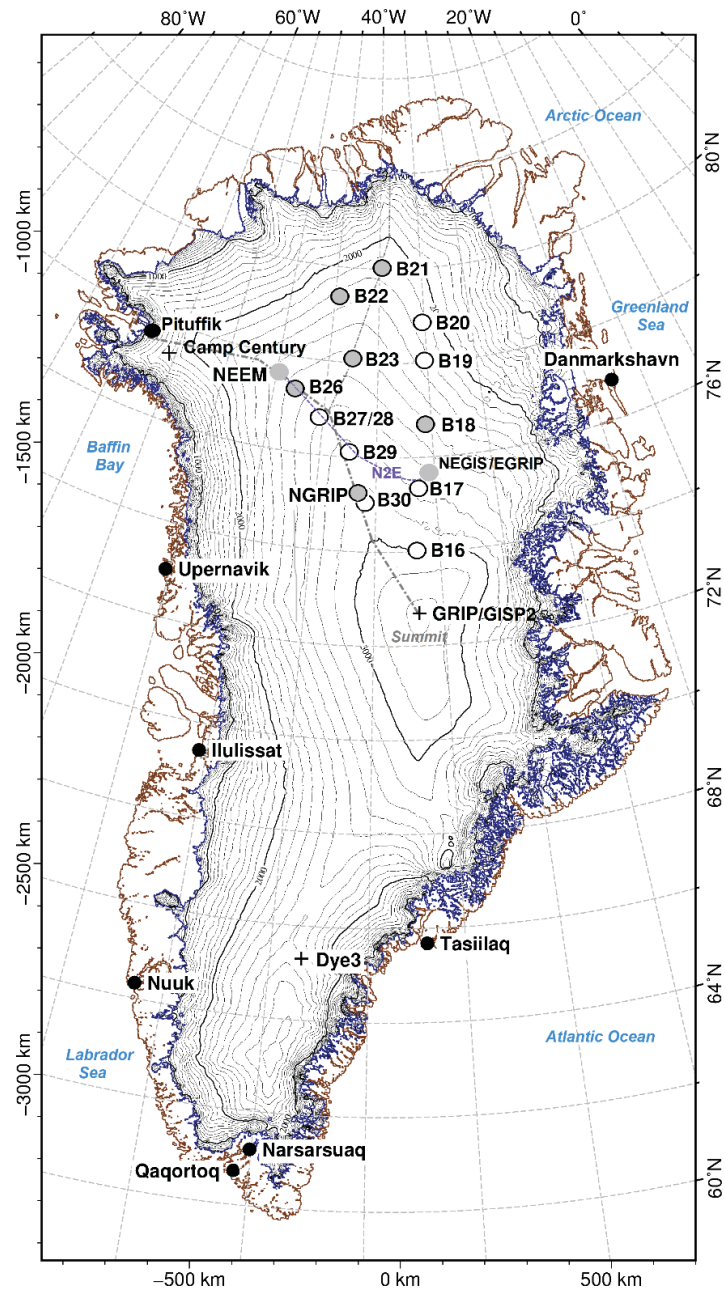
Fig. 3-1 Overview map of Greenland, including marked locations with temperature measurements (black dots) and ice-core drilling sites of the NGT 93/95 (black circles), and some prominent deep drill sites (black crosses). The drilling sites of the NGT-update cores are marked with circles filled in gray. The route of the N2E traverse is shown in violet. The names of bordering seas are shown in blue. The ice sheet topography is according to Bamber et al. (2013). The main ice divide is also indicated on the map (thin gray line).

3.1.1 North Greenland Traverse 1993/1995 (NGT 93/95)

The Greenland Ice Core Project (GRIP) was terminated in 1992. As northern Greenland is one of the least studied regions in the high Arctic, the initial idea was to move the heavy vehicles and camp infrastructure by an overland traverse from the Greenland ice sheet through to Thule (Pituffik) Air Base (Fig. 3-1). The scientific goal of the traverse was to collect as much glaciological data as possible along the way to produce a comprehensive climatic data set, in particular of the stable isotopes of water, the best know temperature proxy, as well as impurities and accumulation rate for northern Greenland over the last 500 years.

The traverse started in 1993 as the "Summit-Thule Traverse". However, it became clear in autumn 1993, that the GRIP and GISP2 Eemian records (115 to 130 kaBP) disagreed and were disturbed by the ice flow (Greenland Ice-core Project, 1993; Taylor et al., 1993). The traverse was renamed to "NGT" in 1994, when it became clear that a new deep drilling project (NGRIP) would be launched to find and retrieve undistributed Eemian ice. Radar data shows a region 300-400 km northwest of Summit on the ice divide to be a promising location. The results of the traverse together with the radar survey should be used to find a new location where the Eemian ice may not be disturbed.

The route of the traverse ran straight northwards first, extending the E.G.I.G. line, passing the beginning of the Fahnestock (today NEGIS) ice stream. In 1994, the team changed direction and designated 80 °N (B21) as the northern most point of the traverse. The direction of the traverse changed again in the third year, following the main ice divide southwards, because of the planned drill of the deep ice core NGRIP. The traverse ended in 1995 with a total length of about 1600 km. In May 1996, the NGT camp became basis for the NGRIP drill camp after being moved it only 15 km from its terminal position at NGT45 (B30).

The 12 NGT shallow ice cores were drilled en route at 100-150 km spacing to depths of 100-175 m deep, except for one 70 m core (Table 3-1). These cores were supplemented by 33 firn cores of 10-15 m length which were collected at about 50 km apart. In addition, snow pits were excavated (Fischer, 1997).

Table 3-1 Overview of NGT 93/95 ice core metadata

Name of ice core	Name of drill site	Longitude [°N]	Latitude [°W]	Length [m]
1993				
B16	NGT 03	73.940	37.630	102.4
B17	NGT 06	75.250	37.625	100.8
B18	NGT 14	76.617	36.403	150.2
B19	NGT 19	78.001	36.398	150.4
1994				
B20	NGT 23	78.833	36.500	150.4
B21	NGT 27	79.999	41.137	100.6
B22	NGT 30	79.341	45.912	150.2
B23	NGT 33	78.000	44.000	150.4
1995				
B26	NGT 37	77.253	49.217	119.7
B27	NGT 39	76.658	46.482	175.0
B28	NGT 39	76.658	46.482	70.7
B29	NGT 42	76.000	43.500	110.5
B30	NGT 45	75.000	42.000	160.8

3.1.2   Northern Greenland 2008-2012 (NGT-update cores)

Factors including the debate about the missing or delayed warming in Greenland, a camp on the inland ice (NEEM), and a ski-equipped plane at NEEM motivated the project to extend the old NGT records to the actual horizon (2011 and 2012, respectively). The distance from NEEM to B26 is only 50 km and was completed by snowmobile already in 2011. The other mentioned sites were visited by plane. Scientists from the Centre for Ice and Climate (CIC, Copenhagen) drilled the 30 m deep cores in only 2-3 hours on the ground. In 2011 and 2012 some of the old NGT drilling sites had been revisited. Firn cores 30 m long were obtained at the 5 northern Greenlandic sites (NGRIP12, B18_12, B21_12, B23_12 and B26_11). Only 6 m of core were drilled at B22_12 due to a power failure. At two sites in southern Greenland, 45 m long firn cores were drilled (Dye3_12, South dome_12 which are not part of this study) (Fig. 3-1, Table 3-2). In addition, there is the NEGIS short core (Vallelonga et al., 2014), which was drilled close to the B17 site and several other shallow drill cores (Masson-Delmotte et al., 2015) around the site of NEEM, which were

drilled for preliminary reconnaissance, but which were used also in this study to extend the northern Greenland ice core records to the recent years.

Table 3-2 Overview of NGT-update firn core metadata

Name of core	Longitude [°N]	Latitude [°W]	Length [m]	Distance to NGT 93/95 drill site [km]
2011				
B26_11	77.253	49.217	30	0
2012				
B18_12	76.62	36.41	30	0.380
B21_12	80.00	41.14	30	0.125
B22_12	79.32	45.91	5.6	2.340
B23_12	78.00	44.00	30	0
NGRIP12	75.1	42.32	17	0
NEGIS (Vallelonga et al., 2014)	75.63	35.95	67	-
NEEM stacked (Masson-Delmotte et al., 2015)	77.45	51.06	52.6-85.3	-

3.1.3   NEEM to EGRIP Traverse 2015 (N2E)

While the NEEM camp was being moved to the new drill site at EGRIP (Fig. 3-1), 44 "liners" of 1 m length were collected (two at each position following in depth) (Schaller et al., 2016) to extend the climate records to the horizon of May 2015.

Collection of liners is a newer method used in glaciology. The upper meters are not studied by snow pits or cores collected by standard drill as the snow is often loose and not possible to keep on shape by drilling. Liners are thin carbon fiber tubes of 1 m length, which can be pushed in the snow and used to collect samples of 1 m length. This method has a time advantage over digging snow pits and is an easy method to derive undisturbed cores of the porous upper meters of the snow. This method also allows an exact study of the snows´ structure. The liners can be cut for smaller samples either directly in the field or later in the lab.

3.2 Available data and prior NGT publications

Plenty of data had been already available at the beginning of this thesis, since the first NGT 93/95 cores were drilled in 1993 (almost 20 years before the start of this thesis).

The following parameters were already available in different depth resolutions and by different measurement methods, in addition to the stable-water isotopes, which had been measured continuously over the last 20 years (see pp.- 26 -):

- Firn temperature at most of the NGT 93/95 sites
- Density (CT, Bulk, Gamma)
- Electrical conductivity (DEP, ECM)
- Impurities (CFA, IC)

An overview of prior publications using NGT 93/95 data is presented below.

Measurements of the electrical properties of the ice (ECM (Werner, 1995) and DEP (Wilhelms, 1996)) give a first idea of the age of the cores by allowing identification of the volcanic marker horizons. Results are presented by Friedmann et al. (1995). The high-resolution NGT 93/95 gamma density data was used to study the impurity impact to the densification of firn (Freitag et al., 2004; Hörhold et al., 2011). Preliminary $\delta^{18}O$ results from some of the NGT 93/95 records are presented by Fischer (B16, B18, B21 e.g. Fischer et al., 1998c) and Schwager (B18, B21, B26 and B29 in Schwager, 2000). These authors describe the distinct occurrence of the LIA and the periodicity from wavelet analysis in the $\delta^{18}O$ values. Preliminary results of the chemical composition from a continuous flow analysis (CFA) are presented by Sommer (1996) and Bigler et al. (2002). They measured parts of the cores of B21 and B29. Fischer et al. (1998a); (1998b) characterize deposition mechanisms for nitrate and sulfate and the impact of industrial emissions on northern Greenland precipitation (using B16-B18). More recently, measurements of sea salt tracers from the NGT 93/95 core B20 were used to investigate inter-annual to multi-decadal modes in atmosphere and ocean dynamics in the North Atlantic over the last 1000 years (Fischer and Mieding, 2005). Rimbu et al. (2007) investigated the connection between frequency of atmospheric blocking circulation and the variability of NGT 93/95 accumulation rate records (B16, B18, B21, B26 and B29). A first presentation of the spatial distribution of the mean accumulation rates was conducted by Jung-Rothenhäusler (1998).

3.3 The stable-water isotope measurements

The ratio of stable isotope content in a sample is given by *δ-notation*. The isotopic content of a sample is given as the relative difference in ‰ between the isotopic ratio of the sample (R_{sample}) compared to the ratio of a standard sample ($R_{standard}$, e.g. Standard Mean Ocean Water, SMOW) (Dansgaard et al., 1973). For example for $\delta^{18}O$ the equation is:

$$\delta^{18}O = 1000 * ((R_{sample}/R_{standard}) -1) \text{ [‰], with } R_{sample} = [H_2^{18}O] / [H_2^{16}O]$$

The isotopic composition of the NGT 93/95 cores was analyzed using mass spectrometers. The NGT-update cores drilled in 2012 as well as the N2E samples were analyzed using Cavity-Ring-Down Spectroscopy (CRDS) instruments. The absolute values of both instruments were calibrated to make it possible to stack and compare the records. The older mass spectrometers measured only one isotopic species ($\delta^{18}O$ for NGT 93/95). The CRDS instruments provide δD in addition to $\delta^{18}O$ and also allow determination of the d-excess. Mainly the $\delta^{18}O$ species are considered for the climatic interpretation in this thesis.

3.3.1 Mass spectrometer (used for NGT 93/95)

The NGT 93/95 isotope data have been measured over the last 20 years (about 77.000 samples) at AWI Bremerhaven. The samples were cut in 1-5 cm thick pieces, and stored in small welded PE-bags. The molten samples were analyzed for $\delta^{18}O$ using a *mass spectrometer* (Finnigan Delta E and Delta S).

Each mass spectrometer consists of three main parts. Standard and sample gas can be entered in alternation through a dual inlet. At the *Ion Source,* the sample is ionized via collision ionization. In the *Mass Analyzer*, the ions are then sorted and separated according to their mass and charge. A combined electric and magnetic field forced the accelerated and directed ions into an orbit. The radii are proportional to their masses. At the *Detector,* the separated ions are measured and the results displayed on a chart. All three devices are stored in a vacuum system.

Using mass spectrometry, it is possible to detect the number of heavy isotopes, here oxygen isotopes (^{18}O), within the sample compared to the lighter ones (^{16}O).

Six out of the 13 records in this thesis were used in prior studies (see- 25 - "Prior NGT publications"). The other records were dated and analyzed for the first time in this thesis. However, the lab measurements had been finished before the beginning of the thesis.

The accuracy for $\delta^{18}O$ measured with the mass spectrometer at AWI Bremerhaven is better than 0.1 $\delta^{18}O$-‰.

3.3.2 Cavity-Ring-Down Spectroscopy (CRDS) (used for updated NGT records and N2E samples)

The cores of the NGT-update and N2E cores were cut in 2 cm thick pieces and measured within the framework of this thesis. The modern system of *Cavity-Ring-Down Spectroscopy (CRDS)* has been used to measure $\delta^{18}O$ and δD. At the AWI Bremerhaven, devices from PICARRO are used (L 1102-I and L 2120 and also first data with L 2130-I).
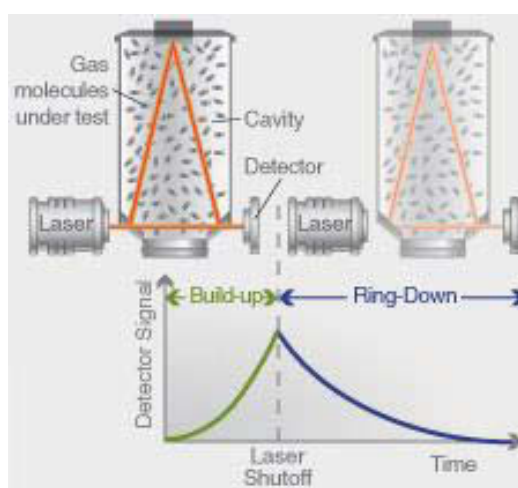
Fig. 3-2 Schematic of a Cavity-Ring-Down Spectroscope
(http://www.picarro.com/assets/images/content/cavity_figure.jpg)

CRDSs uses laser systems (Fig. 3-2). The beam of a single-frequency laser diode (180 Hz) enters a cavity, which is defined by three highly reflective mirrors. When the laser is activated, the cavity quickly fills with circulating laser light. A photodetector senses the small amount of light leaking through one of the mirrors to produce a signal that is directly proportional to the intensity in the cavity. The laser is turned off if the signal from the photodetector reaches a certain threshold level. The remaining light in the cavity continues to bounce between the mirrors. The reflected light steadily leaks out since the mirrors do not have 100% reflectivity. This exponential decay is called the "ring-down" and is measured in real time by a photodetector. PICARRO-instruments measure the time difference between an empty cavity and the cavity filled with a gas as a second absorbing source until zero reflection is reached. Therefore, the ice samples are evaporated by high pressure (~47 mbar) and passed into the cavity.

Four lab standards with known ratios are measured with ten iterations. After these standards, a blank is measured to lower the memory effect. Ten samples are then measured followed by standards once again. Each sample is measured 4 times. The measurement set up is performed

according to the strategy described in van Geldern and Barth (2012). In that way it was possible to assess and correct the data for the memory effect of two following samples as well as the instrumental drift during the whole auto sampling routine.

The accuracy for $\delta^{18}O$ at AWI Bremerhaven is better than 0.07 $\delta^{18}O$-‰ and better than 1 δD-‰ for δD.

4 Methods

Different strategies are used to translate the depth scale of an ice core to an age scale depending on the available data. This translation is called *dating* and makes an interpretation of the data in terms of paleo-climate possible. The separation of the individual years allows for calculation of annual mean values from ice core records. The $\delta^{18}O$ annual mean was calculated as a mean value over all samples between the start and end depth of the calendar year. Knowing the mean thickness and density of the annual layers in an ice core, the annual accumulation rates can be derived by multiplication of both parameters.

In the following the two dating strategies used in this thesis are described.

4.1 Annual layer counting (NGT-update cores, N2E cores and upper NGT 93/95 parts)

The cores of the records that update the NGT 93/95 records, the upper meters of the NGT 93/95 records as well as the N2E records were dated annually by layer counting using the seasonal cycles of $\delta^{18}O$, d-excess and if available Ca^{2+}, electrical conductivity and density data. The local maxima or minima values were selected to mark a cycle of one calendar year (Fig. 4-1). Selected markers (e.g. volcanic events) were used as reference horizons of known age to calculate the maximum dating error (1-3 years).
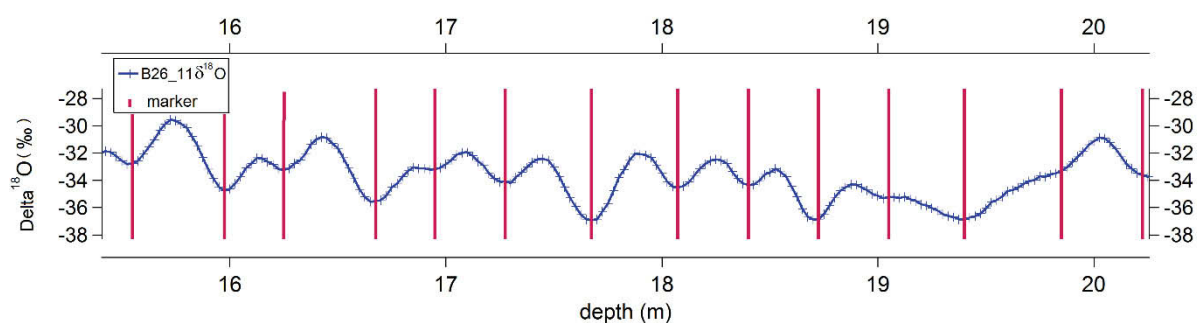
Fig. 4-1 Principal of the annual layer counting method to date an ice core. $\delta^{18}O$ data of B26_11 is shown as an example. Vertical lines mark the end of a calendar year.

Some of the NGT 93/95 records were dated by annual layer counting in prior studies (see 3.2). It was not possible to date all NGT 93/95 cores definitively by annual layer counting (Fig. 4-2)

down to their full length with the available data because of the low accumulation rates and thus small annual layer thickness in northern Greenland (northeast < 100 mm/a). Layer thinning with depth due to gravity and the smoothing of the amplitudes of stable-water isotopes by firn diffusion hamper the counting further. The back diffusion model of Johnsen et al. (2000) can help to reconstruct the initial isotope amplitudes for a more precise dating. However, there is nothing known about the uncertainty of the model results.
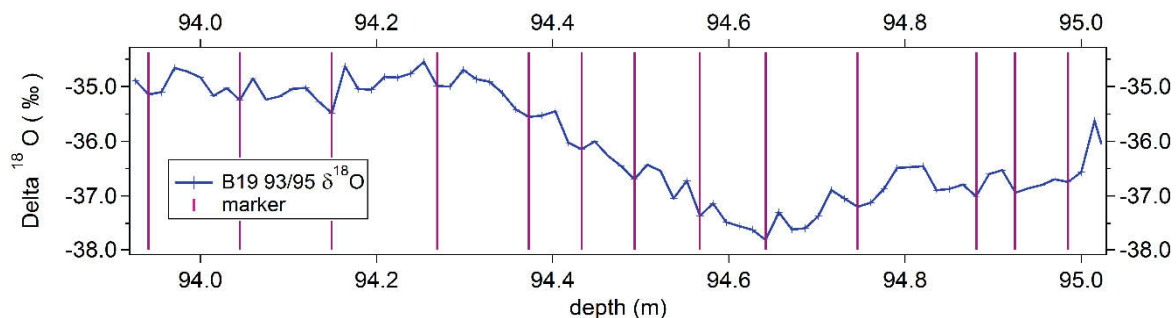
Fig. 4-2 Example where annual layer counting method cannot be used to definitively date an ice core (δ^{18}O data of B19_93/95). Vertical lines mark the end of a calendar year.

4.2 Marker horizons (NGT 93/95)

Marker horizons (melt layers and volcanic events) were selected by electrical conductivity and density records of all NGT 93/95 cores. A volcanic event with a specific age was assigned to the selected depth of observed events, based on the shape of the signal and the depth expected from the known mean accumulation rate at the site (Fig. 4-3). Volcanic events in Greenland are visible in ice core data 1-2 years after the eruption took place. This is due to the residence time, the time the aerosol needs to be transported from the place of eruption over the atmosphere to the place of precipitation on the ice sheet.

A constant accumulation rate between two marker horizons was assumed and annual mean values of δ^{18}O calculated by this strategy. The age between two markers is linear interpolated. This method results in annual δ^{18}O means, but only in mean values of accumulation rates between two marker horizons.
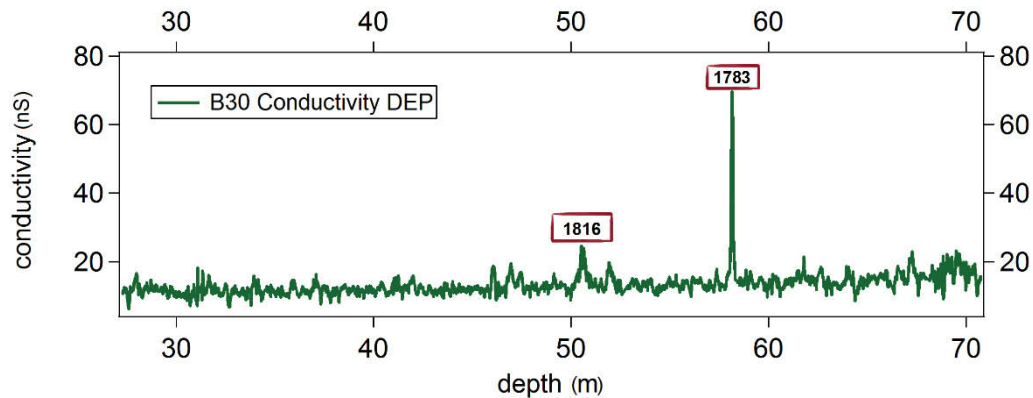
Fig. 4-3 Principal of the method to use marker horizons to date an ice core record. B30 is shown as an example. Two events of high electrical conductivity are marked and associated to the volcanic events of 1816 A.D. (Tambora) and 1783 A.D. (Laki).

Using this above strategy was possible because the last 1000 years were a volcanically active time (Sigl et al., 2013) and a lot of events were preserved in the Greenlandic ice core data. There were only about 100 years or less between any two events.

The described dating strategy was used for all NGT 93/95 cores however, some had been annually layer counted before. It is now possible to better compare the NGT 93/95 $\delta^{18}O$ records because they are all of the same dating quality, independent of their mean accumulation rate or available data.

The data is archived and available for download from:

https://doi.pangaea.de/10.1594/PANGAEA.849161

5 Data analysis

Stacking the northern $\delta^{18}O$ records and to extend the stack to the recent by the NGT-update records discovered first results in the handling and representativity of the data. Furthermore, there are also limits recognized due to the low accumulation rates in northern Greenland, which are described in the following.

5.1 Stacking

Stacking the $\delta^{18}O$ records is comparable to low-pass filtering. It means to lose the local, high-frequency information but making the common supra-regional climate signal obvious.

The $\delta^{18}O$ records of the NGT 93/95 were stacked to construct a representative mean for at least northern Greenland and account for the strong impact of local noise, as the stack covers a large area (680 x 317 km). The annual anomalies relative to a common time window (e.g. 1961 - 1990 A.D.) of the records are stacked. Absolute values were not stacked because of their records´ differences in standard deviation.

It turned out that a stack of sufficient $\delta^{18}O$ records from a representative chosen smaller area can result in the same mean record as a stack of records from a larger area (Fig. 5-1). For instance, four records were stacked to a site mean at NEEM (Masson-Delmotte et al., 2013). There is a strong correlation ($r= 0.81$, $p< 0.05$) of the 11-year running mean of the NEEM stack and a stack over the other 16 here presented northern Greenland records. That means that it is also possible to study the supra-regional climate signals (as in our stack over northern Greenland) from a stack at one position, if the stack includes enough records from a representative chosen position such as the NEEM site. The resulting strong correlation is supported by the findings of Masson-Delmotte et al. (2015), which indicate a positive correlation (annual: $r= 0.48$, 11-year averages: $r= 0.71$) between their NEEM stacked record and that of PC1 (which is comparable to the mean) of all Greenland annual $\delta^{18}O$ records spanning 1761-1966 A.D. (Ortega et al., 2014).
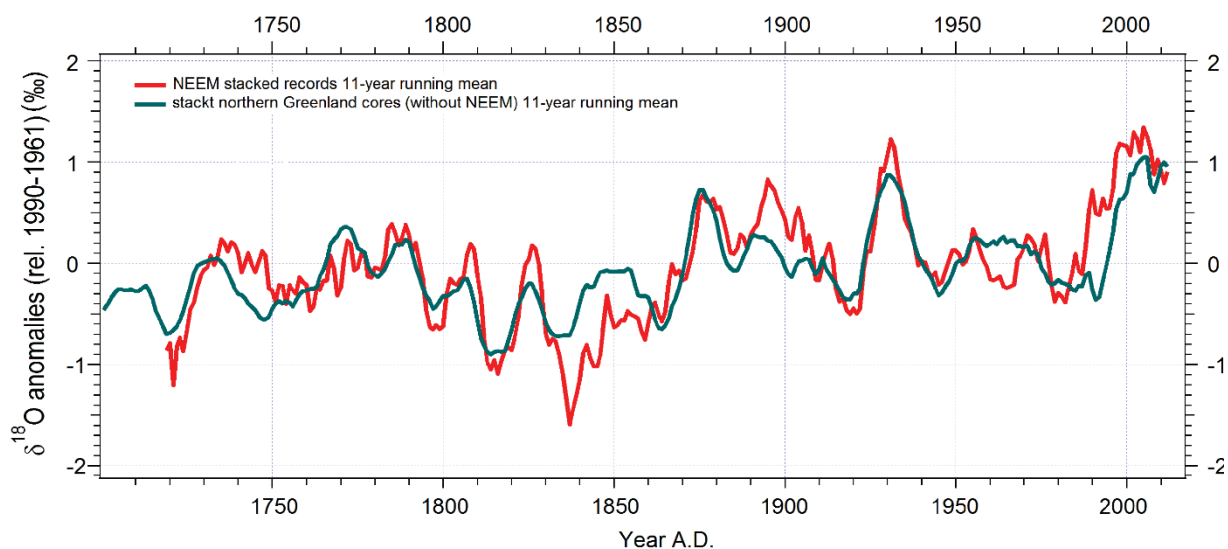
Fig. 5-1 The 11-year running-mean records of stacks of δ¹⁸O anomalies at a single site (NEEM, red) and over a larger area (northern Greenland without NEEM, petrol).

5.2 Update

It was possible to extent the NGT 93/95 stack to the most recent years by stacking their overlapping records. The resulting stacked record is almost identical when stacking all 17 individual records at once or when first stacking the records drilled at comparable sites, then adding the remaining records.

The extension to the recent years became possible because of an overlap of several years (~ 100 years) of the NGT 93/95 records and the records of those cores which were drilled to update them. It was not possible to extent the stacked record any further using the N2E records. Those 22 records were collected only three years after the drills to update the NGT 93/95 were done, but they are just 2 m long. There is an overlap of only two years (2010 and 2011) at some of the lowest accumulation rate sites. Furthermore, only the old drill sites at NEEM and at NEGIS were visited again, which make it difficult to calculate the anomalies relative to the commonly used 1961-1990 time interval. A perfect match is not possible. Two possible options were calculated. In a "positive scenario" the stacked N2E anomalies are fitted to the 2010 level and in the "negative scenario" they are fitted to the 2011 level of the updated-NGT stack (Fig. 5-2). Longer cores with a larger overlap interval have to be collected to further unambiguously extend the northern Greenland δ¹⁸O stack. Single years are affected by local noise. However, a mean over several years would make the level of offset, which is caused by a difference in their local means and the relative values to a not common time interval, clear. A definitely match would help to answer questions about the warming trend in Greenland.

The extension of the NGT 93/95 stack by the stack of the NGT-update records make it possible to assess the recent (ending 2011) years in the context of the last 1000 years. To also access the values of the coming year's further updates of the stack will be necessary.
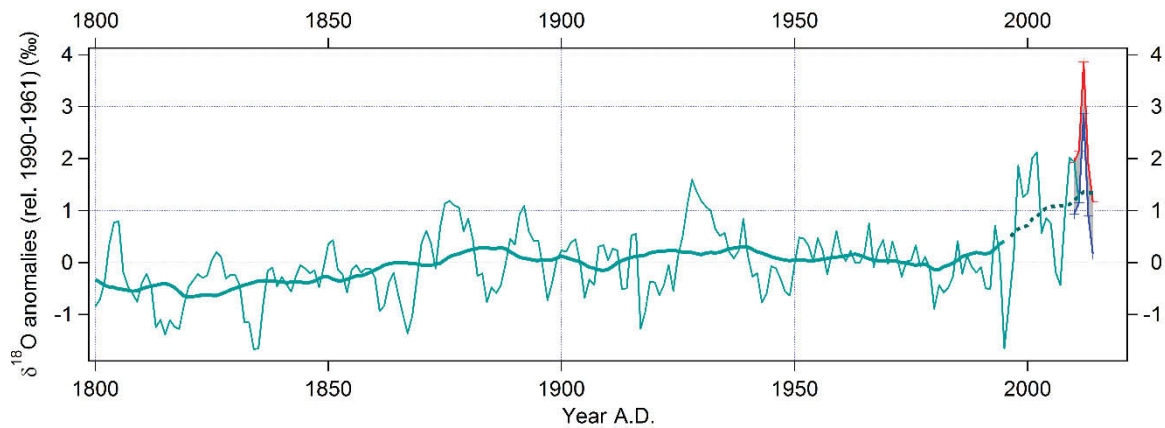
Fig. 5-2 Extension of the northern Greenland stacked δ¹⁸O values (petrol) by the annual means of the stacked N2E liner records (red: "positive scenario", blue: "negative scenario") and their 30-year running mean (petrol thick line, dotted for a mean of the scenarios).

5.3 Local noise and how it hinders the comparison of NGT 93/95 records with the NGT-update records

The NGT-update records and the NGT 93/95 records can be compared in their overlapping intervals. A comparison of the layer thickness of the same years was performed to calculate an annual thinning rate (in firn better named densification rate). That became possible since the top annual layers of the NGT 93/95 records are now located deeper in the core profiles of their updated drill cores and were drilled about 20 years later (Fig. 5-3). It was expected that the layer at the top is thicker than the same layer deeper in the ice, resulting in a positive annual thinning rate. However, some of the calculated thinning rates are negative, meaning that the layer at the surface is thinner than those deeper in the ice. Negative thinning rates were calculated for all compared record pairs from NGT and cannot be attributed to uncertainties in dating. Dating is most reliable in the upper meters of the cores, as the δ¹⁸O signal is not smoothed by diffusion. In addition, a mean over 10 years could not compensate for the negative values. The negative thinning rates are likely caused by the impact of local noise due to the distance between the old and new drill site (2 km – less meters). The linear correlation of the annual means of the B27 and B28, which had been drilled at almost the same position in the same year, has r= 0.6 (p<0.05), much higher than those of the more distantly drilled cores. However, the correlation being

unequal to 1 underlines the strong impact of local effects even on a small spatial scale, causing a low signal-to-noise ratio. Another possible explanation is that layers are not static over time. That might be a hint that there are post depositional effects within the firn column causing a shift of the e.g. $\delta^{18}O$ annual layers.
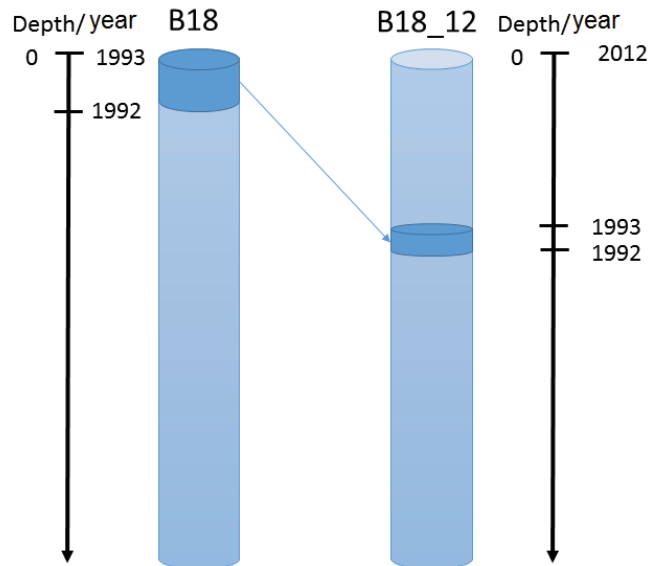
Fig. 5-3 Scheme of annual layer thinning.

Furthermore, it was not possible to derive new information on the quality of the back diffusional model by Johnsen et al. (2000). It was not possible to compare the undiffused signal at the top of the NGT 93/95 records with those in the NGT-update records due to the low correlation of their annual signals. The drill sites need to be spaced less than one meter apart in order to perform such comparative studies or more cores are needed.

6 Results

Summary topic A:

How can the spatial distribution of accumulation rate be characterized in northern Greenland? What about temporal changes of the accumulation rate?

The derived mean snow-accumulation rates support the distribution presented by Ohmura and Reeh (1991) or Bales et al. (2001). Lowest accumulation rates are found in the northeast in the precipitation shadow of the main ice divide. The new data offers the possibility of more detailed studies. On the main divide, there are higher mean accumulation rates but also higher variability than east of it. Further, it became clear that the area of lower accumulation rates (100-150 mm/a) has to be larger than in the map of Ohmura and Reeh (1991).

From the NGT 93/95 records (ending 1994) there are no significant changes observable in the accumulation rates over the last 400 years.

Publication 1: *4.1. Snow accumulation in North Greenland over the last millennium*

Summary topic B:

What was the spatial and temporal distribution of $\delta^{18}O$ in northern Greenland over the last millennium?

The NGT 93/95 cores offered the possibility for a first detailed study of the stable-water isotope distribution in northern Greenland. A preliminary map of representative long-term mean values was made. The area of lowest mean values is east of the main ice divide, north of the summit. Higher values are found west of the main divide. The topography of the ice sheet is confirmed as a main influencing factor of the $\delta^{18}O$ spatial distribution.

The individual NGT 93/95 records are of low correlation. By stacking all the annually dated NGT 93/95 $\delta^{18}O$ records, it was possible to reduce the local noise in the low-accumulation area of northern Greenland. The stack can be interpreted as a temperature record and is representative for at least northern Greenland due to the large area covered for the first time. Global features (e.g. MCA, LIA and ETCW) as well as locally occurring events (warm period 1420 A.D.) are obvious in the stacked record. From the individual records it became clear that climate events (e.g. 1420 A.D. or ETCW) are differently strong pronounced in the different areas in northern Greenland.

Publication 2: 4.2. Spatial and temporal oxygen isotope variability in northern Greenland – implications for a new climate record over the past millennium

Publication 4: 4.4 Using ice core and weather station observations to construct a spatial map of $\delta^{18}O$ and temperature for present-day Greenland.

Summary topic C:

Is there a recent warming trend in northern Greenland?

It was for the first time possible to set the recent northern Greenlandic $\delta^{18}O$ values reliably in the context of history. The stacked and updated $\delta^{18}O$ record is representative for a larger area, at least for northern Greenland and has a higher signal-to-noise ratio, which allows for climate interpretation. Since about 1980 A.D., there has been an increase in $\delta^{18}O$ (and accumulation rate) in northern Greenland. The initiation of this warming is about 15 years later than observed from the global mean temperature but comparable with results from other Arctic records. The slope of the trend is not unusual during the last thousand years however, the reached absolute values are anomalous, and no comparable values can be found during the last millennium.

Publication 3: 4.3. The unusual recent warming trend in northern Greenland

6.1 Snow accumulation in North Greenland over the last millennium

S. Weißbach, A. Wegner and S. Kipfstuhl

Snow Accumulation in North Greenland over the Last Millennium

Stefanie Weißbach, Anna Wegner and Sepp Kipfstuhl

Abstract Knowledge of snow accumulation rates of the large polar ice sheets and their variability over time is crucial for mass budget studies and sea level predictions. Here we present mean long-term snow accumulation rates of 12 shallow ice cores drilled by the North Greenland traverse in the northern part of Greenland. The ice core records cover the last 500–1000 years. We find a trend of decreasing accumulation rate from the southwest ($\sim$180 mmWE/a) to northeast ($\sim$95 mmWE/a). Ice divide sites show higher accumulation rates but also higher variability (up to 20 %) than sites off the ice divides (less than 10 %). Unlike a recent modeling study our results indicate no change in the accumulation in the north of Greenland during the last 400 years.

1 Introduction

Polar ice sheets are unique archives of present and past climatic and environmental conditions. Ice cores drilled on the polar ice sheets provide not only extended records of the Earth's climate in the far past but give also insight into the most recent development in remote parts of the globe where instrumental records are sparse or not available at all. The polar ice sheets are not only unique paleo-archives they are also an important active component of the climate system. Changes in the accumulation rate affect the mass balance of the ice sheets but also reflect changes in the hydrological cycle and atmospheric circulation.

S. Weißbach (✉) · A. Wegner · S. Kipfstuhl
Alfred Wegener Institute Helmholtz Centre for Polar and Marine Research,
Bremerhaven, Germany
e-mail: Stefanie.Weissbach@awi.de

197

Accumulation rates in Greenland were compiled first by Ohmura and Reeh (1991). Updated maps of the accumulation rate were then presented by Ohmura et al. (1999) and Bales et al. (2001, 2009). More recently, maps of the accumulation rate or estimates of the mass balance for varying periods are produced by modeling the precipitation over Greenland using regional atmospheric circulation models (e.g. Dethloff et al. 2002; Burgess et al. 2010; Hanna et al. 2011; Box et al. 2013). Box et al. (2013) reconstructed the accumulation history over the last 400 years and find for example that the Greenland ice sheet net snow accumulation rate increased by 12 % from the end of the Little Ice Age (1840 AD).

Due to the huge dimensions of the polar ice sheets data coverage is not at all evenly distributed (e.g. Ohmura and Reeh 1991; Box et al. 2013). Until the beginning of the era of deep cores in Greenland (GRIP, GISP2, NGRIP and NEEM) at about 1990 most work focused on the central and southern parts of Greenland (e.g. NEEM community members 2013). North Greenland was only covered sparsely, mainly by the PARCA activities (e.g. Mosley-Thompson 2001) and the North Greenland Traverse (NGT). The NGT started at the Summit of the Greenland ice sheet after the GRIP ice core was completed (in summer 1993) and ended at the NGRIP drill site about 350 km northwest of Summit in summer 1996. A total of 13 deep ice cores 70–175 m long were drilled during the NGT (see Fig. 1).

In this contribution within the ESSReS-framework we present an overview of the evolution of the accumulation in North Greenland over the last 500–800 years, the first such overview for the data sparse North Greenland region. The accumulation histories are derived by carefully aligning the time scale for the 13 NGT cores by volcanic matching, and subsequently using measured density data to convert average annual layer thickness between volcanic horizons to accumulation rate estimations.

2 Methods

The lengths of the investigated ice cores and the coordinates of the drill sites are given in Table 1. An overview of their positions is given in Fig. 1.

The drill sites of cores B21–B30 (except B22) are lying on the main ice divide leading from the Summit to the Northwest and then splitting north of site B29 into a branch towards the Northeast (B23 and B21). Core B22 has been drilled in the windward side and all other cores (B16–B20) in the lee-side of the ice divides.

The Di Electric Profiling (DEP)-records of the cores which reflect the impurity content in the ice are used to date the cores. The basis of the dating is the well know pattern of volcanic events present in DEP records (Fig. 2).

The accumulation rate, given here as equivalent height of a water column (mmWE/ a), is derived from the deposited snow mass per time in a core. During the field campaign the length and weight of each single piece of core were measured. From these results and the known diameter of the cores an average density for each single piece was calculated. In the AWI cold room laboratories the density of the cores was additionally measured in millimeter resolution by γ absorption (Wilhelms 1996) or X-
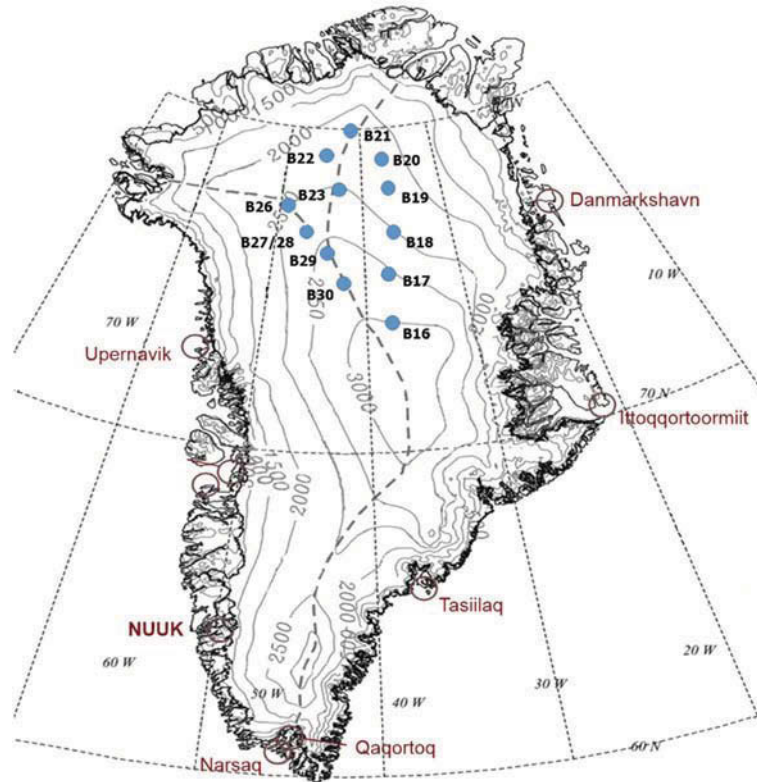
Fig. 1 Map of drill sites of the NGT cores (*blue dots*). The *dashed line* represents present ice divides whereas *solid lines* mark the surface topography

Table 1 Site information about the NGT drill locations

Core	Drill site	Core length (m)	Altitude (m)	Latitude °N	Longitude °W
B16	NGT 03	102.4	3,040	73.94	37.63
B17	NGT 06	100.8	2,820	75.25	37.63
B18	NGT 14	150.2	2,508	76.62	36.40
B19	NGT 19	150.4	2,234	78.00	36.40
B20	NGT 23	150.4	2,147	78.83	36.50
B21	NGT 27	100.6	2,185	80.00	41.14
B22	NGT 30	120.6	2,242	79.34	45.91
B23	NGT 33	150.8	2,543	78.00	44.00
B26	NGT 37	119.7	2,598	77.25	49.22
B27	NGT 39	175.0	2,733	76.66	46.82
B28	NGT 39	70.7	2,733	76.66	46.82
B29	NGT 42	110.5	2,874	76.00	43.50
B30	NGT 45	160.8	2,947	75.00	42.00
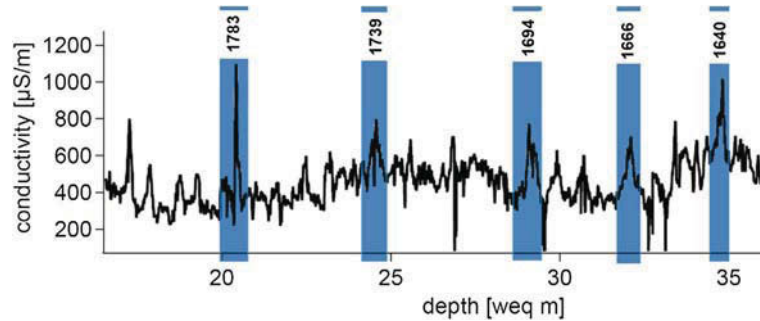
Fig. 2 Dating example. Volcanic marker horizons (*blue bars*) in the DEP record (here core B20 on water equivalent depth scale) provide ice core ages

ray imaging (Freitag et al. 2013). To account for the increase of density in the top 100 m of the ice sheet from about 300 kg/m^3 for the uppermost firn layers to the density of ice (920 kg/m^3) an exponential function was fit to the obtained density profiles.

3 Results

The mean accumulation rates at the 12 drill sites are presented in Table 2. They do not exceed 200 mmWE/a and show a west-east as well as a south-north trend (Fig. 3). The accumulation rates decrease northward from between 150 and 200 mm/a just north of the summit to less than 100 mm/a between 78°N and 79°N, and they are strongly influenced by the ice sheet topography (Fig. 3). The highest accumulation rates (180 and 176 mmWE/a) are found at the B27 and B26 drill sites on the ice divide. The cores with the lowest accumulation rates are B19 and B20 (94 and 98 mmWE/a) with the largest distance to the ice divides in the far northeast. This pattern in the accumulation results probably from a combination of factors. Besides temperature and humidity of the air the shape of the *coastline*, the topography and the inclination of the slopes west of the inland ice plateau play some role for the clouds moving on to the inland ice (Benson 1962). The moisture-

Table 2 Mean accumulation rates for North Greenland at the NGT drill sites

	B16	B17	B18	B19	B20	B21
mm/a	141	114	103	94	98	109
Period	1993–1640	1993–1479	1993–934	1993–934	1994–1179	1994–1514
	B22	B23	B26	B27	B29	B30
mm/a	145	121	176	180	149	166
Period	1994–1479	1994–1179	1995–1601	1995–1783	1995–1479	1995–1259

Given are mean values over the period from present (1993–1995) back to the time of the deepest volcanic event identified in the core
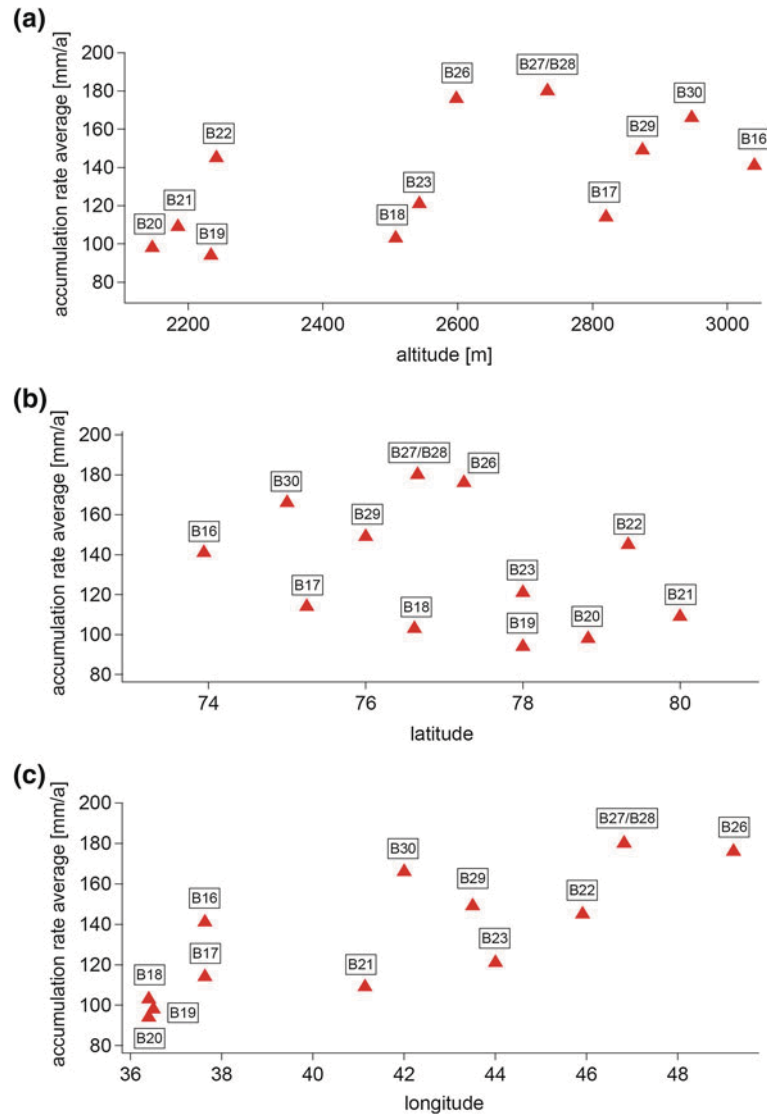
Fig. 3 Accumulation rates at NGT sites versus. **a** Altitude, **b** latitude and **c** longitude

bearing air masses come generally from the west or southwest originating in cyclones forming in the Hudson or Baffin Bay (Chen et al. 1997). They loose most moisture on the coast in front of and on the slopes to the inland ice plateau. East of the ice divide in its wind shadow and at similar or even slightly descending altitude the amount of precipitation is reduced.

Changes in the accumulation rates over the last 400–800 years are given in Table 3 and displayed in Fig. 4. Except for the 33 years lasting period between the

Table 3 Mean accumulation rates (mm/a) for periods between well dated volcanic eruptions of Tambora (1816), Laki (1783) Huyanaputina (1601), Mt. St. Helens (1479) and an unknown event at 1259

Period	B16	B17	B18	B19	B20	B21	B22	B23	B26	B27	B29	B30
1993–1816	138	115	107	95	97	110	144	121	176	174	146	168
1816–1783	148	119	107	96	93	110	154	132	190	184	161	178
1783–1601	143	114	105	95	101	109	144	121	173	171	148	166
1601–1479	142	114	105	90	103	107	144	120		172	152	169
1479–1259			101	90	98					167		161

Fields are blank, when the respective time interval was not covered by the core
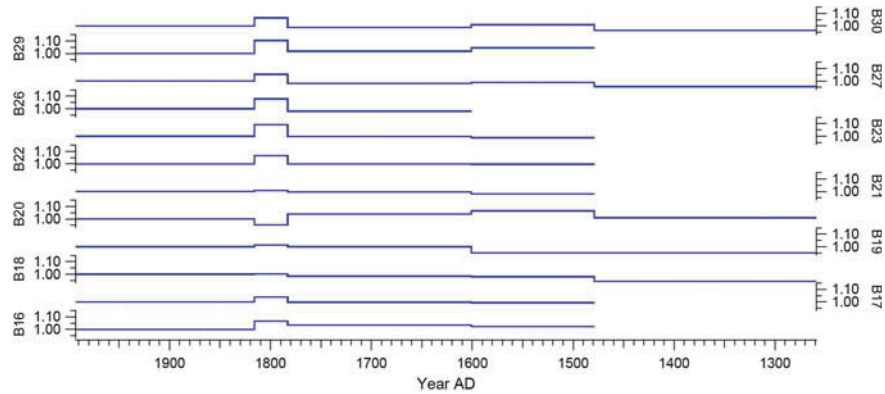
Fig. 4 Relative changes in the accumulation rates for periods between well dated volcanic eruptions (Tambora 1816; Laki 1783; Huyanaputina 1601; Mt. St. Helens 1479; unknown 1259). Reference for each core is the mean accumulation rates over the period between 1816 and present (1993–1995)

Laki and Tambora eruptions (1783–1816) the accumulation rates do not show any significant changes during the entire period of the last millennium. The changes are mostly around 1 % but never exceed 5 % relative to the mean since the Tambora eruption (1816–1993).

4 Discussion and Conclusion

The accumulation rates derived from 12 shallow ice cores in northern central Greenland indicate only little variability over the past millennium. The changes are generally less than 10 % for all sites. Except for the short period between the Laki and Tambora eruptions (1783 and 1816, respectively) the accumulation rates do not show clear trends, however, these changes may be caused by the shortness of this time period.

Our mean accumulation rates agree well with the results of Benson (1962) and Bales et al. (2009). Compared to our accumulation rates the values presented in the map of Ohmura and Reeh (1991) seem to overestimate the accumulation in central parts of North Greenland between 10 and up to more than 30 % (Fig. 5).

In future work the causes of these differences have to be investigated in more detail. They may be explained by the different interpolation techniques or differences in accumulation rates on shorter distances.

A direct comparison to the accumulation rates obtained by Box et al. (2013) is not possible as no details about regional distribution is given.
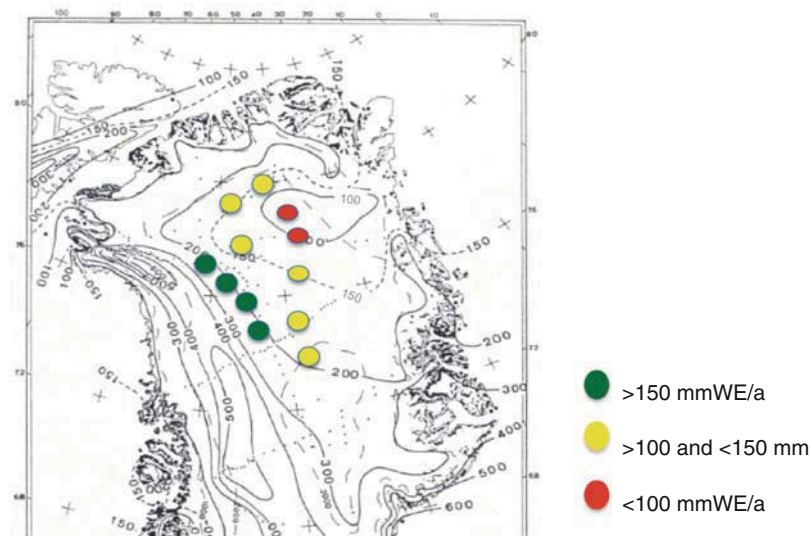
Fig. 5 Accumulation rates from NGT-cores compared to values by Ohmura and Reeh (1991). The color-coded dots represent the accumulation rates from this study, covering up to 1000 years (*red*<100 mmWE/a, *yellow*>100 and <150 mmWE/a, *green*>150 mmWE/a). The *contour line* give accumulation rates as given in Ohmura and Reeh (1991)

References

Bales RC, McConnell JR, Mosley-Thompson E, Csatho B (2001) Accumulation over the Greenland ice sheet from historical and recent records. J Geophys Res 106:33813-33826 (2001)

Bales RC, Guo Q, Shen D, McConnell JR, Du G, Burkhart JF, Spikes VB, Hanna E, Cappelen J (2009) Annual accumulation for Greenland updated using ice core data developed during 2000–2006 and analysis of daily coastal meteorological data. J Geophys Res 114:1–14

Benson CS (1962) Greenland snow pit and core stratigraphic data 1952, 1953, 1954, 1955. U.S. Army Corps Eng Snow Ice Permafrost Res 70:1-182

Box JE, Cressie N, Bromwich DH, Jung J-H, van den Broeke M, van Angelen JH, Forster RR, Miège C, Mosley-Thompson E, Vinther B, McConnell JR (2013) Greenland ice sheet mass balance reconstruction. Part I: net snow accumulation (1600–2009). J Clim 26:3919–3934

Burgess EW, Forster RR, Box JE, Mosley-Thompson E, Bromwich DH, Bales RC, Smith LC (2010) A spatially calibrated model of annual accumulation rate on the Greenland ice sheet (1958–2007). J Geophys Res Earth Surface 115:F02004

Chen QS, Bromwich DH, Bai L (1997) Precipitation over Greenland retrieved by a dynamic method and its relation to cyclonic activity. J Clim 10:839–870

Dethloff K, Schwager M, Christensen JH, Kiilsholm S, Rinke A, Dorn W, Jung-Rothenhäusler F, Fischer H, Kipfstuhl S, Miller H (2002) Recent Greenland accumulation estimated from regional climate model simulations and ice core analysis*. J Clim 15:2821–2832

Freitag J, Kipfstuhl S, Laepple T (2013) Core-scale radioscopic imaging: a new method reveals density-calcium link in Antarctic firn. J Glaciol 59:1009–1014

Hanna E, Huybrechts P, Cappelen J, Steffen K, Bales RC, Burgess E, McConnell JR, Peder Steffensen J, Van den Broeke M, Wake L, Bigg G, Griffiths M, Savas D (2011) Greenland ice

sheet surface mass balance 1870 to 2010 based on twentieth century reanalysis, and links with global climate forcing. J Geophys Res 116:D24121

Mosley-Thompson E, McConnell JR, Bales RC, Li Z, Lin P-N, Steffen K, Thompson LG, Edwards R, Bathke D (2001) Local to regional-scale variability of Greenland accumulation from PARCA cores. J Geophys Res (Atmos) 106(D24):33839–33852

NEEM community membery (2013) Eemian interglacial reconstructed from a Greenland folded ice core. Nature 493:489–494

Ohmura A, Reeh N (1991) New precipitation and accumulation maps for Greenland. J Glaciol 37:140–148

Ohmura A, Calanca P, Wild M, Anklin M (1999) Precipitation, accumulation and mass balance of the Greenland ice sheet. Zeitschrift für Gletscherkunde und Glaziologie 35(1):1–20

Wilhelms F (1996) Leitfähigkeits- und Dichtemessung an Eisbohrkernen. Berichte zur Polarforschung, Bremerhaven

6.2 Spatial and temporal oxygen isotope variability in northern Greenland – implications for a new climate record over the past millennium

S. Weißbach, A. Wegner, T. Opel, H. Oerter, B.M. Vinther, and S. Kipfstuhl

**Climate
of the Past**

Spatial and temporal oxygen isotope variability in northern Greenland – implications for a new climate record over the past millennium

S. Weißbach[1], A. Wegner[1], T. Opel[2], H. Oerter[1], B. M. Vinther[3], and S. Kipfstuhl[1]

[1]Alfred-Wegener-Institut, Helmholtz-Zentrum für Polar- und Meeresforschung, Bremerhaven, Germany
[2]Alfred-Wegener-Institut, Helmholtz-Zentrum für Polar- und Meeresforschung, Potsdam, Germany
[3]Centre for Ice and Climate, Niels Bohr Institute, University of Copenhagen, Copenhagen, Denmark

Correspondence to: S. Weißbach (stefanie.weissbach@awi.de)

Abstract. We present for the first time all 12 δ^{18}O records obtained from ice cores drilled in the framework of the North Greenland Traverse (NGT) between 1993 and 1995 in northern Greenland. The cores cover an area of 680 km × 317 km, 10 % of the Greenland ice sheet. Depending on core length (100–175 m) and accumulation rate (90–200 kg m^{-2} a^{-1}) the single records reflect an isotope–temperature history over the last 500–1100 years.

Lowest δ^{18}O mean values occur north of the summit and east of the main divide as a consequence of Greenland's topography. In general, ice cores drilled on the main ice divide show different results than those drilled east of the main ice divide that might be influenced by secondary regional moisture sources.

A stack of all NGT records and the NGRIP record is presented with improved signal-to-noise ratio. Compared to single records, this stack represents the mean δ^{18}O signal for northern Greenland that is interpreted as proxy for temperature. Our northern Greenland δ^{18}O stack indicates distinctly enriched δ^{18}O values during medieval times, about AD 1420 ± 20 and from AD 1870 onwards. The period between AD 1420 and AD 1850 has depleted δ^{18}O values compared to the average for the entire millennium and represents the Little Ice Age. The δ^{18}O values of the 20th century are comparable to the medieval period but are lower than that about AD 1420.

1 Introduction

During the past decades the Arctic has experienced a pronounced warming exceeding that of other regions (e.g., Masson-Delmotte et al., 2015). To place this warming in a historical context, a profound understanding of natural variability in past Arctic climate is essential. To do so, studying climate records is the first step. However, meteorological measurements in the Arctic are only available for relatively short time periods; only a few time series start as early as in the 19th century. Hence, proxy data from climate archives such as ice cores from the polar ice caps are essential.

Studying the climate of the past centuries allows us to compare the instrumental data with proxy records and therefore to assess the quality of the proxies for climate reconstructions.

Stable water isotopes (here δ^{18}O) in ice cores are commonly used to derive paleotemperatures (e.g., Fischer et al., 1998c; Johnsen et al., 2000; Steffensen et al., 2008). They are largely controlled by equilibrium and kinetic fractionation processes during evaporation at the ocean surface, along the poleward air-mass transport and condensation of precipitation, depending on temperature and moisture conditions (Dansgaard et al., 1969; Jouzel and Merlivat, 1984; Merlivat and Jouzel, 1979).

The isotope ratio is not only driven by local temperature but also affected by several factors like moisture sources and their proximity to the deposition site, the topography of the ice sheet and the seasonality of precipitation (Fisher et al., 1985). In addition the isotope signal is altered by

post-depositional processes like wind-induced redistribution of snow, temperature gradient metamorphism and diffusion (Johnsen et al., 2000; Pinzer et al., 2012; Steen-Larsen et al., 2014). Stacked records are used to compensate for effects due to local to regional differences and to improve the signal-to-noise ratio (Fisher et al., 1985; Masson-Delmotte et al., 2015; White et al., 1997).

To date, most ice core studies on the Greenland ice sheet have been carried out point-wise (e.g., Dye 3, GRIP, GISP2, NGRIP), which begs the question of how representative one single long ice core record is for deriving a comprehensive record of past climate. A study of ice cores from southern Greenland revealed that winter season stable water isotopes are largely influenced by the North Atlantic Oscillation (NAO) and are strongly related to southwestern Greenland air temperatures. On the other hand, summer season stable water isotope ratios show higher correlations with North Atlantic sea surface temperature conditions (Vinther et al., 2010). In particular, northern Greenland has been little investigated so far. The summit in Greenland's center is the highest site and separates Greenland into a northern and southern part. Northern Greenland differs significantly from the south in terms of lower air temperatures and lower snow accumulation rates (Fischer et al., 1998c). Thus, the results from southern Greenland are not directly transferable to the northern part.

Northern Greenland's climate is influenced by different effects than the southern part. One example is the NAO effect, which is present in the southern and western part of Greenland and is discussed to be reduced in northern Greenland (Appenzeller et al., 1998).

The cyclones causing the precipitation over northern Greenland originate in the Baffin Bay and bring dry and cold air masses from the central Arctic to northern Greenland (Chen et al., 1997).

The dominant westerly winds are blocked by the ice divide, while the northeastern part has very low accumulation rates below $100 \, \text{kg} \, \text{m}^{-1} \, \text{a}^{-1}$.

The topographic situation in northern Greenland is special for δ^{18}O studies. In northern Greenland going northward also means to go downward (lower altitudes).

For a correct estimate of mass balances as well as the response to the ongoing climate change, knowledge of accumulation rates and the spatial distribution of δ^{18}O as a temperature proxy is important for the entire Greenland ice sheet. However, due to northern Greenland's remoteness its recent past climate has, up to now, been only scarcely investigated.

Even in the 1990s little was known about northern Greenland. Only few studies had been performed before the Alfred Wegener Institute's (AWI) North Greenland Traverse (NGT) started in 1993. There had been a traverse by Koch and Wegener in 1913 (Koch and Wegener, 1930) and one by Benson in 1952–1953 (Benson, 1962), and there was the British North Greenland Expedition in 1958 (Bull, 1958), which studied the accumulation rate in northern Greenland. How-

ever, there had been no stable water isotope studies in the central part of northern Greenland. Fischer et al. (1998c) and (Schwager, 2000) present the first results from δ^{18}O values of some of the NGT records.

Using the updated accumulation rates of the (compared to Friedmann et al., 1995; Schwager, 2000) NGT, it was possible to show that the area of lower accumulation rates is much larger than expected before, which has an influence on the outlet glaciers (Weißbach et al., 2015).

The NGT ice cores offer, for the first time, the possibility to study the spatial and temporal variability in stable oxygen isotope records from northern Greenland. Furthermore, they allow the analysis of the common spatial stable water isotope signal in northern Greenland by stacking the individual records to significantly reduce the isotopic noise that is present in a single record due to local peculiarities.

The main objectives of this study are (1) to investigate the spatial variability in δ^{18}O in northern Greenland using this new set of δ^{18}O data and to evaluate the influence of isotopic noise on a single record, (2) to assess whether stable water isotope records from sites with low accumulation rates can be interpreted as climate signals, (3) to present a new robust stacked δ^{18}O record for northern Greenland covering the past millennium, and (4) to interpret this record in terms of paleoclimate with respect to temporal variability and relation to large-scale climate information from other proxy records.

2　Material and methods

The ice cores presented here were drilled during the NGT from 1993 to 1995. In total, 13 ice cores (B16-B23, B26-B30) from 12 different sites (Table 1, Fig. 1) were drilled along the traverse route. The ice cores cover the last 500–1000 years. The drillings were accompanied by extensive surface snow studies (e.g., Schwager, 2000).

B21 and B23 as well as B26 to B30 are located on ice divides (Fig. 1), while B16–B20 were drilled east of the main ice divide. The NGRIP core (North Greenland Ice Core Project Members, 2004) was drilled 14.5 km northwest of B30 following the main ice divide and is therefore included in this study.

Before analyzing the stable water isotopes, a density profile of each core was measured. To do so, the single core segments (approximately 1 m long) were weighed in the field. Additional higher-depth-resolution density records were determined using gamma-absorption measurements in the AWI cold lab (Wilhelms, 1996). Finally, in 2012, density of the first 70 m of the three cores B19, B22 and B30 was analyzed by X-ray computer tomography (X-CT; Freitag et al., 2013).

An exponential function fitted to the data taking into account all three types of density data with same respect was used to calculate water equivalent (w.e.) accumulation rates and to synchronize the cores.

Table 1. Overview of all NGT drill sites.

Core	Core length	Elevation	Geographic position	
ID	(m)	(m a.s.l.)	Latitude (° N)	Longitude (° W)
B16	102.4	3040	73.94	37.63
B17	100.8	2820	75.25	37.63
B18	150.2	2508	76.62	36.40
B19	150.4	2234	78.00	36.40
B20	150.4	2147	78.83	36.50
B21	100.6	2185	80.00	41.14
B22	120.6	2242	79.34	45.91
B23	150.8	2543	78.00	44.00
B26	119.7	2598	77.25	49.22
B27	175.0	2733	76.66	46.82
B28	70.7	2733	76.66	46.82
B29	110.5	2874	76.00	43.50
B30	160.8	2947	75.00	42.00

Selected parts of B30 were also analyzed for electrolytic conductivity using high-resolution continuous-flow analysis (Kaufmann et al., 2008).

For the isotopic measurements the ice was cut into samples of 1–5 cm depth resolution, corresponding to 2–10 samples per year. Most of the ice was sampled with 2–2.5 cm depth resolution. Only at the uppermost parts of the core were samples cut with lower depth resolution (up to 5 cm). For some meters of special interest a resolution of 1 cm was used. After melting, $\delta^{18}O$ was determined using Delta E and S mass spectrometers from Finnigan MAT in the AWI laboratory with uncertainties less than 0.1 ‰ as determined from long-term measurements. Cores B27 and B28 were drilled at the same site. Parts of core B27 (8.25–11.38 m w.e.), corresponding to AD 1926–1945) were lost, and these were replaced by the record from B28. For the other parts, the mean of both dated cores was calculated to generate one isotope record for this site.

Six of the NGT cores (B16, B18, B20, B21, B26 and B29) were already dated up to a certain depth by annual layer counting (using density, major ions or $\delta^{18}O$) in prior studies (e.g., Fischer and Mieding, 2005; Fischer et al., 1998a, b; Schwager, 2000). Depending on the availability of data and differences in snow accumulation rates the dating quality of these cores varies between 1- and 5-year accuracy. For the other NGT cores annual layer counting was not possible due to the very low accumulation rates ($< 100\,kg\,m^{-2}\,a^{-1}$). To achieve the same dating quality for all NGT cores for better comparison and to apply the dating on the whole core length, we used a new dating procedure for all cores. From density-corrected (w.e.) high-resolution electrical conductivity profiles (Werner, 1995; Wilhelms, 1996) and SO_4^{2-}-concentration profiles for B16, B18, B21 (Fischer et al., 1998a, b), B20 (Bigler et al., 2002) and an electrolytic conductivity profile (B30), distinct volcanic horizons were iden-
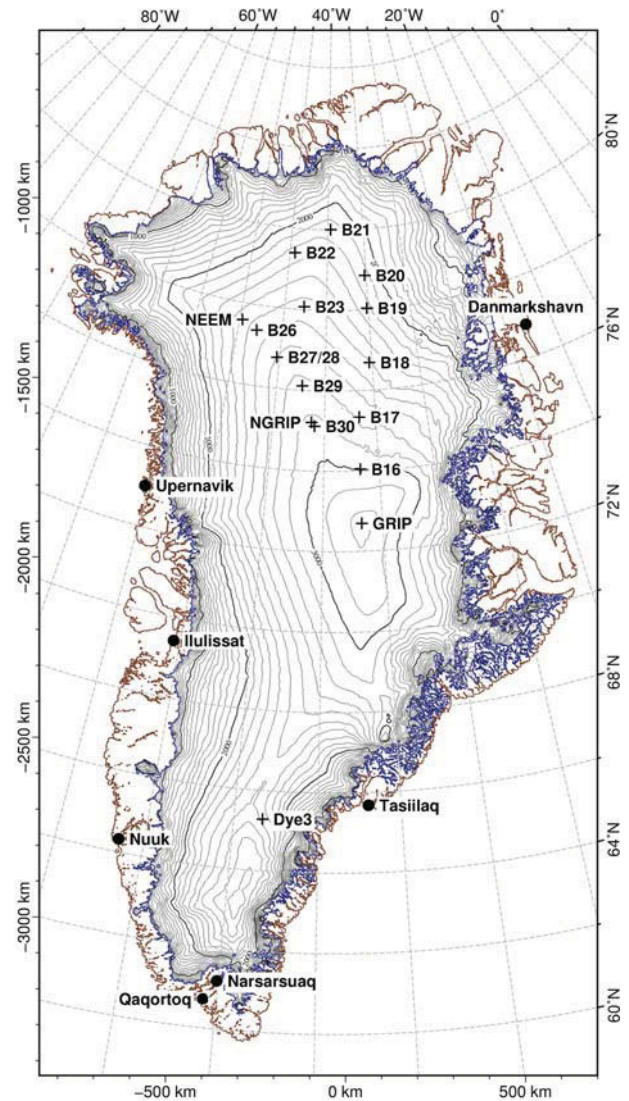
Figure 1. Map of Greenland with NGT ice cores (B16–B23, B26–B30 crosses), deep drilling sites (crosses) and towns (black dots). The ice surface topography is according to Bamber et al. (2013), (mapping: Polar Stereographic (WGS84), Standard Parallel 71, Latitude of Projection Origin −39).

tified and used as match points to synchronize the cores (Table 2). Some of the volcanic eruptions show a more pronounced signal in the Greenlandic ice than others. Thus not all eruptions could be identified in every record.

Between match points, the annual dating was assigned assuming a constant snow accumulation rate. If a volcanic match point could not be clearly identified in an ice core, the next time marker was used to calculate the mean accumulation rate. Below the deepest volcanic match point, the last calculated accumulation rate was extrapolated until the end of the core. As the cores were drilled only in the upper part of the ice sheet (up to 100–175 m depths), layer thinning was not taken into account.

- 51 -

Table 2. Depth of volcanic horizons used for dating. The given year is the time of aerosol deposition on the Greenland ice sheet. All depths are given in meter water equivalent. If a horizon could not be clearly identified a dash is shown in the table. A field is empty if the horizon is deeper than the length of the ice core. The maximum difference is estimated from a comparison between cores dated by annual layer counting (Mieding, 2005; Schwager, 2000) and the dating used for this study. Also given are the volcanic explosivity index (VEI; Newhall and Self, 1982) and the total Northern Hemisphere stratospheric sulfate aerosol injection (Gao et al., 2008) for each volcanic eruption used.

Year [AD]	Event	B16	B17	B18	B19	B20	B21	B22	B23	B26	B27	B28	B29	B30	VEI	Sulfate
1912	Katmai*	11.60	9.31	8.48	7.38	7.86	8.62	11.56	9.49	14.27	13.69	14.44	11.41	13.12	6	11.0
1816	Tambora*	24.49	20.27	18.91	16.77	17.27	19.46	26.17	21.54	31.50	31.13	31.91	25.97	29.91	7	58.7
1783	Laki*	29.36	24.19	22.45	19.94	20.32	23.10	31.25	25.93	37.77	37.19	38.07	31.28	35.80	4	93.0
1739	Tarumai*	35.52	–	26.90	24.10	24.62	–	–	–	–	–		–	43.07	5	0
1694	Hekla**	–	34.47	31.84	28.54	29.16	32.87	44.06	–	–	–		44.22	50.45	4	0
1666	Unknown**	46.22	–	34.75	31.20	32.10	35.93	48.13	–	–	–		48.50	–		0
1640	Komagatake**	49.90	–	37.48	33.69	34.80	–	–	–	–	–		52.36	–	4	33.8
1601	Huaynaputina*		44.97	41.62	–	38.70	42.95	–	48.31	69.22	68.39		58.25	65.94	4	46.1
1479	Mt. St. Helens**		58.84	54.42	–	51.31	56.04	75.09	–		89.42		76.81	86.60		7.4
1259	Samalas*			76.60	68.03	72.86			89.35		126.10			122.10		145.8
1179	Katla*			–	–	80.04			98.60							0
934	Eldgjá*			109.20	99.20											0
Max. age of core [AD]		1470	1363	874	753	775	1372	1372	1023	1505	1195	1763	1471	1242		
Max. difference [a]		7		3		8	6			4			3			

* Sigl et al. (2013); ** Friedmann et al. (1995).

3 Results and discussion

3.1 Depth–age models and snow accumulation rates

The last millennium was a volcanically active time (Sigl et al., 2013). The volcanic aerosols deposited on the Greenland ice sheet can be used as time markers. The depths of peaks in conductivity and sulfate concentration attributed to certain volcanic horizons are given in Table 2 as used for our dating approach.

During the last 500 years, the time period between two detectable eruptions at NGT sites does not exceed 100 years for any of the cores. This leads to a dating uncertainty for each core of smaller than 10 years compared to the annually counted timescales (Mieding, 2005; Schwager, 2000), which is minimal at the matching points. The three youngest volcanic reference horizons (Katmai, Tambora and Laki) and the eruptions from AD 1257 (Samalas; Lavigne et al., 2013) and AD 934 (Eldgjá) were found in all cores, whereas the other eruptions could not be clearly identified in every ice core. We could not find a common pattern (e.g., distance, strength of the eruption) regarding whether or not volcanic horizons could be observed in all records.

This already indicates a high spatial variability within the study region related to significant influences of local to regional peculiarities (e.g., wind drift or sastrugi formation). An overview of the resulting mean accumulation rates for the entire core lengths for all NGT drilling sites, as well as the respective ranges, is given in Table 3. According to our dating, the cores reaching furthest back in time are B18, B19 and B20, covering more than the last 1000 years. These northeasterly cores have the lowest accumulation rates with values below $100 \, \text{kg m}^{-2} \, \text{a}^{-1}$ (B19: $94 \, \text{kg m}^{-2} \, \text{a}^{-1}$; B20: $98 \, \text{kg m}^{-2} \, \text{a}^{-1}$), whereas the highest mean accumulation rate is found for B27/28 in the southwest of our study region with

$180 \, \text{kg m}^{-2} \, \text{a}^{-1}$. Generally, the accumulation rate decreases from the sites located on the main ice divide in the southwest of the study area to the northeast.

The observed range of accumulation at one single site is highest for the southwestern cores (B30 and B29) ranging between 137 and $161 \, \text{kg m}^{-2} \, \text{a}^{-1}$ (B29). Lowest values are found for the cores east of the main ice divide (e.g., B17, B18 and B19) ranging between 113 and $119 \, \text{kg m}^{-2} \, \text{a}^{-1}$ (B17).

The length of the records varies depending on accumulation rate and total length of the core. The longest records are from B19 (back to AD 753) and B20 (back to AD 775). The following comparisons of the individual records refer to the longest common time frame (AD 1505–1953). Although diffusion is known to change isotopic values in the snow, in this study the data were not corrected for diffusion effects. While diffusion length is in the range of annual layer thickness, diffusion might be affecting the absolute difference in isotope content of neighboring years, but the mean over 11 or 30 years will not be affected.

3.2 Regional variability in $\delta^{18}\text{O}$ in northern Greenland

Annual mean $\delta^{18}\text{O}$ records of the NGT cores are displayed in Fig. 2. Table 4 summarizes the main $\delta^{18}\text{O}$ characteristics of each core.

The lowest mean $\delta^{18}\text{O}$ values ($\sim -37\text{‰}$) in northern Greenland (B16–B18) and possibly the lowest in Greenland are found east of the main ice divide and north of the summit, but not at the summit as might be expected. Also, the lowest firn temperatures were measured at B160–B18 (Table 4). This is in contrast to the findings of Ohmura (1987), who suggested temperatures similar to the summit for this region.

- 52 -

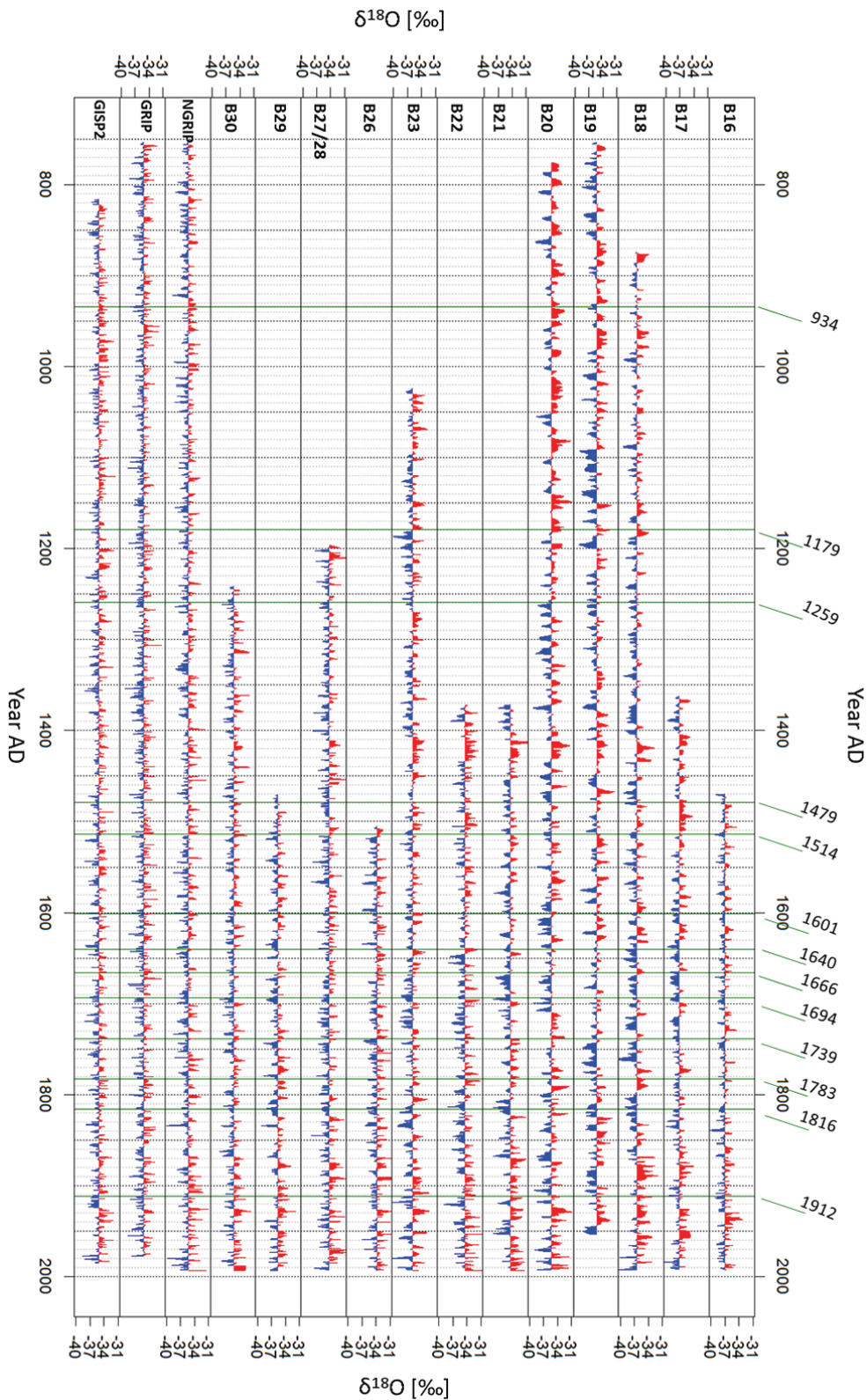**Figure 2.** Annual δ^{18}O records at the 12 NGT sites (this study) and NGRIP (Vinther et al., 2006b), GRIP (Vinther et al., 2010) and GISP2 (Grootes and Stuiver, 1997). Blue values are those below the mean over their common time frame (AD 1505–1953) and red are the higher ones. Dark-green vertical lines mark the volcanic eruptions (years given at top) used as time markers.

Table 3. Resulting mean accumulation rates (from the surface to the deepest volcanic horizon and in brackets for their common time frame (AD 1505–1953)) for each NGT drill site, the lowest and highest rate within the whole core length, the time period from surface to the deepest volcanic horizon, and the age at the bottom of the ice core calculated by extrapolation of the deepest calculated accumulation rate.

Core	Mean accumulation rate [kg m^{-2} a^{-1}]	Accumulation rate range [kg m^{-2} a^{-1}]	Time period [AD]	Age at bottom of core [AD]
B16	141 [141]	134–148	1640–1993	1470
B17	114 [114]	113–119	1479–1993	1363
B18	103 [106]	100–110	934–1993	874
B19	94 [94]	90–99	934–1993	753
B20	98 [100]	90–105	1179–1994	775
B21	109 [109]	105–113	1479–1994	1372
B22	145 [145]	141–154	1479–1994	1372
B23	121 [122]	116–132	1179–1994	1023
B26	176 [176]	172–190	1601–1995	1505
B27/B28	180 [181]	165–187	1783–1995	1195
B29	149 [150]	137–161	1479–1995	1471
B30	166 [169]	158–178	1259–1995	1242

Table 4. The 15 m firn temperature, mean annual δ^{18}O values for each ice core, the range of the highest and lowest δ^{18}O values and the year they occurred as well as the standard deviation (SD) all given for their common time frame (AD 1953–1505).

Core	15 m firn temperature [°C]	Mean δ^{18}O [‰]	δ^{18}O range [‰]	Years [AD] of lowest/highest value	SD δ^{18}O [‰]	Time period [AD] (whole core length)
B16	−32.5***	−37.07	−40.64 to −33.11	1839/1937	0.99	1470–1993
B17	−32.3***	−37.13	−40.06 to −33.89	1835/1879	1.08	1363-1993
B18	−32.3***	−36.53	−41.52 to −31.75	1761/1889	1.44	874–1993
B19	−30.9 (±0.5)**	−35.49	−38.97 to −31.77	1575/1826	1.32	753–1953
B20	−30.4***	−35.41	−39.34 to −30.69	1699/1929	1.42	775–1994
B21	−30.1***	−34.53	−38.29 to −30.95	1814/1871	1.29	1372-1994
B22	−29.8***	−34.54	−39.11 to −29.84	1921/1953	1.34	1372–1994
B23	−29.3 (±0.5)**	−35.98	−42.11 to −32.23	1918/1928	1.28	1023–1994
B26	−30.3***	−33.86	−37.22 to −29.42	1597/1893	1.25	1505–1995
B27/B28	−30.6 (±0.5)**	−34.47	−38.26 to −30.58	1566/1892	1.25	1195–1995
B29	−31.6 (±0.5)**	−35.65	−39.22 to −31.59	1834/1928	1.18	1471–1995
B30	−31.8 (±0.5)**	−35.46	−38.53 to −31.52	1862/1928	1.09	1242–1988
NGRIP*		−35.42	−40.12 to −30.81	1836/1928	1.24	

* Vinther et al. (2006b); ** Schwager (2000); *** interpolated from Schwager (2000).

Generally, the cores located east of the main ice divide show lower mean δ^{18}O values than those located on the ice divide (Fig. 3a). For instance, B29 and B30 are at similar altitudes and latitudes to B16 and B17 but show significantly higher values (Fig. 3a).

Figure 4 indicates that accumulation, latitude and altitude may have a minor impact on the δ^{18}O values here. One possible explanation would be additional moisture isotopically depleted during the transport from directions farther north.

The cores more to the north (B19–B22) were drilled at lower altitude and therefore record different climate signals (i.e., from lower air masses) compared to the high-altitude ice cores that, in turn, record a more smoothed signal of higher atmospheric layers. Similar effects were observed, for exam-

ple, in Svalbard (Isaksson et al., 2005), even though at considerably lower altitudes compared to Greenland.

The maximum difference in mean δ^{18}O values of individual ice cores is 3.3 ‰ (highest mean δ^{18}O in B26: −33.86 ‰; lowest mean δ^{18}O in B17: −37.13 ‰). The standard deviation (SD) for the annual mean values within each core in the common time frame (AD 1505–1953) is lowest for B16 (0.99 ‰) and highest for B18 (1.44 ‰). We found no general relation between accumulation rate and standard deviation of the δ^{18}O values for all individual cores, even though the northern cores with generally lower accumulation rates show higher standard deviations than the southern cores.

The correlation coefficients between the annual δ^{18}O records of individual ice cores are relatively small ($r = 0.1$ to 0.36, $p < 0.05$). This can be partly explained by the fact
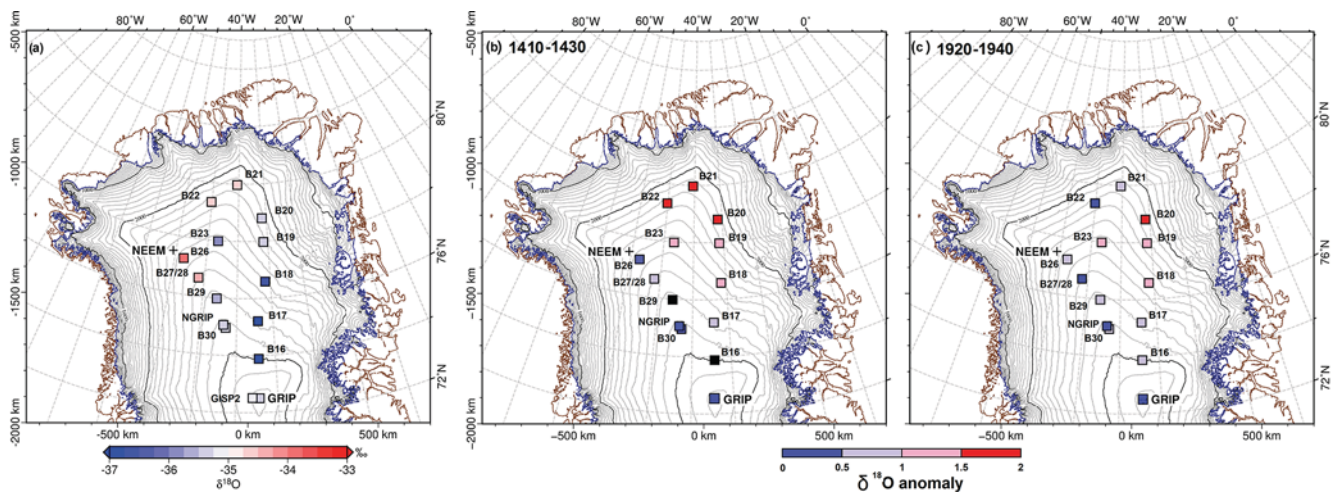
Figure 3. Spatial distribution of δ^{18}O values in northern Greenland. **(a)** The mean δ^{18}O values of the northern Greenland ice cores in their common time frame (AD 1505–1953) are shown with color-coded squares. Blue colors represent lower values and red colors higher values. Mapped mean anomalies of δ^{18}O compared to **(a)** for two different periods: **(b)** AD 1410–1430 and **(c)** AD 1920–1940. If a record does not cover the required time period the square is filled in black.

that the 13 northern Greenland (NG) drilling sites (12 NGT and NGRIP) are up to 680 km apart from each other. In other studies where correlated cores are drilled closer together, at one drill site, higher correlation coefficients were found (e.g., at GRIP $r = 0.41$–0.55 – White et al., 1997; or at NEEM $r \sim 0.54$ – Masson-Delmotte et al., 2015). The strongest correlations are found for the cores from the southwest (B26–B30) and the lowest for those from the northeast (B19, B20). There is a significant linear relationship between the distance between the core sites and their annual δ^{18}O correlation coefficient ($r = -0.44$, $p < 0.05$). However, it is not always true that the cores with smallest distance between them have the highest correlations.

For smoothed values (11-year running mean) the correlation coefficients between the δ^{18}O records are only slightly higher. Only 50 % of the combinations have coefficients higher than 0.3, and 14 % are lower than 0.1. This indicates an important influence of regional site-to-site differences. Variability in δ^{18}O is dependent on local (e.g., wind), regional (e.g., position on the ice sheet) and large-scale (e.g., circulation patterns) processes. Even adjacent cores may differ considerably according to snow drift (Fisher et al., 1985). One further reason for the rather low correlations may be attributed to dating uncertainties.

From Fig. 2, we compare our individual NGT δ^{18}O records to other published central to northern Greenland (GRIP, GISP2, NGRIP) δ^{18}O time series. Prominent decadal-scale maxima and minima occurred mostly isochronally. However, specific events such as warm periods around AD 1420 or AD 1920–1930 or a cold period in the 17th century are more pronounced in the NGT cores compared to summit records.

In Fig. 2 is also obvious that some records show faster changes between warmer and colder events (e.g., GRIP, B30

and B26), while others (e.g., B17–B21) remain longer at values higher or lower than their mean (Fig. 2). The longest warm period (compared to the mean of whole core length) is found in B19 (with 37 subsequent years warmer than the mean), while B17 has the longest cold period (28 subsequent years colder than mean). GRIP, B26, and B27/28 show a higher frequency with a maximum of about 10 subsequent warmer or colder years. A frequency analysis of 11-year running mean smoothed data supports these findings. B18–B21 and B29 show much longer main periods (117–248 a) than B16–B17 and B22–B30 (besides B29, 81–39 a).

In general, the first half of the last millennium was characterized by longer warm or cold anomalies than the second half and records with more rapid fluctuations are from the summit and the main ice divide, while those cores drilled east of the divide have longer periods of positive or negative anomalies. We conclude that, east of the divide, the climate conditions are not as variable and therefore the annual δ^{18}O signal is of greater persistence.

The east-to-west difference is also expressed by the dependency of δ^{18}O values on longitude (Fig. 4). This is in line with results from Box (2002), who found that there is often an opposite trend in air temperatures in east and west Greenland. The antiphase of temperature records from east and west Greenland is possibly explained by the importance of different weather regimes (e.g., Ortega et al., 2014).

The range in δ^{18}O in the different cores is different, too. Cores drilled in the northeast that are characterized by the lowest accumulation rates have the highest standard deviations (SD) in δ^{18}O, which can be partly explained by the fact that a smaller number of accumulation events scatter more easily.
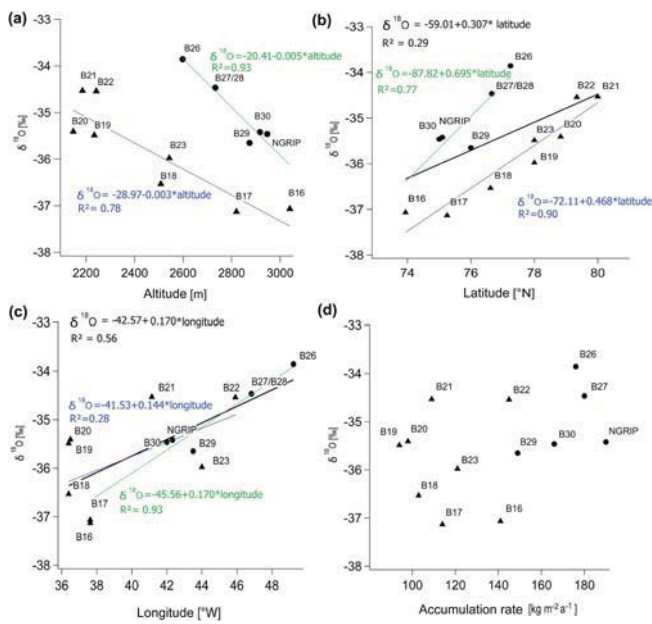
Figure 4. Mean δ^{18}O (AD 1505–1953) as a function of **(a)** altitude, **(b)** latitude, **(c)** longitude and **(d)** accumulation rate of northern Greenland ice core drill sites. Cores with higher accumulation rates (> 145 kg m^{-2} a^{-1}) are given as black dots and lower rates as black triangles, which is similar to the differentiation between east of and on the main ice divide. For statistically significant correlations the lines give the linear regression functions (black: mean; green: higher accumulation rates; blue: lower accumulation rates).

We investigated the relationship between the altitude, latitude and longitude of the drilling sites and the mean δ^{18}O values (Fig. 4a, b, c), which are, when considering all records, statistically significant ($p < 0.05$) only for longitude and latitude. Regarding their snow accumulation rate we differentiate between two groups: (i) cores with accumulation rates lower than 145 kg m^{-2} a^{-1} mainly located east of the main ice divide (B16–B21 and B23) and (ii) cores with higher accumulation rates (B22, B26–B30 and NGRIP). We find higher δ^{18}O ratios for sites with higher accumulation rates (Fig. 4d). The relationship is weak but becomes stronger for higher accumulation rates. Buchardt et al. (2012) noted that the relationship between accumulation rate and δ^{18}O is not distinct for Greenland. Furthermore, Buchardt et al. (2012) found that the sensitivity of δ^{18}O changes to accumulation rate is smallest in northeastern Greenland (North Central and North 1972), which is in agreement with our findings.

Among the factors influencing the mean isotopic composition, longitude has the strongest impact ($R^2 = 0.56$), which becomes clearest when looking only at the data of group I ($R^2 = 0.93$). Figure 4c shows the clear east-to-west gradient in the mean δ^{18}O values in northern Greenland.

If separating between group I ("East") and group II ("Divide") there is a strong altitude effect ($R^2 = 0.93$ and 0.78) in the data, too.

These patterns may be explained by different atmospheric circulation conditions allowing additional moisture from other sources to reach the region east of the ice divide. This is supported by the finding of Friedmann et al. (1995), who suppose, based on data from B16 to B19, that northeastern Greenland receives more moisture from local sources as the Greenland Sea, Atlantic Ocean and the Canadian wetlands, in particular during summer.

We found lower δ^{18}O values in the southern and eastern part of northern Greenland in contrast to the general ideas of Dansgaard (1954), who expected lower values northward. That we do not find the lowest values north is a consequence of different factors in northern Greenland that balance each other out. More to the north, where we would expect lower δ^{18}O values, the altitude in northern Greenland is decreasing, which causes higher δ^{18}O values (Fig. 1). A multiple linear regression becomes necessary, as Johnsen et al. (1989) did before.

Applying this approach to our data, we find $\delta(\delta^{18}\text{O})/(\delta(\text{latitude}) = -0.30$ (± 0.40) ‰ degree^{-1} and $\delta(\delta^{18}\text{O})/\delta(\text{altitude}) = -0.0035$ (± 0.0024) ‰ m^{-1}. The regression residuals are linearly related to longitude as well as accumulation rate.

In general, we found correlations with altitude, latitude and longitude, but the balancing-out effects because of the special topography in northern Greenland have to be taken into account.

To study the regional-scale patterns of common variability in all annual δ^{18}O records, we performed a principal component analysis (PCA). All calculations are done for the largest common time frame of all cores (AD 1505–1953). Other time periods were used as well, and they show similar results.

Only the first two principal components (PC1 and PC2) are above the noise level. The first two eigenvectors of the isotopic time series explain 34.1 % of the total variance (PC1: 21.8 %; PC2: 12.3 %). PC1 is similar to the mean of all records ($r = 0.97$, $p \ll 0.01$). It was not possible to assign PC2 to any climatic relevant signal. The other PCs are dominant in one or two records but are not significant for the total variance of the entire data set. The loading patterns show a homogeneous pattern for EOF1 and a bipolar (west–east) result for EOF2.

To summarize, the spatial differences in mean δ^{18}O values in northern Greenland can be largely explained by the influence of the topography of the ice sheet on the regional climate system. The main ice divide influences the pathways of air masses, causing lower accumulation rates in the east.

We assume that the temporal variability in a stacked NG δ^{18}O record represents past temperature development.

3.3 The northern Greenland δ^{18}O stack and its paleoclimatic significance

Stable water isotope ratios in ice are widely used as a proxy for air temperature (Dansgaard, 1964; Johnsen et al.,

1995; Jouzel et al., 1997b). The comparison to direct air-temperature observation data and proxy data allows for assessment of the quality of the proxy in terms of paleoclimatological interpretation.

To reduce the noise in the single $\delta^{18}O$ records, we calculated a stacked record by averaging the 13 annual NG $\delta^{18}O$ records in their overlapping time periods (NG stack, Fig. 5). Before stacking, all records were centered and normalized regarding their common time frame (AD 1505–1953). The SD of the NG stack (0.44 for AD 1505–1953) is less than half of the SD in annual $\delta^{18}O$ records of the individual cores. Vinther et al. (2010) also point out that stacking is important to improve the signal-to-noise ratio in areas with low accumulation rate. Local drift noise accounts for half of the total variance in single-site annual series (Fisher et al., 1985). As the NG stack before AD 1000 is based on only four records (< 25 % of the total core numbers), we decided to focus in the following only on the time period after AD 1000.

As the NG stack is a result of 13 ice cores over a large area, we assume it is regionally representative.

To investigate the relationship of the NG stack with air temperature, we used monthly meteorological observations from coastal southwestern Greenland sites and Stykkishólmur in northwestern Iceland available from the Danish Meteorological Institute (DMI; http://www.dmi.dk; AD 1784–1993) and the Icelandic Met Office (http://en.vedur.is/; back to AD 1830), respectively. We selected only the Greenlandic temperature records longer than 200 years for our study even though they are at a large distance to the NGT drill sites (706–2206 km).

The correlation coefficients between the NG stack and these air-temperature records are shown in Table 5. Dating uncertainties are taken into account by comparing 5-year running means. The NG stack shows low but significant ($p < 0.001$) correlations with the air temperatures at all sites (Table 5).

The strongest correlation with annual mean temperature was found for the merged station data at Greenland's southeast coast ($r = 0.51$), and the temperature reconstruction for the North Atlantic Arctic boundary region of Wood et al. (2010) ($r = 0.55$); the lowest was also found for Qaqortoq ($r = 0.39$) in the south of Greenland (Table 5). For Stykkishólmur the correlation is in the range of the Greenlandic ones ($r = 0.41$). Slightly higher correlations are obtained by comparing the NG stack to seasonal data. Except for Ilulissat, winter months (DJF) show weaker correlations; spring (MAM) and summer (JJA) months show stronger correlations with the NG stack.

Comparably low correlations between annual $\delta^{18}O$ means and measured temperatures from coastal stations are also reported for the NEEM record (Steen-Larsen et al., 2011).

However, the rather low correlation coefficients might underestimate the real regional $\delta^{18}O$–temperature relations because of different reasons.

We expect that the most important reasons are the large distances and the difference in altitude (i.e., more than 2000 m) between drill sites and the meteorological stations, which cause them to receive different atmospheric signals. The stations are located at the coast and are in turn also likely influenced by local factors such as the occurrence of sea ice.

One other aspect might be seasonality, as argued by Steen-Larsen et al. (2011) for the NEEM site. The snowfall in northern Greenland may be unevenly distributed seasonally. However, it is not possible to generate sub-annual data for northern Greenland ice cores due to low accumulation rates. We find a tendency towards stronger correlation between the annual $\delta^{18}O$ and summer (JJA, $r = 0.35$–0.51) and spring (MAM, $r = 0.36$–0.62) temperatures for most of the stations. This points to a higher proportion of summer snow in the annual accumulation in northern Greenland, too. SON has slightly weaker correlation coefficients ($r = 0.31$–0.5), while DJF is only significant for Ilulissat and the merged southern station.

In addition, regional noise factors such as wind drift and sastrugi formation as well as uncertainties in ice core dating and the usage of very old observation data have to be taken into account.

In summary, we consider the northern Greenland $\delta^{18}O$ stacked record as a reliable proxy for annual temperature for northern Greenland. The regional representativeness of the NG stack is supported by the general similarity to the NEEM $\delta^{18}O$ record (Masson-Delmotte et al., 2015) for the period AD 1724–1994. We found a strong correlation between both records ($r = 0.83$ for 30-year running mean). Even single events such as the highest values in AD 1928 and the AD 1810–1830 cooling occur in both records.

Although the NG stack record shows some correlation with temperature data from coastal Greenland sites, it remains an open question as to how the NG stack $\delta^{18}O$ variations can be converted into absolute temperature changes within northeastern Greenland during the last millennium. In the past, such conversion of isotopic time series of Greenland ice cores was based on a modern analogue approach taking the observed spatial isotope–temperature gradient of $0.67 \pm 0.2\,‰\,°C^{-1}$ (Dansgaard, 1964; Johnsen et al., 1989) as a valid calibration for converting isotope records of Greenland ice cores into temperature changes (e.g., Grootes et al., 1993). The strong confidence of glaciologists in this approach came principally from two observations. (1) Over both polar ice sheets, the spatial correlation between modern isotope and annual mean temperature is very high and significant. (2) This empirical observation was theoretically understood as a consequence of a Rayleigh rainout system controlling the isotopic composition of meteoric water.

However, for the Greenland area this long-accepted approach has been challenged during the last decade. Two entirely independent analytic techniques, one based on the numerical interpretation of borehole temperatures (e.g., Dahl-Jensen et al., 1998) and the other based on the occlusion pro-
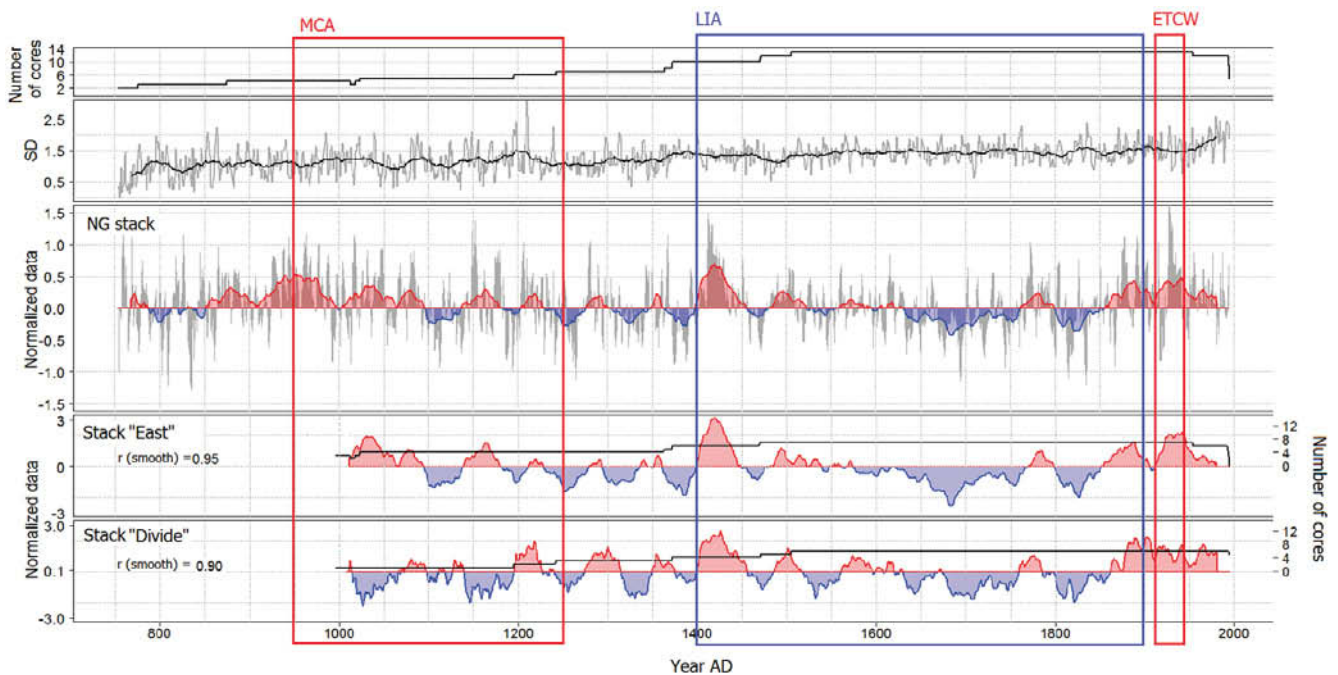
Figure 5. Top two panels: the number of cores used for the stack and the standard deviation (SD; gray: annual values; black: 30-year running mean) of all times. Middle: annual stacked $\delta^{18}O$ (gray) and smoothed record (30-year running mean). Values more enriched compared to the mean (AD 1953–1505) are shown in red, while values less enriched are shown in blue. Known climate anomalies are marked: Medieval Climate Anomaly (MCA, AD 950–1250; Mann et al., 2009), the Little Ice Age (LIA, AD 1400–1900; Mann et al., 1998), and early twentieth century warming (ETCW, 1920–1940; Semenov and Latif, 2012; Wood and Overland, 2010). Bottom two panels: 30-year running mean on z levels (centered and normalized data) of stacked northern Greenland $\delta^{18}O$ records over the last 1000 years. Stack "East": B16, B17, B18, B19, B20, B21 and B23. Stack "Divide": B22, B26, B27, B29, B30 and NGRIP. Values in red are more enriched compared to the mean over their last 1000 years, and those in blue are less enriched. Also given is the correlation coefficient of 30-year running means between the NG stack and the sub-stacks (AD 1505–1993). The coefficient for a similar correlation between the two sub-stacks is calculated with $r = 0.71$.

cess of gases into the ice (e.g., Buizert et al., 2014; Severinghaus et al., 1998), allow for a direct temperature reconstruction at least for some periods of the past. In agreement with this, both methods point to much lower temporal $\delta^{18}O\,T^{-1}$ slopes ranging between 0.4 and 0.3 ‰ °C^{-1} (Jouzel et al., 1997a). Consequently, they indicate a much higher temperature variability in Greenland during the last glacial period. For the period of the last 9000 years the Greenland average Holocene isotope–temperature relationship has been estimated to be 0.44–0.53 ‰ °C^{-1}, again substantially lower compared to the modern spatial gradient (Vinther et al., 2009). However, as all these studies cover much longer time periods as compared to our NG stack records, no firm conclusion can be drawn from these studies about an appropriate isotope–temperature relationship for the last millennium.

Along the NGT firn, temperature measurements at about 15 m depth have been done (Table 4). However, due to their small range of about 2 K difference, it is difficult to reassess the general Greenland isotope–temperature relationship from Johnsen et al. (1989) from the NGT data alone. Schwager (2000) added data from Dansgaard et al. (1969) from along the EGIG traverse, which was also used in Johnsen et

al. (1989), to expand the temperature range to derive a more reliable isotope–temperature gradient. This calculated gradient of 0.7 ± 0.2 ‰ °C^{-1} is within the gradient uncertainty range given by Johnsen et al. (1989). Using our updated NGT data set we get the same results.

If we apply the spatial isotope–temperature gradient of 0.7 ‰ °C^{-1} from Schwager (2000) for the range of isotope variations (-1.4 to 2.5 ‰) of the NG stack record, the isotope data translate into temperature changes of -2.0 to 3.6°C (5.6 K) within the last millennium. However, applying instead a temporal gradient of 0.48 ‰ °C^{-1} as suggested by Vinther et al. (2009) results in possible temperature changes of -2.9 to 5.2 °C (8.1 K) within the last 1000 years. Using the most recent temporal glacial–interglacial isotope–temperature gradients reported by Buizert et al. (2014) would result in comparable temperature changes. If using the NEEM gradient of 1.1 ± 0.2 ‰ °C^{-1} (Masson-Delmotte et al., 2015), which is valid for AD 2007–1979 in the area of NEEM, the resulting temperature range of the NG stack is, at -1.3 to 2.3 °C (3.6 K), a bit smaller than compared to the Johnsen or Schwager gradient. Nevertheless, the resulting temperature ranges are larger than expected (e.g., Dahl-

Table 5. Correlation coefficients (r) of the stacked $\delta^{18}O$ record with annual and seasonal (DJF, MAM, JJA and SON) extended Greenland temperature records * (Vinther et al., 2006a), northwestern Iceland instrumental data** (Hanna et al., 2004; Jónsson, 1989), annual mean Greenland ice sheet near-surface air temperatures from combined instrumental and model output *** (Box et al., 2009) and Arctic temperature reconstruction **** (Wood et al., 2010). All correlations are done with 5-year running means and are significant at the 95 % level ($p < 0.05$).

	r_{annual}	$r_{seasonal}$		Years of overlap
Merged South (Greenland)*	0.51	DJF	0.47	1784–1994
		MAM	0.62	
		JJA	0.51	
		SON	0.5	
Ilulissat (Greenland)*	0.46	DJF	0.50	1784–1994
		MAM	0.42	
		JJA	0.36	
		SON	0.45	
Nuuk (Greenland)*	0.41	DJF	–	1784–1994
		MAM	0.55	
		JJA	0.47	
		SON	0.47	
Qaqortoq (Greenland)*	0.39	DJF	–	1784–1994
		MAM	0.50	
		JJA	0.50	
		SON	0.36	
Stykkishólmur (Iceland)**	0.41	DJF	–	1830–1994
		MAM	0.36	
		JJA	0.35	
		SON	0.31	
Mean Greenland surface air temperature***	0.50			1840–1994
Extended instrumental temperature record****	0.55			1802–1994

Jensen et al., 1998), which is an additional argument for not calculating absolute temperatures from the NG stack with the given gradients.

We conclude that any conversion of the NG stack isotope record into absolute temperature variations during the last millennium is highly uncertain. Thus, for the following part of the manuscript, we will refer to NG stack isotope anomalies as relative temperature changes in terms of "warmer" (i.e., isotopically enriched) and "colder" (isotopically depleted) only, but will refrain from converting our ice core data into absolute temperature changes.

To assess regional differences within northern Greenland, stacks of subsets of cores will be discussed in terms of interpretation as a temperature proxy. As illustrated in Fig. 4, we differentiate between two different types of cores: cores drilled on the ice divide and cores drilled east of the ice divide. Accordingly, in Fig. 5 the overall northern Greenland $\delta^{18}O$ stack used in this study is compared to a stack of the cores of lower accumulation rate drilled east of the main ice divide (B16, B17, B18, B19, B20, B21 and B23) (stack "East") and a stack of those on the ice divide (B22, B26, B27, B29, B30 and NGRIP) (stack "Divide") (Fig. 5).

Even though there is a similar overall trend, the three records show differences in amplitude and timing of warm and cool events. The correlation between the two sub-stacks is rather low ($r = 0.71$ of 30-year running means). In the 11th

and 12th centuries, we observe a quasi-anti-correlation between stack "East" and stack "Divide". Even during well-known climate events such as the Medieval Climate Anomaly (MCA, AD 950–1250; Mann et al., 2009), the Little Ice Age (LIA, 1400–1900; Mann et al., 1998) and the early twentieth century warming (ETCW, AD 1920–1940; Semenov and Latif, 2012), there are significantly different $\delta^{18}O$ patterns. For example, stack "Divide" shows colder temperatures during AD 1000–1200. Also, during the 16th century we notice substantial differences between the two sub-stacks. In stack "East" events like the AD 1420 or the first part of the LIA show a higher amplitude.

Stack "East" has a higher correlation to the total NG stack ($r = 0.96$) compared to stack "Divide" ($r = 0.68$) for the period AD 994–1994. When looking at the time period AD 1505–1993 with a high number of cores included in both sub-stacks, it can be seen that the correlation coefficients to the total NG stack are almost equal (stack "East": $r = 0.95$; stack "Divide": $r = 0.90$, $p < 0.1$). Here, both records reflect the mean changes in $\delta^{18}O$ for northern Greenland. Differences before AD 1505 may be artifacts of low core numbers even though regional differences in climate conditions cannot be ruled out.

We consider the NG stack to be a climate record that displays the overall climate variation independent of local influences such as topography or accumulation rate. In con-

trast, results from studies with only one record become less spatially representative, as they may be affected by a lower signal-to-noise ratio and a higher influence of other local non-climate effects.

3.4 Last millennium climate from a stacked NG δ^{18}O record in relation to other proxy records and possible forcing factors

The NG stack covers the time between AD 753 and AD 1994 (Fig. 5). For a better visualization of decadal- to centennial-scale variability, a 30-year running mean is added. The running mean shows the warmest period around AD 1420 and the coldest at about AD 1680. The isotopically warmest single year during the last 1000 years in northern Greenland was AD 1928, whereas AD 1835 was the coldest.

Distinct decadal- to centennial-scale warm and cold anomalies can be detected in the stacked (Fig. 5) as well as individual δ^{18}O records (Fig. 2) and coincide with well-known climate anomalies (MCA, LIA, ETCW, marked in Fig. 5).

We find a pronounced warm period from AD 850 to 1100 which has its maximum between AD 900 and 1000. This is about 100 years earlier than the described MCA in Mann et al. (2009). The warm period is followed by a quasi-periodical change of warm and cold phases observed approximately every 60 to 80 years until about AD 1600. During this phase, the most distinct warm period is observed around AD 1420.

A longer period of cold temperatures occurred during the 17th and early 19th century and has already been attributed to the LIA by a prior NGT study that used only four cores (B16, B18, B21 and B29; Fischer et al., 1998c). A cold period in northern Greenland corresponding to the LIA is later than reconstructed for the entire Northern Hemisphere by Mann et al. (1998), with lowest values during AD 1620–1780 and in the first half of the 19th century. Interestingly, the warmest mean values of the last 1000 years at AD 1420 lie within the time frame of the LIA.

A distinct but, compared to other periods, not exceptional warm event in the early 20th century corresponds to the ETCW. Since the 1870s, the values are above the 1000-year mean. At the end of the 20th century, the temperature stagnates at a high mean level. However, as the NGT cores were drilled between AD 1993 and 1995, the warmest years of the recent decades (Wood et al., 2010) are not included in our record.

For the NG stack as well as most of the individual NGT cores, the isotopically warmest periods besides the AD 1420 event were in the 10th and 20th centuries, in particular between AD 1900 and 1950. These years are even warmer than the most recent years covered by the NGT cores (i.e., the 1980s).

To place the results in an Arctic-wide context, we compare our northern Greenland temperature record (NG stack) to ice core records from the Russian Arctic (Akademii Nauk

– AN; Opel et al., 2013), Canada (Agassiz Ice Cap – Agassiz; Vinther et al., 2008), Svalbard (Lomonosovfonna – Lomo; Divine et al., 2011) and southern Greenland (Dye3; Vinther et al., 2006b), as well as a multi-proxy reconstruction of annual Arctic SAT (Arctic2k; Pages 2k Consortium, 2013; Fig. 6) that covers our time period.

Note that some of these time series (Agassiz, Arctic2k) are also stacked records with a wider regional representativeness, whereas others are single records (Dye3, AN, Lomo), which influences the strength of correlation due to different signal-to-noise ratios. For the discussion of the temperature record, we concentrate on the smoothed values (30-year running means).

The strongest correlations with our NG stack are found for the Agassiz and Arctic2k records ($r = 0.58$ and 0.66, respectively). For the latter, we have to consider that some of the NGT cores (B16, B18 and B21 on the old timescale) are used to generate this multi-proxy record. In total, 59 records including 16 ice cores were used. NGT cores represent only 3 out of these 59 records. The correlation coefficient between the stacked anomalies of B16, B18 and B21 and the Arctic2k temperature is small ($r = 0.24$), so we can assume that the NGT records do not dominate the reconstruction.

We conclude that a good correlation between the NG stack and the Arctic2k record shows that the temperature in northern Greenland generally follows the Arctic-wide mean temperature.

The Lomonosovfonna record is interpreted as a winter record and has only a weak correlation with the NG stack ($r = 0.22$). More summer snow in northern Greenland compared to Lomonosovfonna could be one possible explanation for the weak correlation between both records. While for the other drill sites we have comparable r values for both sub-stacks as for the NG stack, the Lomonosovfonna record has a stronger correlation to stack "East" ($r = 0.2$) than to stack "Divide" ($r = -0.12$), which supports the argument of different moisture sources or seasonal distribution of snowfall in the northeast of Greenland.

The Lomonosovfonna, Akademii Nauk and Arctic2k records show significantly more enriched δ^{18}O values during the MCA. However, smaller events of abnormal warm temperatures during the MCA are observed for Agassiz and Dye3. Our NG stack shows warmer values earlier than the MCA time period given by Mann et al. (1998). We conclude that, further north in the Arctic, the warm events during MCA may be less pronounced or earlier in timing.

The Lomonosovfonna and Arctic2k records show a dominant cold period during the LIA from AD 1580 to 1870. Also, our northern Greenland ice cores, as well as those of Agassiz and Akademii Nauk, reveal distinct LIA cooling periods in contrast to the Dye3 ice core from southern Greenland. Like in our NG stack, the cooling appears in two phases and some decades later than described by Mann et al. (2009). For the NG stack, the younger phase (AD 1800–1850) is of minor amplitude and shorter duration.
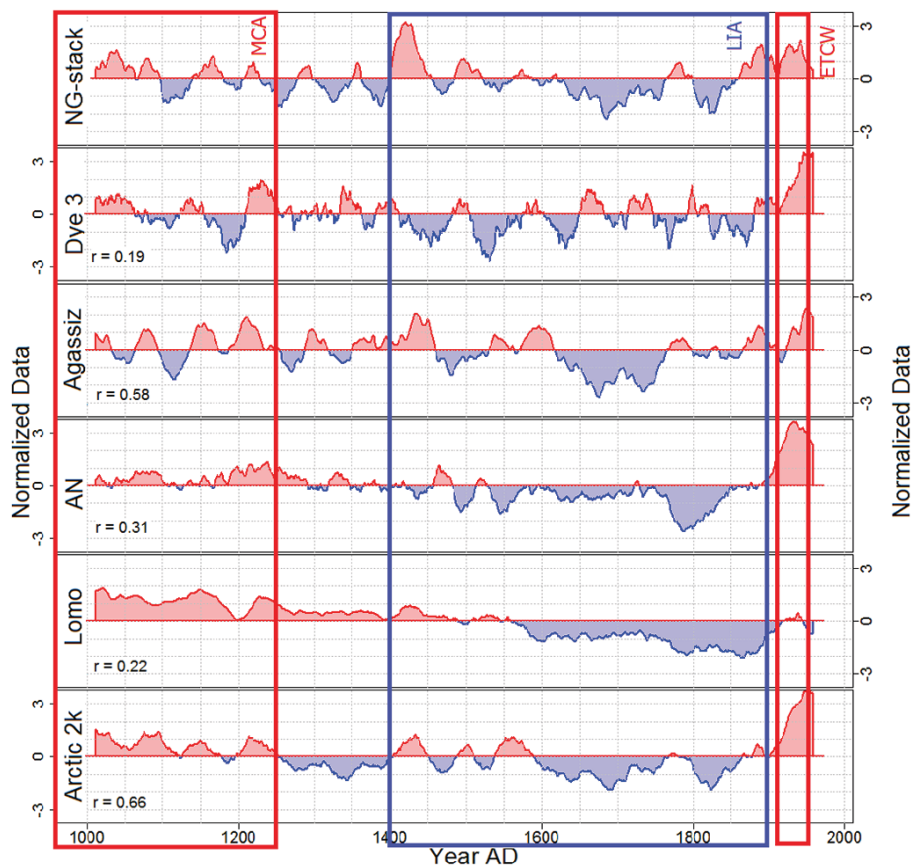
Figure 6. Thirty-year running mean for δ^{18}O values from different Arctic regions – northern Greenland (NG stack, this study), southern Greenland (Dye3; Vinther et al., 2006b), Canada (Agassiz Ice Cap, Agassiz; Vinther et al., 2008), Russian Arctic (Akademii Nauk, AN; Opel et al., 2013) and Svalbard (Lomonosovfonna, Lomo, Divine et al., 2011) – as well as a reconstructed record (Arctic2k; Pages 2k Consortium, 2013). All records are given on z-level scales (centered and normalized data). The correlation coefficient for the smoothed values with regard to our stack is also given.

Between AD 1920 and 1940, there was a major warming period in the Arctic, known as the ETCW, which was observed in all records shown here. Chylek et al. (2006) determined from meteorological data that the 1920–1930 warming was stronger than the 1995–2005 warming. For the NG stack and Akademii Nauk record, the ETCW was warmer than the second half of the 20th century, which distinguishes them from other shown records. The ETCW is assumed to be independent of external forcing but caused by internal climate variability, in particular sea-ice–atmosphere feedbacks (Wood and Overland, 2010). This led us to conclude that northern Greenland may also be a good place to study forcing-independent (i.e., internal) climate changes.

However, natural external forcing (i.e., insolation, solar irradiance and volcanic eruptions) is assumed to influence the temperature that can be studied from northern Greenland's ice cores.

In general, higher solar activity causes higher temperatures (as during the MCA), whereas cold periods (e.g., LIA) are dominated by lower solar activity (Ammann et al., 2007).

Based on some of the NGT records (B16, B18, B21 and B29), Fischer et al. (1998c) explained most of the long-term variation in northern Greenland through changes in solar activity.

Volcanism causes strong negative radiative forcing (Robock, 2000). It is assumed that volcanic eruptions inject large quantities of sulfur-rich gases into the stratosphere and global climate can be cooled by 0.2–0.3 °C for several years after the eruption (Zielinski, 2000). Results from Crowley (2000) indicate that volcanism generally explains roughly 15–30 % of the variability in global temperatures.

Miller et al. (2012) argued that century-scale cold summer anomalies, of which the LIA represents the coldest, occur because natural forcing is either weak or, in the case of volcanism, short-lived. Pages 2k Consortium (2013) shows that periods with strong volcanic activity correspond to a reduced mean temperature. The LIA may be therefore caused by a 50-year-long episode of volcanism and kept persistently cold because of ocean feedback and a summer insolation minimum.
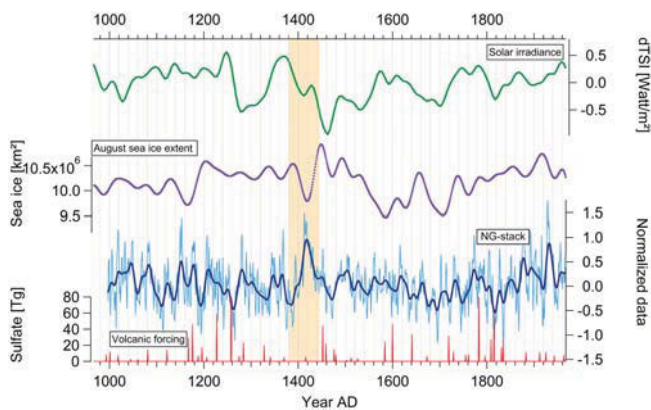
Figure 7. The northern Greenland stack (NG stack; blue: annual; dark blue: smoothed) is shown with possible forcing factors. Green represents the reconstructed total solar irradiance (Steinhilber et al., 2009), purple the reconstructed August Arctic sea-ice extent (Kinnard et al., 2011), and red at the bottom the stratospheric sulfate aerosol injection for the Northern Hemisphere (Gao et al., 2008). All values are 40-year low-pass-filtered. The discussed AD 1420 event is marked in beige.

Between about AD 1100 and 1600 we observe quasi-periodic (60–80 a) cold and warm anomalies in the NG stack which are not present in the other Arctic records shown (Fig. 6). The main period determined using Fourier decomposition between AD 1100 and 1600 for 30-year running mean smoothed values is calculated with 76.31 a.

The Atlantic Multidecadal Oscillation (AMO) could be one possible influence causing these low-frequency oscillations. Chylek et al. (2012) explain that the AMO is visible in $\delta^{18}O$ values from central Greenland. As the AMO index reconstruction (Gray et al., 2004) does not cover the time between AD 1100 and 1600, we can only speculate about an influence in that time due to the similar periodicity. For the time period AD 1567–1990, the correlation between the NG stack and the AMO index is weak ($r = 0.06$), which might be due to the uncertainties in historical AMO data. However, after AD 1800 we observe a higher correlation coefficient ($r = 0.66$, $p < 0.05$) implying a possible relation.

One of these warmer periods is at about AD 1420 ± 20, an abnormal warm event which is observed in our northern Greenland record and has not been pointed out in other ice core studies before. The event is observable in all nine NGT cores covering this time (Fig. 2) as well as in NGRIP but not in the isotope records from southern Greenland such as the Dye3 ice core (Fig. 6). One reason here might be the specific geographical position in the north.

Furthermore, we observe a difference between the Canadian and Russian Arctic regarding the 1420 event. Unlike the Russian Akademii Nauk ice core, the $\delta^{18}O$ values of the Agassiz cores from Ellesmere Island also show a tendency towards more enriched values in that period but which is not as strong as in northern Greenland.

The fact that the 1420 event is not clearly noticeable in other surrounding Arctic ice cores emphasizes that this event may have occurred on a smaller regional scale. However, it seems to have been of dominant influence and is also reflected in a smaller warming for the Arctic2k record (Fig. 6).

The spatial distribution of the 1420 event in northern Greenland is mapped in Fig. 3b. The event is strongest in the upper north and shows a different pattern than the $\delta^{18}O$ anomalies of the 1920/1930 warm phase, which is also attributed to internal variability and is strongest in the northeast of Greenland.

Figure 7 shows possible forcing factors that might be related to the AD 1420 event. According to the reconstructed total solar irradiance record of Steinhilber et al. (2009), there was no solar maximum observed for AD 1420 that could explain the warmer temperatures in northern Greenland. As we see no forcing anomaly, we interpret the 1420 event as likely be caused by internal Arctic climate dynamics with a sea-ice–atmosphere feedback.

Box (2002) argued that climate variability in Greenland is linked to the North Atlantic Oscillation (NAO), volcanism and sea-ice extent. NAO (Vinther et al., 2003) is calculated to be weakly reflected ($r = -0.2$, $p < 0.01$) in the NG stack, similar to the results of White et al. (1997) for summit ice cores, whereas none of the single NGT records is significantly correlated ($p < 0.05$) with the NAO index. The NG stack has an increased signal-to-noise level, which is why the correlation here might be clearer than from individual records. Also, the sub-stacks of the records on the ice divide (stack "Divide") as well as those east (stack "East") are significantly correlated ($r = -0.19$ and -0.17, $p < 0.05$) with the NAO index. The cores east of the main ice divide are expected to be out of the major cyclonic track. We conclude that NAO is not of major importance for northern Greenland $\delta^{18}O$ values.

Around AD 1420, an anti-correlation between sea-ice extent in the Arctic Ocean (Kinnard et al., 2011) and the $\delta^{18}O$ values is observed (Fig. 7). The sea-ice extent reconstruction of Kinnard et al. (2011) is based on 69 proxy records, of which 22 are $\delta^{18}O$ records. Out of these 22 $\delta^{18}O$, records 5 (NGRIP, B16, B18, B21 and B26) are also used in our NG stack. We do not expect circular reasoning in the interpretation of the 1420 event because B16 and B26 do not reach the age of AD 1420 and we do not see a strong anti-correlation during any other time period.

The sea ice in the Arctic Ocean shows a recession only during that warm period in northern Greenland. A diminished sea-ice extent would cause higher temperatures on a regional scale and would increase the amount of water vapor from local sources. Therefore, compared to distant sources, more isotopically enriched moisture (Sime et al., 2013) may contribute to precipitation in northern Greenland, in particular east of the main ice divide.

However, we do not see any direct relationship between sea-ice extent and our NG stack during the rest of time, which

does not exclude the relationship between sea-ice extent and δ^{18}O in northern Greenland. The sea-ice reconstruction used is Arctic-wide, which means that the climatic events of regional extent, like an additional moisture source for northern Greenland's δ^{18}O, do not always have to be reflected. Nevertheless, the recent NEEM δ^{18}O record from northwestern Greenland also shows a generally close relationship with the Labrador Sea/Baffin Bay sea-ice extent (Masson-Delmotte et al., 2015; Steen-Larsen et al., 2011).

4 Conclusions

With the full set of the NGT records, it was, for the first time, possible to describe regional differences in the δ^{18}O values in northern Greenland over the last 1000 years.

Because of the ice sheet topography we see a clear east-to-west difference in northern Greenland δ^{18}O distribution. In total, 12 % of the spatial δ^{18}O variability is attributed to ice sheet topography. The east-to-west gradient is larger than the north-to-south gradient. We find a more pronounced persistence of warm or cold events east of the main ice divide and assume more stable climate conditions there. The eastern part is more influenced by local effects like changes in the Arctic Ocean. However, these findings need to be supported by the results of climate models. For the first time, a local warm event at AD 1420 ± 20 has been pointed out. We assume an atmosphere–sea-ice feedback to be one possible reason for this event.

Due to the shadowing effect of the main ice divide we find the lowest accumulation rates in the northeast, whereas the lowest mean δ^{18}O values are found east of the main ice divide north of the summit. The lowest δ^{18}O mean values seem to be independent of accumulation rate.

We have presented a new 1000-year stacked δ^{18}O record for northern Greenland covering 10 % of the area of Greenland. We found this NG stack to be representative of the northern Greenland temperature.

Northern Greenland δ^{18}O represents known climatic variations of the last millennium. We see a warm MCA and can derive distinct LIA cooling from our NG stack.

The results of single-site ice core studies are likely weakened by the finding that there is only 22 % common variability in the 13 NGT cores.

The solar activity and internal Arctic climate dynamics are likely the main factors influencing the temperature in northern Greenland. In contrast, we could not find a general cooling effect of volcanic eruptions in our data.

References

Ammann, C. M., Joos, F., Schimel, D. S., Otto-Bliesner, B. L., and Tomas, R. A.: Solar influence on climate during the past millennium: results from transient simulations with the NCAR Climate System Model, P. Natl. Acad. Sci. USA, 104, 3713–3718, 2007.

Appenzeller, C., Schwander, J., Sommer, S., and Stocker, T. F.: The North Atlantic Oscillation and its imprint on precipitation and ice accumulation in Greenland, Geophys. Res. Lett., 25, 11, 1939–1942, 1998.

Bamber, J. L., Griggs, J. A., Hurkmans, R. T. W. L., Dowdeswell, J. A., Gogineni, S. P., Howat, I., Mouginot, J., Paden, J., Palmer, S., Rignot, E., and Steinhage, D.: A new bed elevation dataset for Greenland, The Cryosphere, 7, 499-510, doi:10.5194/tc-7-499-2013, 2013.

Benson, C. S.: Greenland snow pit and core stratigraphic data 1952, 1953, 1954, 1955, U.S. Army Corps of Engineers Snow Ice and Permafrost Res, 70, 39–47, 1962.

Bigler, M., Wagenbach, D., Fischer, H., Kipfstuhl, J., Miller, H., Sommer, S., and Stauffer, B.: Sulphate record from a northeast Greenland ice core over the last 1200 years based on continuous flow analysis, in: Annals of Glaciology, vol. 35, edited by: Wolff, E. W., Int. Glaciological Soc., Cambridge, 250–256, 2002.

Box, J. E.: Survey of Greenland instrumental temperature records: 1873–2001, Int. J. Climatol., 22, 1829–1847, 2002.

Box, J. E., Yang, L., Bromwich, D. H., and Bai, L.-S.: Greenland Ice Sheet Surface Air Temperature Variability: 1840–2007*, J. Climate, 22, 4029–4049, 2009.

Buchardt, S. L., Clausen, H. B., Vinther, B. M., and Dahl-Jensen, D.: Investigating the past and recent δ^{18}O-accumulation relationship seen in Greenland ice cores, Clim. Past, 8, 2053–2059, doi:10.5194/cp-8-2053-2012, 2012.

Buizert, C., Gkinis, V., Severinghaus, J. P., He, F., Lecavalier, B. S., Kindler, P., Leuenberger, M., Carlson, A. E., Vinther, B., Masson-Delmotte, V., White, J. W. C., Liu, Z., Otto-Bliesner, B., and Brook, E. J.: Greenland temperature response to climate forcing during the last deglaciation, Science, 345, 1177–1180, 2014.

Bull, C.: Snow accumulation in north Greenland, J. Glaciol., 3, 237–248, 1958.

Chen, Q. S., Bromwich, D. H., and Bai, L. S.: Precipitation over Greenland retrieved by a dynamic method and its relation to cyclonic activity, J. Climate, 10, 839–870, 1997.

Chylek, P., Dubey, M. K., and Lesins, G.: Greenland warming of 1920–1930 and 1995–2005, Geophys. Res. Lett., 33, L11707, doi:10.1029/2006GL026510, 2006.

Chylek, P., Folland, C., Frankcombe, L., Dijkstra, H., Lesins, G., and Dubey, M.: Greenland ice core evidence for spatial and temporal variability of the Atlantic Multidecadal Oscillation, Geophys. Res. Lett., 39, L09705, doi:10.1029/2012GL051241, 2012.

Crowley, T. J.: Causes of Climate Change Over the Past 1000 Years, Science, 289, 270–277, 2000.

Dahl-Jensen, D., Mosegaard, K., Gundestrup, N., Clow, G. D., Johnsen, S. J., Hansen, A. W., and Balling, N.: Past temperatures directly from the Greenland Ice Sheet, Science, 282, 268–271, 1998.

Dansgaard, W.: The O^{18}-abundance in fresh water, Geochim. Cosmochim. Ac., 6, 241–260, 1954.

Dansgaard, W.: Stable isotopes in precipitation, Tellus, 16, 436–468, 1964.

Dansgaard, W., Johnsen, S. J., and Moeller, J.: One Thousand Centuries of Climatic Record from Camp Century on the Greenland Ice Sheet, Science, 166, 377–380, 1969.

Divine, D., Isaksson, E., Martma, T., Meijer, H. A. J., Moore, J., Pohjola, V., van de Wal, R. S. W., and Godtliebsen, F.: Thousand years of winter surface air temperature variations in Svalbard and northern Norway reconstructed from ice core data, Polar Res., 30, 7379, doi:10.3402/polar.v30i0.7379, 2011.

Fischer, H. and Mieding, B.: A 1,000-year ice core record of interannual to multidecadal variations in atmospheric circulation over the North Atlantic, Clim. Dynam., 25, 65–74, 2005.

Fischer, H., Wagenbach, D., and Kipfstuhl, J.: Sulfate and nitrate firn concentrations on the Greenland ice sheet: 1. Large-scale geographical deposition changes, J. Geophys. Res., 103, 21927–21930, 1998a.

Fischer, H., Wagenbach, D., and Kipfstuhl, J.: Sulfate and nitrate firn concentrations on the Greenland ice sheet: 2. Temporal anthropogenic deposition changes, J. Geophys. Res.-Atmos., 103, 21935–21942, 1998b.

Fischer, H., Werner, M., Wagenbach, D., Schwager, M., Thorsteinnson, T., Wilhelms, F., Kipfstuhl, J., and Sommer, S.: Little Ice Age clearly recorded in northern Greenland ice cores, Geophys. Res. Lett., 25, 1749–1752, 1998c.

Fisher, D. A., Reeh, N., and Clausen, H. B.: Stratigraphic noise in time series derived from ice cores, Ann. Glaciol, 7, 76–83, 1985.

Freitag, J., Kipfstuhl, S., and Laepple, T.: Core-scale radioscopic imaging: a new method reveals density & calcium link in Antarctic firn, J. Glaciol., 59, 1009–1014, 2013.

Friedmann, A., Moore, J. C., Thorsteinnson, T., Kipfstuhl, J., and Fischer, H.: A 1200 year record of accumulation from northern Greenland, Ann. Glaciol, 21, 19–25, 1995.

Gao, C., Robock, A., and Ammann, C.: Volcanic forcing of climate over the past 1500 years: An improved ice core-based index for climate models, J. Geophys. Res.-Atmos., 113, D23111, doi:10.1029/2008JD010239, 2008.

Gray, S. T., Graumlich, L. J., Betancourt, J. L., and Pederson, G. T.: A tree-ring based reconstruction of the Atlantic Multidecadal Oscillation since 1567 A.D, Geophys. Res. Lett., 31, L12205, doi:10.1029/2004GL019932, 2004.

Grootes, P. M. and Stuiver, M.: Oxygen 18/16 variability in Greenland snow and ice with 10^{-3}- to 10^5-year time resolution, J. Geophys. Res.-Oceans, 102, 26455–26470, 1997.

Grootes, P. M., Stuiver, M., White, J. W. C., Johnsen, S., and Jouzel, J.: Comparison of oxygen isotope records from the GISP2 and GRIP Greenland ice cores, Nature, 366, 552–554, 1993.

Hanna, E., Jónsson, T., and Box, J. E.: An analysis of Icelandic climate since the nineteenth century, Int. J. Climatol., 24, 1193–1210, 2004.

Isaksson, E., Kohler, J., Pohjola, V., Moore, J. C., Igarashi, M., Karlöf, L., Martma, T., Meijer, H. A. J., Motoyama, H., Vaikmäe, R., and Van de Wal, R. S. W.: Two ice-core $\delta^{18}O$ records from Svalbard illustrating climate and sea-ice variability over the last 400 years, Holocene, 15, 501–509, 2005.

Johnsen, S. J., Dansgaard, W., and White, J. W. C.: The origin of Arctic precipitation under present and glacial conditions, Tellus Ser. B, 41, 452–468, 1989.

Johnsen, S. J., Hammer, C. U., Dansgaard, W., Gundestrup, N. S., and Clausen, H. B.: The Eem stable isotope record along the GRIP ice core and its interpretation, Quaternary Res., 42, 117–124, 1995.

Johnsen, S. J., Clausen, H. B., Cuffey, K. M., Hoffmann, G., Schwander, J., and Creyts, T.: Diffusion of stable isotopes in polar firn and ice: the isotope effect in firn diffusion, in: Physics of Ice Core Records, Hokkaido University, Place Hokkaido, 121–140, 2000.

Jónsson, T.: the observations of Jon Thorsteinsson in Nes and Reykjavik 1820–1854, Icel. Met. Office Report, Reykjavik, 1989.

Jouzel, J., Alley, R. B., Cuffey, K. M., Dansgaard, W., Grootes, P., Hoffmann, G., Johnsen, S. J., Koster, R. D., Peel, D., Shuman, C. A., Stievenard, M., Stuiver, M., and White, J.: Validity of the temperature reconstruction from water isotopes in ice cores, J. Geophys. Res.-Oceans, 102, 26471–26487, 1997a.

Jouzel, J., Froehlich, K., and Schotterer, U.: Deuterium and oxygen-18 in present-day precipitation: data and modelling, Hydrogeological Science, 42, 747–763, 1997b.

Jouzel, J. and Merlivat, L.: Deuterium and O-18 in precipitation-Modelling of the isotopic effects during snow formation, J. Geophys. Res.-Atmos., 89, 1749–1757, 1984.

Kaufmann, P., Federer, U., Hutterli, M. A., Bigler, M., Schüpbach, S., Ruth, U., Schmitt, J., and Stocker, T. F.: An Improved Continuous Flow Analysis System for High-Resolution Field Measurements on Ice Cores, Environ. Sci. Technol., 42, 8044–8050, doi:10.1021/es8007722, 2008.

Kinnard, C., Zdanowicz, C. M., Fisher, D. A., Isaksson, E., de Vernal, A., and Thompson, L. G.: Reconstructed changes in Arctic sea ice over the past 1,450 years, Nature, 479, 509–512, 2011.

Koch, J. P. and Wegener, A.: Wissenschaftliche Ergebnisse der dänischen Expedition nach Dronning Louises-Land und quer über das Inlandeis von Nordgrönland 1912–13, Reitzel, 1930.

Lavigne, F., Degeai, J.-P., Komorowski, J.-C., Guillet, S., Robert, V., Lahitte, P., Oppenheimer, C., Stoffel, M., Vidal, C. M., Surono, Pratomo, I., Wassmer, P., Hajdas, I., Hadmoko, D. S., and de Belizal, E.: Source of the great A.D. 1257 mystery eruption unveiled, Samalas volcano, Rinjani Volcanic Complex, Indonesia, P. Natl. Acad. Sci., 110, 16742–16747, 2013.

Mann, M. E., Bradley, R. S., and Hughes, M. K.: Global-scale temperature patterns and climate forcing over the past six centuries, Nature, 392, 779–787, 1998.

Mann, M. E., Zhang, Z., Rutherford, S., Bradley, R. S., Hughes, M. K., Shindell, D., Ammann, C., Faluvegi, G., and Ni, F.: Global Signatures and Dynamical Origins of the Little Ice Age and Medieval Climate Anomaly, Science, 326, 1256–1260, 2009.

Masson-Delmotte, V., Steen-Larsen, H. C., Ortega, P., Swingedouw, D., Popp, T., Vinther, B. M., Oerter, H., Sveinbjornsdottir, A. E., Gudlaugsdottir, H., Box, J. E., Falourd, S., Fettweis, X., Gallée, H., Garnier, E., Gkinis, V., Jouzel, J., Landais, A., Minster, B., Paradis, N., Orsi, A., Risi, C., Werner, M., and White, J. W. C.: Recent changes in north-west Greenland climate documented by NEEM shallow ice core data and simulations, and implications for past-temperature reconstructions, The Cryosphere, 9, 1481–1504, doi:10.5194/tc-9-1481-2015, 2015.

Merlivat, L. and Jouzel, J.: Global climatic interpretation of the deuterium-oxygen 18 relationship for precipitation, J. Geophys. Res.-Oc. Atmos., 84, 5029–5033, 1979.

Mieding, B.: Reconstruction of millennial aerosol-chemical ice core records from the northeast Greenland: Quantification of temporal changes in atmospheric circulation, emission and deposition, Reports on Polar and Marine Reports, 513, Alfred Wegener Institute for Polar and Marine Research, Bremerhaven, 2005.

Miller, G. H., Geirsdóttir, Á., Zhong, Y., Larsen, D. J., Otto-Bliesner, B. L., Holland, M. M., Bailey, D. A., Refsnider, K. A., Lehman, S. J., Southon, J. R., Anderson, C., Björnsson, H., and Thordarson, T.: Abrupt onset of the Little Ice Age triggered by volcanism and sustained by sea-ice/ocean feedbacks, Geophys. Res. Lett., 39, L02708, doi:10.1029/2011GL050168, 2012.

Newhall, C. G. and Self, S.: The volcanic explosivity index (VEI) an estimate of explosive magnitude for historical volcanism, J. Geophys. Res.-Oceans, 87, 1231–1238, 1982.

North Greenland Ice Core Project Members: Andersen, K. K., Azuma, N., Barnola, J.-M., Bigler, M., Biscaye, P., Caillon, N., Chappellaz, J., Clausen, H. B., Dahl-Jensen, D., Fischer, H., Flückiger, J., Fritzsche, D., Fujii, Y., Goto-Azuma, K., Grønvold, K., Gundestrup, N. S., Hansson, M., Huber, C., Hvidberg, C. S., Johnsen, S. J., Jonsell, U., Jouzel, J., Kipfstuhl, S., Landais, A., Leuenberger, M., Lorrain, R., Masson-Delmotte, V., Miller, H., Motoyama, H., Narita, H., Popp, T., Rasmussen, S. O., Raynaud, D., Röthlisberger, R., Ruth, U., Samyn, D., Schwander, J., Shoji, H., Siggard-Andersen, M.-L., Steffensen, J. P., Stocker, T. F., Sveinbjörnsdóttir, A. E., Svensson, A., Takata, M., Tison, J.-L., Thorsteinsson, T., Watanabe, O., Wilhelms, F., and White, J. W. C.: High-resolution record of Northern Hemisphere climate extending into the last interglacial period, Nature, 431, 147–151, 2004.

Ohmura, A.: New temperature distribution maps for Greenland, Zeitschrift für Gletscherkunde und Glaziologie, 35, 1–20, 1987.

Opel, T., Fritzsche, D., and Meyer, H.: Eurasian Arctic climate over the past millennium as recorded in the Akademii Nauk ice core (Severnaya Zemlya), Clim. Past, 9, 2379–2389, doi:10.5194/cp-9-2379-2013, 2013.

Ortega, P., Swingedouw, D., Masson-Delmotte, V., Risi, C., Vinther, B., Yiou, P., Vautard, R., and Yoshimura, K.: Characterizing atmospheric circulation signals in Greenland ice cores: insights from a weather regime approach, Clim. Dynam., 43, 2585–2605, 2014.

Pages 2k Consortium: Continental-scale temperature variability during the past two millennia, Nat. Geosci., 6, 339–346, 2013.

Pinzer, B. R., Schneebeli, M., and Kaempfer, T. U.: Vapor flux and recrystallization during dry snow metamorphism under a steady temperature gradient as observed by time-lapse microtomography, The Cryosphere, 6, 1141–1155, doi:10.5194/tc-6-1141-2012, 2012.

Robock, A.: Volcanic eruptions and climate, Rev. Geophys., 38, 191–219, 2000.

Schwager, M.: Ice core analysis on the spatial and temporal variability of temperature and precipitation during the late Holocene in North Greenland, Reports on Polar and Marine Research, 362, Alfred Wegener Institute for Polar and Marine Research, Bremen, 2000.

Semenov, V. A. and Latif, M.: The early twentieth century warming and winter Arctic sea ice, The Cryosphere, 6, 1231–1237, doi:10.5194/tc-6-1231-2012, 2012.

Severinghaus, J. P., Sowers, T., Brook, E. J., Alley, R. B., and Bender, M. L.: Timing of abrupt climate change at the end of the Younger Dryas interval from thermally fractionated gases in polar ice, Nature, 391, 141–146, 1998.

Sigl, M., McConnell, J. R., Layman, L., Maselli, O., McGwire, K., Pasteris, D., Dahl-Jensen, D., Steffensen, J. P., Vinther, B., Edwards, R., Mulvaney, R., and Kipfstuhl, S.: A new bipolar ice core record of volcanism from WAIS Divide and NEEM and implications for climate forcing of the last 2000 years, J. Geophys. Res.-Atmos., 118, 1151–1169, 2013.

Sime, L. C., Risi, C., Tindall, J. C., Sjolte, J., Wolff, E. W., Masson-Delmotte, V., and Capron, E.: Warm climate isotopic simulations: what do we learn about interglacial signals in Greenland ice cores?, Quaternary Sci. Rev., 67, 59–80, 2013.

Steen-Larsen, H. C., Masson-Delmotte, V., Sjolte, J., Johnsen, S. J., Vinther, B. M., Bréon, F. M., Clausen, H. B., Dahl-Jensen, D., Falourd, S., Fettweis, X., Gallée, H., Jouzel, J., Kageyama, M., Lerche, H., Minster, B., Picard, G., Punge, H. J., Risi, C., Salas, D., Schwander, J., Steffen, K., Sveinbjörnsdóttir, A. E., Svensson, A., and White, J.: Understanding the climatic signal in the water stable isotope records from the NEEM shallow firn/ice cores in northwest Greenland, J. Geophys. Res.-Atmos., 116, D06108, doi:10.1029/2010JD014311, 2011.

Steen-Larsen, H. C., Masson-Delmotte, V., Hirabayashi, M., Winkler, R., Satow, K., Prié, F., Bayou, N., Brun, E., Cuffey, K. M., Dahl-Jensen, D., Dumont, M., Guillevic, M., Kipfstuhl, S., Landais, A., Popp, T., Risi, C., Steffen, K., Stenni, B., and Sveinbjörnsdottír, A. E.: What controls the isotopic composition of Greenland surface snow?, Clim. Past, 10, 377–392, doi:10.5194/cp-10-377-2014, 2014.

Steffensen, J. P., Andersen, K. K., Bigler, M., Clausen, H. B., Dahl-Jensen, D., Fischer, H., Goto-Azuma, K., Hansson, M., Johnsen, S. J., Jouzel, J., Masson-Delmotte, V., Popp, T., Rasmussen, S. O., Röthlisberger, R., Ruth, U., Stauffer, B., Siggaard-Andersen, M. L., Sveinbjornsdottir, A. E., Svensson, A., and White, J. W.: High-resolution Greenland ice core data show abrupt climate change happens in few years, Science, 321, 680–684, 2008.

Steinhilber, F., Beer, J., and Fröhlich, C.: Total solar irradiance during the Holocene, Geophys. Res. Lett., 36, L19704, doi:1029/2009GL040142, 2009.

Vinther, B. M., Andersen, K. K., Hansen, A. W., Schmith, T., and Jones, P. D.: Improving the Gibraltar/Reykjavik NAO index, Geophys. Res. Lett., 30, 2222, doi:10.1029/2003GL018220, 2003.

Vinther, B. M., Andersen, K. K., Jones, P. D., Briffa, K. R., and Cappelen, J.: Extending Greenland temperature records into the late eighteenth century, J. Geophys. Res.-Atmos., 111, D11105, doi:10.1029/2005JD006810, 2006a.

Vinther, B. M., Clausen, H. B., Johnsen, S. J., Rasmussen, S. O., Andersen, K. K., Buchardt, S. L., Dahl-Jensen, D., Seierstad, I. K., Siggaard-Andersen, M. L., Steffensen, J. P., Svensson, A., Olsen, J., and Heinemeier, J.: A synchronized dating of three Greenland ice cores throughout the Holocene, J. Geophys. Res.-Atmos., 111, D13102, doi:10.1029/2005JD006921, 2006b.

Vinther, B. M., Clausen, H. B., Fisher, D. A., Koerner, R. M., Johnsen, S. J., Andersen, K. K., Dahl-Jensen, D., Rasmussen, S. O., Steffensen, J. P., and Svensson, A. M.: Synchronizing ice cores from the Renland and Agassiz ice caps to the Greenland Ice Core Chronology, J. Geophys. Res.-Atmos., 113, D08115, doi:10.1029/2007JD009143, 2008.

Vinther, B. M., Buchardt, S. L., Clausen, H. B., Dahl-Jensen, D., Johnsen, S. J., Fisher, D. A., Koerner, R. M., Raynaud, D., Lipenkov, V., Andersen, K. K., Blunier, T., Rasmussen, S. O., Steffensen, J. P., and Svensson, A. M.: Holocene thinning of the Greenland ice sheet, Nature, 461, 385–388, 2009.

Vinther, B. M., Jones, P. D., Briffa, K. R., Clausen, H. B., Andersen, K. K., Dahl-Jensen, D., and Johnsen, S. J.: Climatic signals in multiple highly resolved stable isotope records from Greenland, Quaternary Sci. Rev., 29, 522–538, 2010.

Weißbach, S., Wegener, A., and Kipfstuhl, J.: Snow accumulation in North Greenland over the last millennium, in: Towards an interdisciplinary approach in earth system science, edited by: Lohmann, G., Meggers, H., Unnithan, V., Wolf-Gladrow, D., Notholt, J., and Bracher, A., Springer Earth System Science, London, 197–205, 2015.

Werner, M.: Vergleichende Studie ueber die Verteilung vulkanogener Spurenstoffdepositionen in Nord-Ost-Groenland, Diplom, Institut fuer Umweltphysik, Heidelberg, 85 pp., 1995.

White, J. W. C., Barlow, L. K., Fisher, D., Grootes, P., Jouzel, J., Johnsen, S. J., Stuiver, M., and Clausen, H.: The climate signal in the stable isotopes of snow from Summit, Greenland: Results of comparisons with modern climate observations, J. Geophys. Res.-Oceans, 102, 26425–26439, 1997.

Wilhelms, F.: Leitfähigkeits- und Dichtemessung an Eisbohrkernen, Reports on Polar and Marine Research, 191, Alfred Wegener Institute for Polar and Marine Research, Bremerhaven, 1996.

Wood, K. R. and Overland, J. E.: Early 20th century Arctic warming in retrospect, Int. J. Climatol., 30, 1269–1279, 2010.

Wood, K. R., Overland, J. E., Jónsson, T., and Smoliak, B. V.: Air temperature variations on the Atlantic-Arctic boundary since 1802, Geophys. Res. Lett., 37, L17708, doi:10.1029/2010GL044176, 2010.

Zielinski, G. A.: Use of paleo-records in determining variability within the volcanism–climate system, Quaternary Sci. Rev., 19, 417-438, 2000.

- 66 -

6.3 The unusual recent warming trend in northern Greenland

S. Weißbach, S. Kipfstuhl, J. Freitag, M. Hörhold, G. Lohmann and T. Laepple

The following points will be worked on before submission:

- Compare results to global climate model outputs
- Studying the reasons of the 1930/40 warm event (ETCW)
- Make clear whether recent warming can be explained by natural variability
- Determine common intervals of smoothing, slopes and diffusion calculations and adjust figures and recalculate histograms

1   The unusual recent warming trend in northern Greenland

2   S. Weißbach[1], S. Kipfstuhl[1], J. Freitag[1], M. Hörhold[1], G. Lohmann[1,2], T. Laepple[3], *[4]

3

4   [1] Alfred Wegener Institute Helmholtz Centre for Polar and Marine Research, Bremerhaven,
5   Germany

6   [2] MARUM – Center for Marine Environmental Sciences, University of Bremen, Bremen, Germany

7   [3] Alfred Wegener Institute Helmholtz Centre for Polar and Marine Research, Potsdam, Germany

8   [4] Contributions Centre Ice Climate, Niels Bohr Institute, University of Copenhagen, Denmark

9

10

11   **Summary paragraph**

12   Greenland currently shows record warm temperatures, early melting season, area-wide melting[1–
13   [4] and a loss in mass of the ice sheet[5,6]. To assess these findings it is necessary to set the recent
14   temperature values into historical context. However, instrumental temperature records are
15   short-termed and geographically sparse. Millennium reconstructions exist but they merge
16   different proxies and instrumental datasets and thus might be biased towards underestimating
17   past changes. Further, they are not specific for Greenland. Here we provide the most
18   comprehensive ice-core compilation of Greenland allowing us to reconstruct the millennium
19   climate signal in an unprecedented quality. The gradient of the actual warming is not unusual
20   while recent values haven´t been found comparable during the last thousand years. It shows that
21   the recent warming is unusual in the context of the last millennium.

22

23   Main

24   The recent global air temperature has a clear warming trend[7]. The high latitudes are known to
25   be extra sensitive to a rise in temperature[7,8]. Recent instrumental records show, that during the
26   20th century the air temperature over land in the Arctic rises by up to 5 °C[9] which is about twice
27   as fast as temperature in lower latitudes[10,11]. Satellite observations show a huge loss in mass for
28   Greenland during the last years[5,6], surface melting at higher altitudes on the Greenland Ice Sheet,

29 extremely in 2012[1-4], and a decline in Arctic sea ice cover[12,13], which all pretends an ongoing

30 warming trend in air temperature.

31 The recent values have to be set in context of natural variability to definitely assess the observed

32 Arctic trend[14]. However, there is a lack in Arctic temperature data. Instrumental temperature

33 data are too short in time and cannot be used to reconstruct preindustrial climate variability,

34 and no Arctic annual one-proxy record of the necessary length exists until now. Another

35 problem is the merge of different proxy-record sources, as they are associated with calibration

36 uncertainties as well as seasonal bias. Tree-ring records for example are summer proxies and

37 cannot represent the evolution of annual mean values in Greenland[15]. Single-spot studies carry

38 high local noise (e.g. NGRIP) and are not representative for a larger area. Local noise is assumed

39 to be so high in low accumulation rate sites that it possibly hides the Holocene climate

40 variability.

41 In our study we use stable water isotopes as a proxy of temperature. This method is well

42 established in ice core studies[16,17]. Enriched $\delta^{18}O$ values are interpreted as warmer temperatures

43 whereas depleted values are referred to colder temperature conditions.

44 In our new approach, we used 16 instead of one, equally distributed firn cores over northern

45 Greenland (fig.1). By stacking we reduce the local noise[18] and show the result to be correlated to

46 temperature time series of coastal stations (methods). The stack proofs to be representative for

47 decadal temperature variability (methods). Our stacked record covers more than the last 1000

48 years (2011-775 C.E.) back in time and extends till 2011. By that, it is possible to set the recent

49 trend into the context of natural climate variability.

50 The annual stacked $\delta^{18}O$ record has the three most enriched values (from highest to third

51 highest) in the years 2002, 2009 and 2001 C.E. and the three most depleted (from most depleted

52 to third) annual values in 810, 1265 and 862 C.E.

53 We see a clear warmer medieval time, a positive extreme event around 1400-1450 C.E. and a

54 colder Little Ice Age which is ended by the recent warming. The decadal natural variability is

55 reflected in the stacked record which is by now not possible to show with climate models. Clearly

56 observable from the stack is for example a warm event around 1930/40 C.E. which is attributed

57 to the Early Twentieth Century Warming (ETCW). This event is explained by anomalies in the

58 atmospheric flow. A low NAO and a blocking situation over Greenland were likely causing the

59 warm years.

60 The last decade (2002-2011) has compared to the mean of the meteorological reference interval

61 (1961 - 1990 C.E.) which is used in this study as reference interval, a 0.97 ‰ higher mean value.

62   Using following the α-value of 0.67 regarding Johnsen et al[19], this is equal to a warming of about
63   1.45°C which can be comparably found in a stacked record of the coastal DMI automatic weather
64   stations in Greenland[20] (+1.62°C). Even warmer than the last decade and any other covered
65   decade in our stacked firn core record was 1997 to 2006 (~1 ‰, +1.5°C).

66   There is a first downward (from approx. 950 C.E.) than upward (to approx. 1950 C.E.) long-term
67   trend in the stacked firn core data. We observe more enriched $\delta^{18}O$ values since about 1850 C.E.
68   The $\delta^{18}O$ stack shows a clear increasing trend since about 1980 C.E. This start is about 15 years
69   later than the start of rising in the global mean temperature (fig. 2).

70   To exclude that the different core number changes our findings we calculated a stack of a
71   constant max. core number (7 records, 2011-1372 C.E.), which is used in further calculations
72   (methods).

73   Assessing the recent trend two facts are of interest: the gradient of the trend and the absolute
74   level of the values.

75   The gradient of the recent rise is not unusual and can be found comparable during the last years
76   (e.g. around 1400 and 1860 C.E.) (fig.3). The trend of the most recent 20 years has only the fourth
77   steepest slope of the 11-year running mean record.

78   However, the level of the values is unusual. The distribution of the annual stacked values makes
79   the abnormality of the recent values clear. High values occurred during the 1420-event but all
80   values of the last 15 years are significantly higher compared to the 1961-1990 mean (fig.3). The
81   three highest values are younger than 2000 C.E. Most of the values higher than the 2-sigma
82   interval are values of the last 15 years. This is at variance with studies which show that the recent
83   values are within the natural variability. One example is the study of Kobashi et al.[21] which
84   however covers 4000 years back in time while our study only goes back to 775 C.E., further our
85   stacked data includes more latest values.

86   The recent values have already been on a high level before 1980 C.E. when the rise started. That
87   is why the values rise up to an unusual high level. Before the recent rise the Greenland and global
88   temperature records are more or less independent. However, since 1980 they show same positive
89   trend. We suppose that the anthropogenic effect affects the Greenland temperatures now,
90   additional to the already natural high level. This is an important information to predict future
91   temperature values in the right way, as proxy data also show the natural decadal variability
92   which is still underestimated by climate models. Later than global, but the anthropogenic effect
93   is now also obvious in the Arctic temperatures.

94   With the presented data it is for the first time possible to definitively show and asses the recent

95   warming trend from a one-proxy record over the last more than 1000 years on a decadal time

96   scale. The abnormality of the recent values can now be verified by a record of large regional

97   representativity. We can say that the last years in Greenland were the abnormal warmest in the

98   last millennium. Further we can exclude the rise to be an artefact of other than climatic reasons.

99   The northern Greenland firn cores can close the Arctic gap in the worldwide measuring network

100 for a more representative global mean temperature and to help to verify climate model outputs.

101

102 **REFERENCES**

103 1. Hanna, E. *et al.* Atmospheric and oceanic climate forcing of the exceptional Greenland ice
104   sheet surface melt in summer 2012. *Int. J. Climatol.* **34,** 1022–1037 (2014).

105 2. Rignot, E., Velicogna, I., van den Broeke, M. R., Monaghan, A. & Lenaerts, J. T. M.
106   Acceleration of the contribution of the Greenland and Antarctic ice sheets to sea level rise.
107   *Geophys. Res. Lett.* **38,** L05503 (2011).

108 3. Nghiem, S. V. *et al.* The extreme melt across the Greenland ice sheet in 2012. *Geophys. Res.*
109   *Lett.* **39,** L20502 (2012).

110 4. Tedesco, M. *et al.* Evidence and analysis of 2012 Greenland records from spaceborne
111   observations, a regional climate model and reanalysis data. *The Cryosphere* **7,** 615–630 (2013).

112 5. Khan, S. A. *et al.* Sustained mass loss of the northeast Greenland ice sheet triggered by
113   regional warming. *Nat. Clim Change* **4,** 292–299 (2014).

114 6. Shepherd, A. *et al.* A Reconciled Estimate of Ice-Sheet Mass Balance. *Science* **338,** 1183–1189
115   (2012).

116 7. IPCC. *Climate Change 2013: The Physical Science Basis. Contribution of Working Group I to the*
117   *Fifth Assessment Report of the Intergovernmental Panel on Climate Change*. (Cambridge
118   University Press, 2013).

119 8. Walsh, J. E. Intensified warming of the Arctic: Causes and impacts on middle latitudes. *Glob.*
120   *Planet. Change* **117,** 52–63 (2014).

121 9. IPCC. Climate Change 2007: *The Physical Science Basis. Fourth Assessment Report of the*
122   *Intergovernmental Panel on Climate Change.* (Cambridge University Press, 2007).

123 10. Knutson, T. R. *et al.* Assessment of Twentieth-Century Regional Surface Temperature Trends
124   Using the GFDL CM2 Coupled Models. *J. Clim.* **19,** 1624–1651 (2006).

125 11. Delworth, T. L. & Knutson, T. R. Simulation of Early 20th Century Global Warming. *Science*
126   **287,** 2246–2250 (2000).

127 12. Comiso, J. C., Parkinson, C. L., Gersten, R. & Stock, L. Accelerated decline in the Arctic sea
128   ice cover. *Geophys. Res. Lett.* **35,** L01703 (2008).

129   13. Serreze, M. C., Holland, M. M. & Stroeve, J. Perspectives on the Arctic's Shrinking Sea-Ice
130   Cover. *Science* **315,** 1533–1536 (2007).

131   14. Tingley, M. P. & Huybers, P. Recent temperature extremes at high northern latitudes
132   unprecedented in the past 600 years. *Nature* **496,** 201–205 (2013).

133   15. Esper, J. *et al.* Orbital forcing of tree-ring data. *Nat. Clim. Change* **2,** 862–866 (2012).

134   16. Vinther, B. M. *et al.* Climatic signals in multiple highly resolved stable isotope records from
135   Greenland. *Quat. Sci. Rev.* **29,** 522–538 (2010).

136   17. Masson-Delmotte, V. *et al.* Recent changes in north-west Greenland climate documented by
137   NEEM shallow ice core data and simulations, and implications for past-temperature
138   reconstructions, *The Cryosphere*, **9**, 1481-1504, (2015).

139   18. Fisher, D. A., Reeh, N. & Clausen, H. B. Stratigraphic noise in time series derived from ice
140   cores. *Ann. Glaciol.* **7,** 76–83 (1985).

141   19. Johnsen, S. J. Stable isotope profiles compared with temperature profiles in firn with historical
142   temperature records. Proc. of symp. on isotopes and impurities in snow and ice, *Int. Assoc.*
143   *Hydrol. Sci. Commission of Snow and Ice, I. U. G.G. XVI, Genera Assembly, Grenoble Aug. Sept.*
144   *1975, IAHS-AISH Publication* **118,** 388–392 (1977).

145   20. Cappelen, J. Greenland - DMI Historical Climate Data Collection 1784-2014, Danish
146   Meteorological Institute, Copenhagen, 1-97 (2015).

147
148   21. Kobashi, T. *et al.* High variability of Greenland surface temperature over the past 4000 years
149   estimated from trapped air in an ice core. *Geophys. Res. Lett.* **38,** L21501 (2011).
150
151   22. Rohde, R. et al. Berkeley earth temperature averaging process, Geoinfor Geostat: An
152   Overview, **1:2**, 1-13, (2013).

153

154   **Figures**
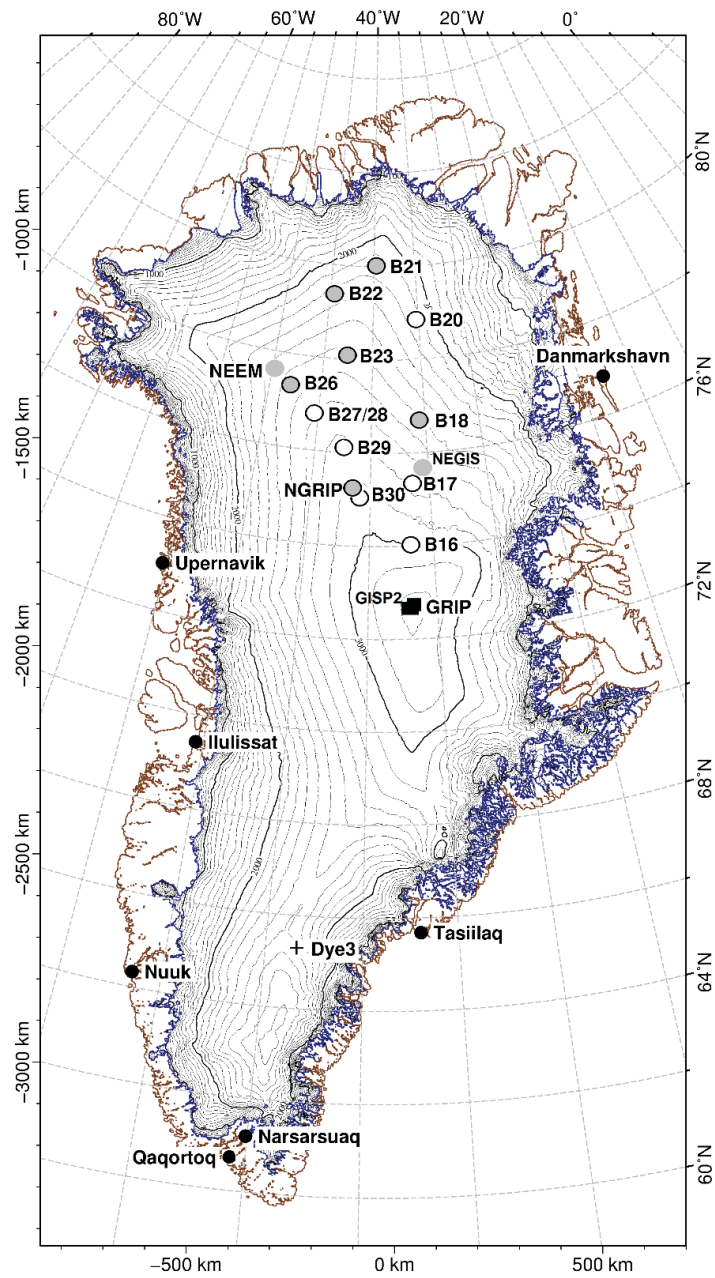
155

156   **Fig. 1** Overview drill sites. Black circles mark drill site positions of cores from the AWI NGT
157   traverse 1993/1995, grey dots mark drill sites of cores drilled 2011/20012. Black squares mark older
158   drills used in this study. With crosses are deep drill sites market for orientation and black dots
159   show settlements with longer DMI temperature measurements.
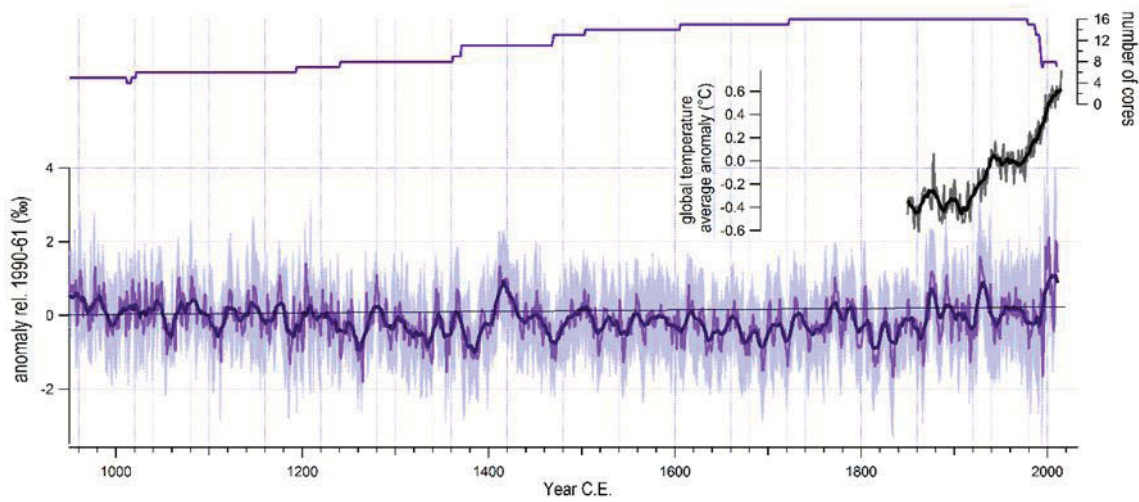
Fig.2 Anomalies (relative to 1990-1961 C.E.) of the stacked annual northern Greenland $\delta^{18}O$ data (thick: 11-year running mean, violet: annual values, light violet: ±1 standard deviation. The number of stacked cores is given at top. In gray the global mean temperature anomaly record[21] (relative to 1980-1950 C.E.) (thick: 11-year running mean, thinner: annual) is displayed.

179   a)
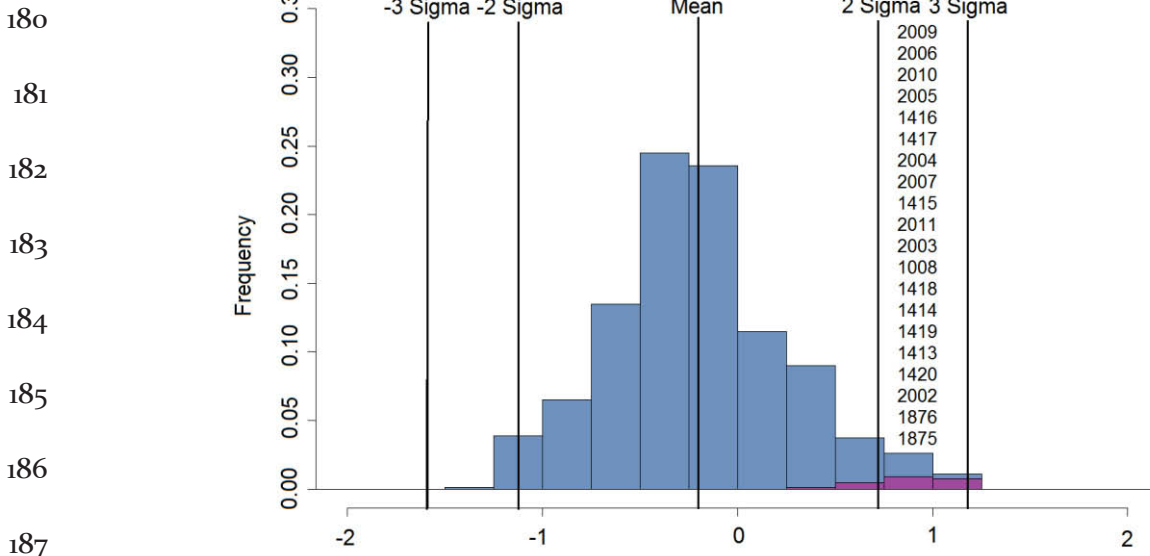
188   b)
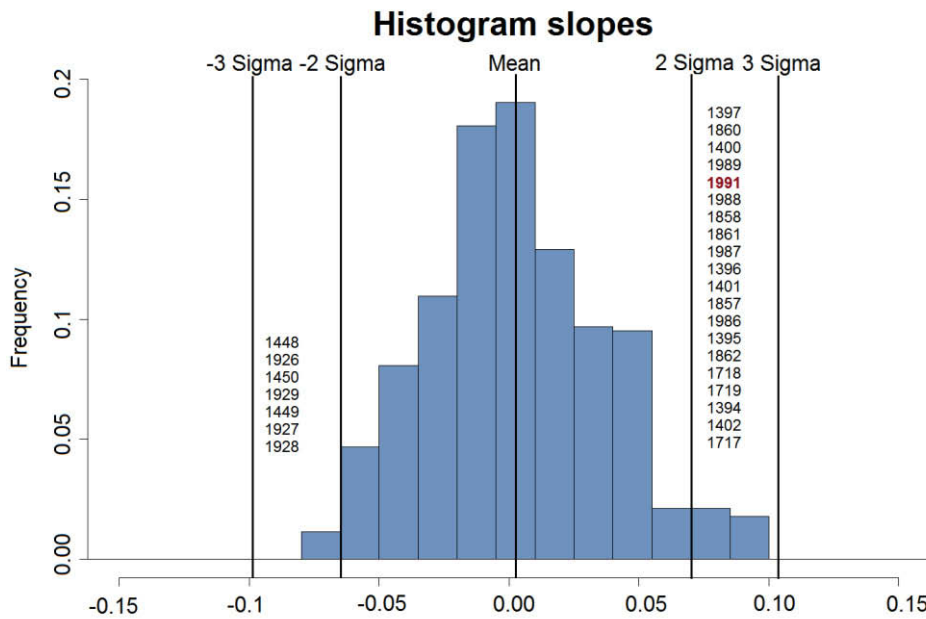
189

190   **Fig. 3** Abnormity of recent temperatures from histograms.

191   Histogram (2011-1372 C.E.) of a) the 11-year running mean smoothed stacked record with constant

192   core number (highlighted in violet are the values of the last 15 years) and b) linear regression

193   slopes of 20 year intervals of the same record.

194   The years with the highest values and the start year interval with steepest slopes are given in

195   order with the warmest and steepest years at top.

196

197   **Methods**

198   **Stacking the data**

199   The annual δ¹⁸O values of 16 ice core records from northern Greenland were stacked to a mean
200   record.

201   First 5 NGT 93/95 records (B18, B21, B22, B23, B26) (Weißbach et al., 2016) and the NGRIP record
202   (Vinther et al., 2006) were extended to the recent years by the data of the NGT-update cores
203   drilled in the years 2011 and 2012 (not published data). For their overlapping interval the annual
204   values of the NGT-update records were used. There was no mean calculated for the overlapping
205   interval to not smooth the amplitude of variability.

206   Additional to the in total used 11 NGT 93/95 records, NGRIP and their updated records the
207   annual records of GRIP (Vinther et al., 2010), GISP2 (Grootes and Stuiver, 1997), NEGIS
208   (Vallelonga et al., 2014) and NEEM (Masson-Delmotte et al., 2015) were used to calculate a
209   representative stack for northern Greenland.

210   The annual anomalies relative to their mean of 1961-1990 C.E. have been averaged to calculate
211   the stack.

212   **Stack with constant core number**

213   As the records used to calculate the stack are of different lengths also a second stack with a
214   constant number of records was calculated. Therefore the annual NGRIP, B18, B21, B22, B23,
215   NEEM and NEGIS records were stacked. Two of the seven records (NEEM and NEGIS) were
216   continued by other records (B27/28 and B17) of comparable variance and with adjusted mean
217   values to extend their length to the same time interval. The so produced stack and the stack with
218   different core numbers are of high similarity (r = 0.95). However, for further calculations the
219   stack of constant core number was used.

220   **Finding right smoothing interval and boundary value method**

221   The stacked δ¹⁸O record was smoothed to take into account for dating uncertainties. To find the
222   best method to do so, correlations to a stacked record of DMI southern Greenland coastal
223   temperature data were made. We tested for different time intervals and different filter types
224   (Gaussian and moving average) as well as 3 different alternatives (1) minimum norm, 2)
225   minimum slope, 3) minimum roughness) according to Mann (2004) to account for the
226   boundary-value problem. We find the highest correlation coefficients for the records performing
227   a 9-year running mean average padding the series with values using the methods of minimum

228   slope beyond the boundaries. That method pad the series with the values within one filter width

229   of the boundary reflected about the time boundary and continues in that way the rising trend.

230   Using the results of this study we decided to use an 11-year running mean and padding the record

231   by continuing the rising trend before for further calculations.

232
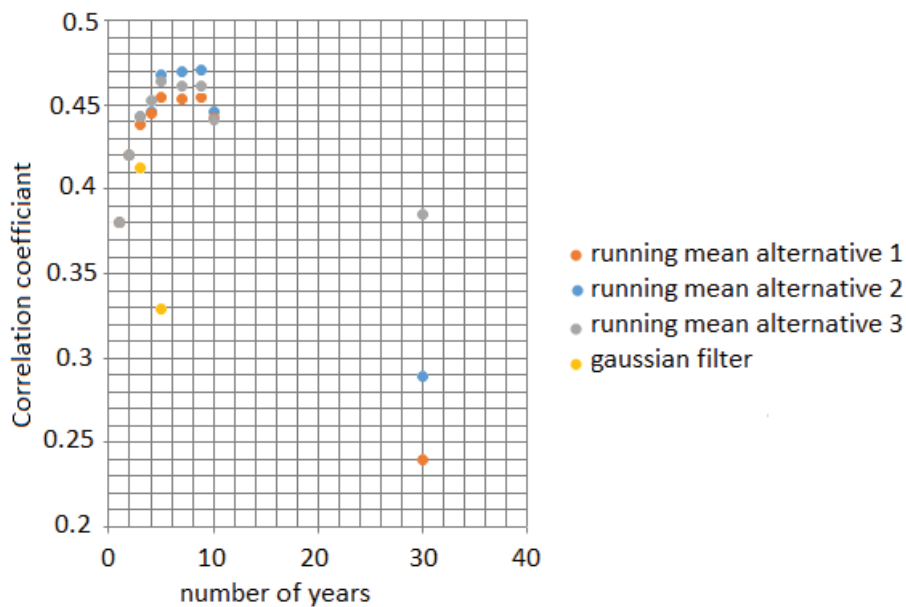
233

234   **Fig. 4** Correlation of DMI coastal temperature data and stacked $\delta^{18}O$ northern Greenland ice

235   core data. The correlation coefficients for different tested smoothing methods (colors) and

236   different filter widths are shown.

237

238   **Representativity studies**

239   To check the spatial representativity of the stack we correlated the data to reanalysis data (20C).

240   We find high correlations between the stacked $\delta^{18}O$ record and the gridded $\delta^{18}O$ temperature

241   data for whole Greenland. This supports our statement that the stack is at least representative

242   for northern Greenland. Also high correlation coefficients were found for the subtropics but not

243   to northeast Pacific or Asia.
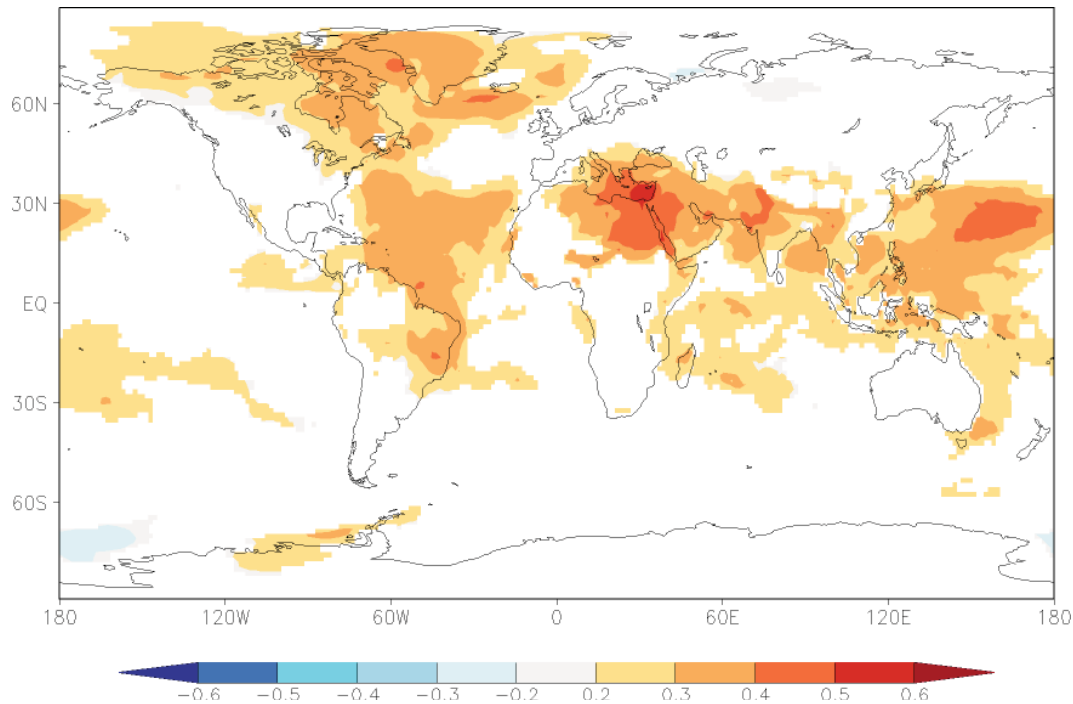
Fig.5 Correlation map of 20C temperature data and stacked northern Greenland δ¹⁸O data.

Exclusion of other factors causing the recent values to be unusually high

There are several factors that might be influence the annual $\delta^{18}O$ vales. In the following we discuss the main points: $\delta^{18}O$ diffusion, dating uncertainty and core number, which might be change the extraordinary values after 1980 C.E.

Diffusion

Diffusion smooths the high frequency changes in $\delta^{18}O$ data. Regarding Johnsen et al. (2000) the annual mean data is unaffected by that smoothing and only the sub-annual differences are reduced. However, we checked that fact by using an 8 cm w.eq. long Gaussian filter to smooth the high-resolution records of each of the individual cores. The filter length was chosen as an extreme but realistic case following the study of Johnsen et al. (2000). The filter is constantly used for the total length of the individual records to calculate the extreme. In reality the filter length should be decrease with depth because further down in the ice core the real diffusion has already been carried out. From the filtered high-resolution records annual means were calculated and the resulting annual records stacked to one record.

Our results show, that the 30-year running mean is not affected by the diffusion experiment.

Smaller differences are in the annual data, which might be are because of the chosen extreme case.

264

265
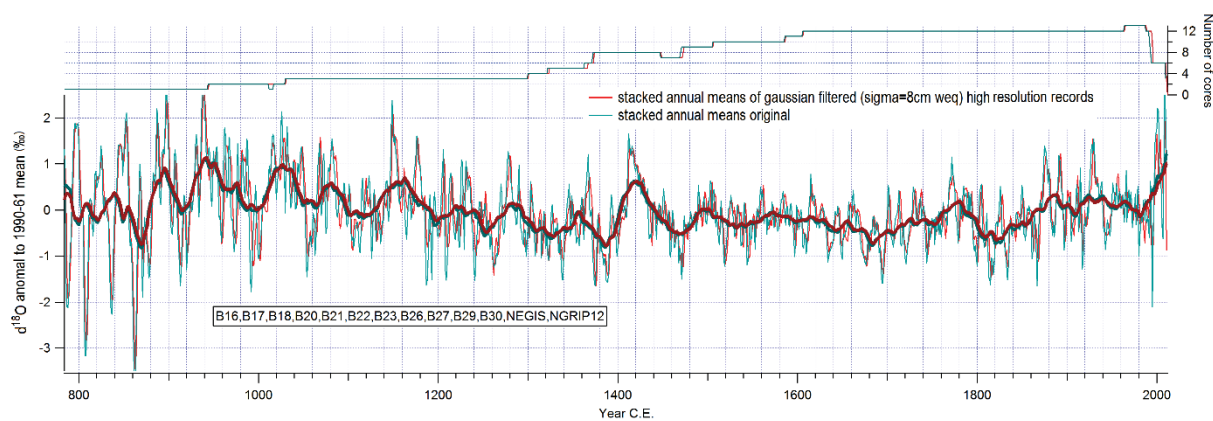
Fig.6 Stacked records of northern Greenland δ¹⁸O values. In red the high-resolution records have been filtered before stacking their annual records (thin: annual values, thick 30-year running mean. In red the stack of the unfiltered, original diffused values is given (thin: annual values, thick: 30-year running mean). At top the number of cores used to produce the stack is given.

270

Dating uncertainty

Annual layer counting, especially in low accumulation rate areas as northern Greenland, are most certain for the youngest years and get more uncertain with age. Therefore it could be the case that the annual amplitude is reduced with age because of the increasing dating uncertainties. That would result in an unrealistic assessment of the recent amplitudes compared to the older ones.

We performed a MonteCarlo method to check if the dating uncertainty can explain the high recent annual amplitudes and cause the trend which is interpreted as a recent warming trend. With the mean accumulation rate and known standard deviation from the original layer counted results at each drill site we calculated 1000 random Gaussian distributed annual accumulation rates for each site. We used those accumulation rate records to calculate annual δ¹⁸O means. From the 1000 runs we calculated the annual standard error/deviation at each drill site. The mean annual standard deviation is then used for an error band. We added the annual standard error to the mean value of all records relative to the 1961-1990 mean.

The band has an increasing trend also since 1980 C.E. The random counted stacked record has unusual high recent values as well. This suspends the increasing dating uncertainty with depth as a factor causing the abnormal recent high annual values obvious from our northern Greenland stacked record.
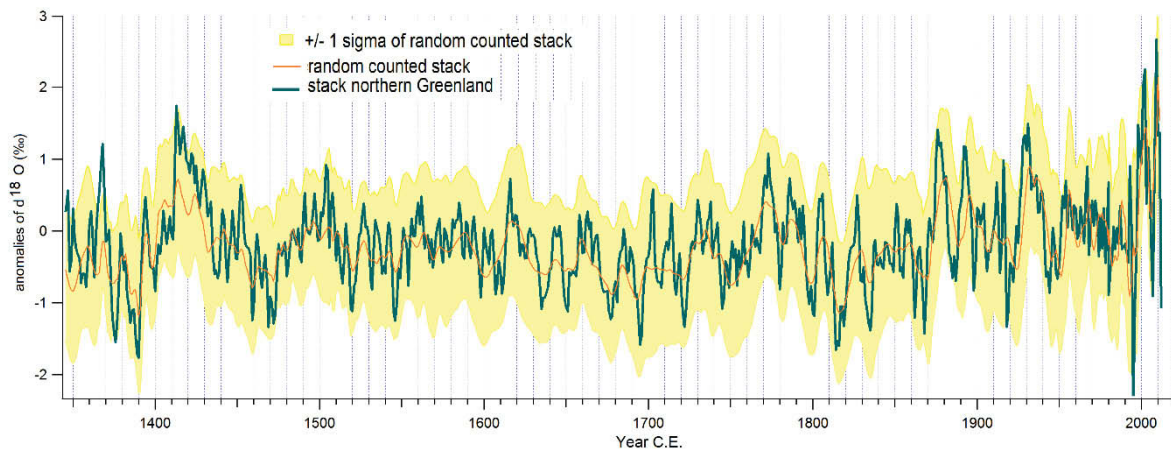
Fig. 7 Original stacked record (petrol) and the resulting stack of the same records randomly counted (thin orange line, +/- 1 standard deviation error band given in yellow).

Number of cores

The number of stacked records defines by definition the standard error. The result of a higher number of records is more precise. As our stack has a higher number of records starting about 1400 and ending 1995 compared to other intervals we check the argument of different core number by stacking only those records of same length. The resulting stack has the same characteristics as the original with is of different core numbers.

References methods

Grootes, P. M. and Stuiver, M.: Oxygen 18/16 variability in Greenland snow and ice with 10–3- to 105-year time resolution, J. Geophys. Res. Oceans, 102, 26455-26470, 1997.

Johnsen, S. J., Clausen, H. B., Cuffey, K. M., Hoffmann, G., Schwander, J., and Creyts, T.: Diffusion of stable isotopes in polar firn and ice : the isotope effect in firn diffusion. In: Physics of Ice Core Records:, Hokkaido University, 2000.

Mann, M. E.: On smoothing potentially non-stationary climate time series, Geophys. Res. Lett., 31, L07214, 2004.

Masson-Delmotte, V., Steen-Larsen, H. C., Ortega, P., Swingedouw, D., Popp, T., Vinther, B. M., Oerter, H., Sveinbjornsdottir, A. E., Gudlaugsdottir, H., Box, J. E., Falourd, S., Fettweis, X., Gallée, H., Garnier, E., Gkinis, V., Jouzel, J., Landais, A., Minster, B., Paradis, N., Orsi, A., Risi, C., Werner, M., and White, J. W. C.: Recent changes in north-west Greenland climate documented by NEEM shallow ice core data and simulations, and implications for past-temperature reconstructions, The Cryosphere, 9, 1481-1504, 2015.

Vallelonga, P., Christianson, K., Alley, R. B., Anandakrishnan, S., Christian, J. E. M., Dahl-Jensen, D., Gkinis, V., Holme, C., Jacobel, R. W., Karlsson, N. B., Keisling, B. A., Kipfstuhl, S.,

318   Kjær, H. A., Kristensen, M. E. L., Muto, A., Peters, L. E., Popp, T., Riverman, K. L.,
319   Svensson, A. M., Tibuleac, C., Vinther, B. M., Weng, Y., and Winstrup, M.: Initial
320   results from geophysical surveys and shallow coring of the Northeast Greenland Ice
321   Stream (NEGIS), The Cryosphere, 8, 1275-1287, 2014.
322   Vinther, B. M., Clausen, H. B., Johnsen, S. J., Rasmussen, S. O., Andersen, K. K., Buchardt, S. L.,
323   Dahl-Jensen, D., Seierstad, I. K., Siggaard-Andersen, M. L., Steffensen, J. P., Svensson,
324   A., Olsen, J., and Heinemeier, J.: A synchronized dating of three Greenland ice cores
325   throughout the Holocene, J. Geophys. Res.-Atmos., 111, D13102, 2006.
326   Vinther, B. M., Jones, P. D., Briffa, K. R., Clausen, H. B., Andersen, K. K., Dahl-Jensen, D., and
327   Johnsen, S. J.: Climatic signals in multiple highly resolved stable isotope records from
328   Greenland, Quat. Sci. Rev., 29, 522-538, 2010.
329   Weißbach, S., Wegner, A., Opel, T., Oerter, H., Vinther, B. M., and Kipfstuhl, S.: Spatial and
330   temporal oxygen isotope variability in northern Greenland – implications for a new
331   climate record over the past millennium, Clim. Past, 12, 171-188, 2016.

332

6.4 Using ice core and weather station observations to construct a spatial map of δ¹⁸O and temperature for present-day Greenland

A-K. Faber, B.M. Vinther, <u>S. Weißbach</u>, S. Kipfstuhl, N.O. Ørum

Using ice core and weather station observations to construct a spatial map of $\delta^{18}O$ and temperature for present-day Greenland

A-K Faber[1]**, B. M. Vinther** [1]**, S. Weissbach**[2]**, S. Kipfstuhl** [2]**, N. O. Ørum** [1]

[1]Centre for Ice and Climate, Niels Bohr Institute, University of Copenhagen, Juliane Maries Vej 30, 2100 København Ø, Denmark.

[2]Alfred-Wegener-Institut, Helmholtz-Zentrum für Polar- und Meeresforschung, Bremerhaven, Germany

Key Points:

- A database is created from 326 observations from ice core and weather stations at Greenland
- The spatial distribution of T and d18O are described by means of elevation and latitude
- Gridded maps of temperature and d18O are created for Greenland

Corresponding author: Anne-Katrine Faber, `akfaber@nbi.ku.dk`

–1–

Abstract

This study presents a comprehensive database of ice core and weather station data from Greenland. Based on time series within the period 1890-2014, present day annual and seasonal mean values are computed for 326 locations in Greenland. The database comprises measurements of near-surface temperature, ice core borehole temperature, accumulation, precipitation, $\delta^{18}O$, δD and d-excess. The values are compared to existing re-analysis and gridded data products for Greenland.

Based on multiple linear regression it is found that for present-day, the spatial distribution of annual mean δ^{18}O of Greenland precipitation can be described using linear parameterizations of the form $\delta^{18}O_{ann} = a * elev_{site} + b * lat_{site} + c$ with $R^2 = 0.98$. Similarly present-day annual mean surface temperature can be described as $T_{ann} = a * elev_{site} + b * lat_{site} + c$ with $R^2 = 0.93$. It is not possible to express the spatial distribution of accumulation data using the same approach. Thorough analysis of geographical subregions of the data reveals that both the temperature and $\delta^{18}O_{ann}$ decrease with elevation at different rates in the west and in the east of Greenland. Differences in the rate of temperature and $\delta^{18}O_{ann}$ decrease with elevation are also observed between coastal regions and high elevation regions.

The parameterizations are combined with a digital elevation model of Greenland to create the first data-based gridded map of δ^{18}O of precipitation for Greenland and the first gridded map of Greenland temperature where ice core borehole temperatures are included. The map of δ^{18}O is corrected for residuals errors and the robustness of the parameterizations in space and time are assessed.

1 Introduction

Ice cores form a cornerstone in the study of past climates. Isotopic measurements of the layers of past snowfall contained in the ice cores provide a vertical timeline of past climate conditions stored in the ice [*Dansgaard*, 1964; *Johnsen et al.*, 1989; *Vinther et al.*, 2010]. The isotopic composition of the Greenland precipitation comprises information of fractionation processes during the moisture pathway from source to deposition (e.g. [*Steen-Larsen et al.*, 2011; *Bonne et al.*, 2014]).

Climatic influences of the isotopic composition of Greenland snow can be studied using isotope-enabled general circulation models (GCMs). Such models are GCMs with an additional isotope module that simulates the isotopic fractionation processes throughout the hydrological cycle. This has the advantage that all physical processes influencing the isotopic fractionation in the model are known. Water isotope modules are available as a feature in several state-of-the-art atmosphere or fully coupled general circulation models (GCMs), earth system models (ESMs) and regional models; GISS [*Jouzel et al.*, 1987; *Schmidt et al.*, 2007]; ECHAM [*Hoffmann et al.*, 1998; *Werner et al.*, 2011, 2016], LMDZ [*Risi et al.*, 2010], GSM [*Yoshimura et al.*, 2008], CAM [*Lee et al.*, 2007; *Noone*, 2003], Hadley GCM [*Tindall et al.*, 2009], GENESIS[*Mathieu et al.*, 2002],MIROC[*Kurita et al.*, 2011], iLOVECLIM [*Roche*, 2013], SPEEDYier [*Dee et al.*, 2015], REMO-iso [*Sturm et al.*, 2005], RSM [*Yoshimura et al.*, 2010], SAM [*Blossey et al.*, 2010] and COSMO [*Pfahl et al.*, 2012].

Model validation of an isotope-enabled model yield crucial information on strength and weaknesses of the given model. Such model validation needs to be done globally and for the region of interest. The Greenland ice core records play a key role in benchmarking paleo-climate model simulations and therefore Greenland and specifically the Greenland Ice Sheet (GrIS) is a region of specific interest for isotope modeling. Model evaluation is therefore essential, however the weather and isotope observations from Greenland are limited in both time and space. This challenges the data-foundation for an isotope-enabled model validation for Greenland.

Weather observations from Greenland comprise the following:

Temperature and precipitation observations (Danish Meteorological Institute (DMI) *Cappelen et al.* [2013a,b], coastal observations and few GrIS). Temperature and isotopic composition of precipitation (Global Network of Isotope Precipitation (GNIP), coastal observations). Near surface air temperature (Greenland Climate Network (GC-Net) *Steffen and Box* [2001], GrIS observations). Near surface air temperature (Programme for Monitoring of the Greenland Ice Sheet (PROMICE) *van As et al.* [2011], observations from GrIS and outlet glaciers).

Before 1995, the main part of long-term instrumental records comes from coastal weather stations. Since 1995, the air temperatures at the Greenland Ice Sheet have been monitored by an increasing network of automatic weather stations (AWS).

Ice core records provide an excellent opportunity to expand the spatial and temporal coverage of isotopic composition of precipitation, accumulation and borehole temperatures at Greenland. [*Johnsen et al.*, 1989; *Vinther et al.*, 2010]. Borehole temperatures provide isotope-independent temperature reconstructions of the Greenland Ice Sheet [*Dahl-Jensen et al.*, 1998]. The temperature of a borehole close to the surface (normally measured at either 10 or 20 m depth) is used to represent the present-day annual mean temperature at the ice core site [*Johnsen et al.*, 1989].

Gridded maps of climate observations provide a tool for easier model-data comparison. For Greenland, surface mass balance studies have used ice core data as a foundation for accumulation maps [*Calanca et al.*, 2000; *Ohmura and Reeh*, 1991; *Bales et al.*, 2009; *Burgess et al.*, 2010; *Shen et al.*, 2012]. Similarly gridded maps of Greenland temperature have been created using weather station data [*Steffen and Box*, 2001; *Fausto et al.*, 2009], yet none have included ice core borehole data. So far maps of isotopic composition of precipitation (e.g. $\delta^{18}O$) have not been created for Greenland.

Knowledge of the spatial distribution of present-day Greenland conditions is essential in order to conduct inter-model and model-data comparison. Inherently, this requires a dataset where trends in data, natural variability, data uncertainties and spatial representation of regional differences must be considered.

The main objective of this study is to exploit the opportunities of combining weather station and ice core data in order to describe the spatial variations in present-day climate and isotopic conditions. This approach covers both conditions of coastal and interior regions of Greenland. The manuscript is structured as follows; (1) A comprehensive collection of ice core data and meteorological observations are combined into a dataset of mean values for present-day Greenland. (2) Parameterizations of the spatial distribution of respectively temperature and δ^{18}O are constructed based on the linear dependency on elevation and latitude. Sensitivities of the parameterization coefficients are tested using selected subsets of data. (3) Spatial gridded maps of surface temperature and δ^{18}O for Greenland are created using the parameterizations and refined by correcting for the residuals. (4) Robustness testing is conducted to assess the robustness of the mean data and the parameterizations in space and time.

The combination of the database and the gridded maps constitute a framework for isotope-model performance testing for Greenland. The gridded maps are model-independent data-transparent products, which aim to supplement, rather than replace, the original data and allow analysis of the spatial features of the data.

2 Data description

A database is generated based on annual and seasonal means of data spanning the time period 1890-2014 from ice cores and meteorological observations in Greenland. Note that each dataset covers slightly different time periods; Ice core data covers the period 1890-2010, DMI data covers respectively 1890-2012 and 1958-2012, PROMICE covers 2007-2014, GC-net covers 1995-2014, and GNIP covers 1961-2013. Mean values are chosen over individual time se-

–3–

110 ries of each location in order to facilitate model-data comparison with modeled mean values

111 and yield a representation of the spatial distribution of the values.

112 Mean values are computed for temperature, precipitation, accumulation, $\delta^{18}O$, δD and

113 d-excess. These parameters are selected as they are all important for isotope modeling and be-

114 cause many long-term time series exist that cover a wide spatial range.

115 A complicating factor for this dataset is that no period exists for which there is data from

116 all different locations. Therefore the combined data synthesis is based on data that represent

117 different subsets of time periods within the full time period 1890-2014. This years spanning

118 this time period was chosen as a compromise between the length of time and the number of

119 records that span the period.

120 The mean values of the data are collected in a common dataset with geospatial infor-

121 mation and metadata. This dataset is available in both Excel spread sheet and netCDF format.

122 The netCDF format has several advantages. It is universally readable, self-described and widely

123 used in the modeling community. Details on the measurements for the different types of data

124 are described in the following.

2.1 Greenland ice core data

126 The ice core data consist of measurements from 185 different ice cores, firn core and

127 snow pit drillings. All measurements span different subsets of time within the period 1890-

128 2010. The period 2011-2014 is not covered in this data set. pit studies of data less than 2 years

129 are excluded from this study. Cores from the North Greenland Traverse (NGT) [*Weissbach et al.*,

130 2016] span larger time periods.

131 The measurements obtained from the ice cores are mean annual $\delta^{18}O$, δD and d-excess.

132 Also mean annual accumulation values from the ice core sites are included as well as the tem-

133 perature of the borehole from 10 m or 20 m depth. This is used to represent annual mean tem-

134 peratures at the ice core site [*Johnsen et al.*, 1989]. The time span that an ice core record cov-

135 ers varies depending on the depth of the ice core and the year of drilling. In this study all cores

136 are treated independently thus no stacking and extension of several cores are conducted. This

137 implies that each ice core record cover different time periods.

138 The ice core measurements are conducted by analyzing the discrete ice core samples cut

139 in a given resolution (e.g. 2.5 or 5 cm). The mean annual accumulation for the full available

140 time periods are computed based on data from *Buchardt et al.* [2012]. Here the accumulation

141 is estimated by counting the annual layers in the ice core [*Hammer et al.*, 1978] and correct

142 the layer thickness for density changes with depth [*Herron and Langway Jr*, 1980; *Dansgaard*

143 *and Johnsen*, 1969] (see *Buchardt et al.* [2012] for details).

144 The annual mean isotopic composition is computed using isotope measurements and the

145 annual layer counting to obtain individual means of the given annual layer weighted with re-

146 spect to the amount of samples for the given year, and hereafter compute the annual mean val-

147 ues of $\delta^{18}O$, δD and d-excess. This is done for all annual layers within the time period of in-

148 terest 1890-2010. At the time of this analysis, no accurately dated ice core data was avaliable

149 for years after 2010. The number of samples per ice core is included in the database.

150 A total of 14 ice cores from this study have data resolved in half-year time resolution,

151 respectively representing winter and summer values. This data origins from *Vinther et al.* [2010]

152 and seasonal data from the NEEM core is added. All seasonal resolved data are diffusion cor-

153 rected to account for the dampening of the annual oscillations in $\delta^{18}O$ signal post deposition

154 for the upper 60 meter of firn [*Johnsen et al.*, 2000]. In cases with summer melt layers, the

155 signal obtained from traditional diffusion correction is distorted. The only seasonal resolved

156 cores that experience frequent summer melting are Dye 3 and Renland. Thus these cores have

157 been corrected using a different approach and dampening of the climate signal in these cores

–4–

must therefore be considered, however the high accumulation rates at the sites ensure that a signal is still detected [*Vinther et al.*, 2010].

Borehole temperatures present the direct memory of the past surface temperature, this approach is isotope-independent and have shown to be a useful source of past climate information from the Greenland Ice Sheet [*Dahl-Jensen et al.*, 1998]. The temperatures of the ice at different depths depend on the geothermal heat flow density (heat flux), the ice-flow pattern, and the past surface temperatures and accumulation rates. Because seasonal variations of the borehole temperature are smoothed out at 10 m and below, this temperature represents the annual mean surface temperature, following *Johnsen et al.* [1989]. In this study we assume that the temperature represent the mean of the last 3 years before the measurement. E.g. a measurement from summer 1975 represents the annual mean surface temperatures of the years 1972-1974. Borehole temperatures have the advantages that they are undisturbed by instrumental calibration drift in time.

Precipitation intermittency and post-depositional processes influence the ice core data. The robustness of the accumulation from ice core records relies on the assumption that the ice core represents the annual mean accumulation amount and isotopic composition of the snow at the given location. However temporal averaging of the core data is found to minimize the effects of wind drift, sastrugi formation and dating errors on the accumulation [*Mosley-Thompson et al.*, 2001; *Cogley*, 2004]. Therefore it is here assumed that temporal averaging also minimizes changes in the isotopic composition, seasonality of the precipitation, and diffusion [*Johnsen et al.*, 2000].

2.2 Danish Meteorological Institute (DMI) datasets

This dataset consist of temperature (dry bulb air temperature) and precipitation from automatic and manned weather stations primarily located near the Greenland coast. This comprises a total of 90 stations, spanning different subsets of time within the years 1890-2012. The data have been collected by the Danish Meteorological Institute (DMI), and two datasets are included. The long-term historical climate data collection (1890-2012) [*Cappelen et al.*, 2013a] and weather observations (1958-2012) [*Cappelen et al.*, 2013b]. Precipitation is here only included where available for the long-term measurements, in total 8 stations. The weather stations have been operated with different degrees of automation over time. In cases where the location of the weather station has changed during the measurement period the coordinates of the location that covers the largest percentage of the time period is chosen. Coastal stations with missing elevation data are set to $20m$.

2.3 PROMICE dataset

This dataset consists of near surface air temperature data from 22 automatic weather stations (AWS) located on the mid and exterior part of the Greenland ice sheet. Stations are often in sets located close to each other either in the upper ablation zone near the equilibrium line or at a lower elevation in the ablation zone. All stations are part of the Programme for Monitoring of the Greenland Ice Sheet (PROMICE) lead by the Geological Survey of Denmark and Greenland (GEUS) (e.g. [*van As et al.*, 2011]). The data used here cover the full time period from 2007 - 2014, with varying length of time series for the individual stations. The positions from 2015 are set as stations coordinates. Each station has two temperature sensors, the data from these are averaged and hereafter monthly means of the sensor-averaged daily means are used to compute seasonal and annual means of this data.

2.4 GC-Net dataset

This dataset consist of near surface air temperature data from 23 AWS located on the interior of the Greenland ice sheet. All stations are part of the Greenland Climate Network (GC-Net) [*Steffen et al.*, 1996; *Steffen and Box*, 2001]. Quality control procedures are applied to all

206 AWS data sets. The data used here cover the full time period from 1995-2014, with varying
207 length of time series for the individual stations. Data from four temperature sensors are av-
208 eraged and hereafter monthly means of the sensor-averaged daily means are used to compute
209 seasonal and annual means of this data.

210 ### 2.5 GNIP dataset

211 This dataset consists of 6 station measurements of isotope and meteorological coastal
212 observation from Greenland as part of the Global Network of Isotopes in Precipitation (GNIP)
213 network [*IAEA and WMO*, 2015]. The data includes data of δ^{18}O, d-excess and air temper-
214 ature. Due to the short time span of these records precipitation amount of these coastal sta-
215 tions is not included here and seasonal means are not computed.

216 ### 2.6 General data overview

217 The database includes a total of 326 different locations of observations. Here 185 ice
218 core locations on the Greenland ice sheet, 6 coastal GNIP stations, 43 ice sheet automatic weather
219 station locations (out of these 23 stations are from GC-Net and 22 from PROMICE). DMI data
220 comprises 90 weather and climate observations mainly from the coast. Overview of the num-
221 ber of different measurements are shown in table 1.

Number of observations

Datasets	No. of obs. ‖	T	Acc./Precip.,	δ^{18}O	δD	d-excess	$\delta^{18}O_{seasonal}$
Ice cores	185 ‖	77	101	153	41	40	14
DMI	90 ‖	81	8	0	0	0	0
PROMICE	22 ‖	17	0	0	0	0	0
GC-Net	23 ‖	19	0	0	0	0	0
GNIP	6 ‖	6	0	6	4	4	0
Total	326 ‖	200	109	159	45	44	14

222 **Table 1.** Number of observations for the dataset and for the individual variables in each of those data sets.
223 These numbers refer to the observations included in this analysis.

224 The main purpose of this database is to provide information on the spatial distribution
225 of present day mean conditions. Annual and seasonal mean values and standard deviations are
226 calculated for the entire timespan of the individual station or core site. Missing data is a chal-
227 lenge for weather stations at the Greenland Ice Sheet as the rough climate and remote loca-
228 tion of the stations complicates the maintenance and calibration of the stations. Therefore only
229 stations are included where monthly mean values, for all of the months, can be computed on
230 data from 3 months or more. The spatial range of the annual mean data varies greatly over
231 GrIS. The spatial range of the annual mean values of different data types is shown in table 2.

234 ## 3 Method

235 The created database is used to analyze the spatial characteristics of annual mean sur-
236 face temperature ($T_{surface}$), δ^{18}O and accumulation for Greenland. This is done by conduct-
237 ing multiple linear regression by means of latitude and elevation. Observations from nearby
238 but different drilling sites are treated independently. To represent the spatial variability of the
239 observations, no combination of core or stacking of data from several ice cores or observa-

–6–

Spatial range of variables

T [°C]	min	max
Ice cores	-32.9	-9.5
DMI	-29.7	2.6
PROMICE	-17.6	-1.7
GC-Net	-30.1	-5.8
GNIP	-17.6	1.7

Acc./Precip. [w.eq. m/yr.]	min	max
Ice cores	0.09	1.11
DMI	0.13	0.96

δ^{18}O [‰]	min	max
Ice cores	-39.59	-22.82
GNIP	-25.02	-11.17

δD [‰]	min	max
Ice cores	-304.9	-253.3
GNIP	-184.4	-87.5

d-excess	min	max
Ice cores	6.32	11.96
GNIP	2.76	11.23

$\delta^{18}O_{seasonal}$* [‰]	min	max
Ice cores	1.74	7.89

Table 2. Spatial range of the individual variables and data types. All values are computed based on annual mean values. Except $\delta^{18}O_{seasonal}$* computed as $\delta^{18}O_{summer}$-$\delta^{18}O_{winter}$.

tions is conducted. The sensitivity to individual datasets and geographical regions is tested by performing the regression analysis on the full data set as well as for different subgroups of data.

3.1 Spatial characteristics of temperature

Previous studies have described the spatial variability of the Greenland annual mean temperature using weather stations [*Ritz et al.*, 1996; *Steffen and Box*, 2001; *Fausto et al.*, 2009]. In order to provide the most extensive spatial and temporal coverage, all types of annual mean temperature data are treated similarly as representing the present-day mean surface conditions in Greenland.

–7–

248   The datasets used in this study comprise both borehole temperatures, near surface tem-
249 peratures from AWS at the GrIS and T_{2m} from coastal meteorological stations. In total 200
250 observations of temperature spanning both land and ice sheet regions. Borehole data from ice
251 cores is here for the first time included together with AWS observations. A dominant amount
252 of the total ice core borehole temperatures are measured in the years 1970-1995. Thus inclu-
253 sion of the borehole data aids to constrain the spatial variation of GrIS surface temperatures
254 to conditions before the recent warming. The advantages and difficulties that arise from us-
255 ing all types of temperature data to represent surface temperature are treated in the discussion
256 (see section 5).

        The resulting parameterization of the annual mean temperature T_{ann} in Greenland is found
using multiple linear regression, similar to *Ritz et al.* [1996]; *Steffen and Box* [2001]; *Fausto
et al.* [2009]. Thus we describe the surface temperature in Greenland as

$$T_{ann} = \mathbf{a} * elev_{site} + \mathbf{b} * lat_{site} + \mathbf{c} \tag{1}$$

257 where $elev_s$ and lat_{site} describes respectively the elevation and latitude of the site of the ob-
258 servation, the coefficients **a, b** and **c** determine the dependence of elevation, latitude and the
259 intercept value. This approach yield a description of annual mean temperature in Greenland
260 that associated with the expected radiative cooling of an air mass northwards and for higher
261 elevation. The advantage of this parameterization is the data-transparent, model-independent
262 approach, using only geographical parameters that are constant in time for present day timescales.

263   The sensitivity of the parameterization is tested for different geographical regions and
264 different data sets, thus also analysing the influence of different types of temperature measure-
265 ments. Regression analysis is also used to analyse regional differences in the regression of the
266 data. This is done by subgrouping the observations in regions determined by either latitude,
267 longitude or elevation, and hereafter test regional differences for one of these at a time. A caveat
268 of this approach is that this limits the range of elevation and latitude values which the subgroup-
269 regressions are based on. Therefore the subgroups are defined so that each subgroup includes
270 locations spanning a wide range of elevation and latitude. Results are shown in table 3. DMI
271 and GNIP data are combined in the same subgroup to improve statistics. All combination of
272 data sets show a good fit with data with values of $R^2 > 0.9$. The sensitivity to latitude are
273 within the range -0.79 to $-0.83\ °C/°N$ for all dataset combinations, except the PROMICE
274 dataset. A likely cause for this exception might be that many PROMICE stations are located
275 in association to outlet glaciers, where local climate conditions and glacial melt might be dom-
276 inating the temperatures.

277   GC-Net temperatures on the GrIS are higher than neighbouring borehole temperatures.
278 Multiple linear regression using all data except GC-Net yields comparable results to the all-
279 data parameter and thus we find that $a = -0.0076 \pm 0.0001\ °C/m$, $b = -0.78 \pm 0.02\ °C/°N$,
280 and $c = 49.38 \pm 1.52\ °C$ with $R^2 = 0.98$ and RMSE=1.77 $°C$ for 181 observations. Dif-
281 ferent coefficient values are achieved when ice core borehole temperatures are excluded from
282 the regression. Here $a = -0.0063 \pm 0.0001\ °C/m$, $b = -0.78 \pm 0.02\ °C/°N$, and $c =$
283 $49.19 \pm 1.46\ °C$ with $R^2 = 0.97$ and RMSE=1.44 $°C$ for 123 observations. Explanations
284 for this difference might be attributed to changes in GrIS temperature, differences in the ice
285 sheet surface temperature and the AWS near-surface temperature as well as temperature trends
286 as ice core boreholes temperature are measured mainly in before the period 1995 in contrast
287 to the AWS stations. Different regimes of temperature lapse rate for high, medium and coastal
288 elevation regions of Greenland [*Hanna et al.*, 2011], most likely a result of a transition from
289 moist-adiabatic to more dry-adiabatic lapse rate conditions with height might also explain the
290 different sensitivity.

292   The geographical distribution of the data is shown in tab.4. For elevation it is found that
293 high (elevation $2300 - 3300m$) and medium and low (elevation $0 - 1500m$) show $a_{high,elev.} =$
294 $-0.0080 \pm 0.0008°C/m$, $a_{low,elev.} = -0.0045 \pm 0.0005\ °C/m$ confirms that Greenland tem-
295 perature lapse rate depends on the elevation. At the same time the latitude coefficients b is within
296 the same range, and does not show a sensitivity to elevation regions. Different latitude sub-

–8–

Temperature parameterization coefficients

$$T_{ann} = a * elev_{site} + b * lat_{site} + c$$

	a [°C/m]	b [°C/°N]	c [°C]	R^2	# obs.	RMSE [°C]
Data set combinations						
Ice cores	-0.0096 ± 0.0005	-0.82 ± 0.04	57.46 ± 3.14	0.9	77	1.71
GC-Net	-0.0065 ± 0.0004	-0.83 ± 0.07	53.12 ± 5.49	0.96	19	1.55
PROMICE	-0.0069 ± 0.0007	-0.61 ± 0.05	38.84 ± 3.67	0.94	17	1.12
DMI + GNIP	-0.0063 ± 0.0002	-0.79 ± 0.02	49.71 ± 1.59	0.95	87	1.39
Ice cores + GC-Net	-0.0085 ± 0.0003	-0.81 ± 0.04	54.02 ± 3.07	0.91	96	1.96
Ice cores + PROMICE	-0.0086 ± 0.0002	-0.76 ± 0.03	50.78 ± 2.31	0.96	94	1.71
GC-Net+ PROMICE	-0.0069 ± 0.0003	-0.75 ± 0.05	48.04 ± 3.32	0.97	36	1.5
Ice cores + GC-Net + PROMICE	-0.0083 ± 0.0002	-0.78 ± 0.03	51.48 ± 2.38	0.95	113	1.89
Ice cores + DMI + GNIP	-0.0075 ± 0.0001	-0.78 ± 0.02	49.60 ± 1.54	0.98	164	1.73
GC-Net+PROMICE+DMI+GNIP	-0.0063 ± 0.0001	-0.78 ± 0.02	49.19 ± 1.46	0.97	123	1.44
Ice cores +PROMICE+DMI+GNIP	-0.0076 ± 0.0001	-0.78 ± 0.02	49.38 ± 1.52	0.98	181	1.77
Latitude						
North (> 75°N)	-0.0075 ± 0.0003	-0.76 ± 0.18	47.62 ± 14.52	0.92	56	2.53
Central (75°N -69°N)	-0.0077 ± 0.0002	-0.88 ± 0.14	57.59 ± 10.27	0.98	57	1.72
South (< 69°N)	-0.0074 ± 0.0001	-0.52 ± 0.05	32.52 ± 3.45	0.99	87	1.16
Longitude						
West (> 47°W)	-0.0065 ± 0.0002	-0.79 ± 0.03	50.3 ± 2.38	0.97	69	1.48
Central (47°W- 37°W)	-0.0074 ± 0.0002	-0.75 ± 0.03	47.62 ± 2.09	0.99	87	1.43
East (< 37°W)	-0.0078 ± 0.0003	-0.82 ± 0.09	51.85 ± 6.62	0.95	44	2.42
Elevation						
High (> 2300m)	-0.0080 ± 0.0008	-0.82 ± 0.04	53.82 ± 3.43	0.88	79	1.78
Medium and low (< 1500m)	-0.0045 ± 0.0005	-0.75 ± 0.02	47.23 ± 1.64	0.92	106	1.59
All non-coastal (> 500m)	-0.0087 ± 0.0002	-0.79 ± 0.03	53.13 ± 2.45	0.95	111	1.87
All data (the coefficients used in this study)	**-0.0075± 0.0001**	**-0.78 ± 0.02**	**49.53 ± 1.53**	**0.98**	**200**	**1.85**

Table 3. Temperature parameterization coefficients for different subsets of the full dataset.

–9–

Geographical distribution of observations

Elevation	Very high (> 2800 m)	High (2300 − 2800 m)	Medium (1500 − 2300 m)	Low (200 − 1500 m)	Coast (< 200 m)
	21.47 %	29.14 %	10.43 %	11.66 %	27.3 %

Latitude	North (> 75°N)	Central (75°N -69°N)	South (< 69°N)
	33.13 %	25.77 %	41.4 %

Longitude	West (> 47°W)	Central (47°W- 37°W)	East (< 37°W)
	27.91 %	53.37 %	18.71 %

Table 4. Geographical distribution of the observations.

groups (north, central and south) do not show changes in the temperature decrease with height. They all show values of a within the range -0.0074 to $-0.0077 \, °C/m$.

Interestingly, the data show a clear separation in eastern and western conditions. The eastern part of Greenland (here defined as longitude $< 37°W$) show significantly higher sensitivity to elevation with $a_{east} = -0.0087 \, °C/m$) than the western side (here defined as longitude $> 47°W$) $a_{west} = -0.0065 \, °C/m$. This difference is also found in other temperature studies [*Fausto et al.*, 2009; *Steffen and Box*, 2001] and might be a result of different air mass characteristics on the east and west sides of the ice divide of GrIS, respectively.

Fausto et al. [2009] argues that adding a longitudinal component to the temperature parameterization improves the match to observations. However, based on the results of *Buchardt et al.* [2012], we argue that in order to create a temperature parameterization with considerations on longitude, then the position of the observation in relation to the ice divide is more descriptive for the temperature characteristics than the absolute longitude coordinates. However such information was not provided in this database. To summarize, it is found that the above analysis of geographical subsets of the data reveals geographical differences in the sensitivity to temperature with elevation, both for different elevation regions and for the eastern and western side of the ice divide.

3.2 Spatial characteristics of $\delta^{18}O$

The spatial distribution of annual mean $\delta^{18}O$ ($\delta^{18}O_{ann}$) is described in terms of elevation and latitude, using the same approach as for temperature. From a physical perspective this empirical relation reproduce the two classical Greenland isotopic features; the elevation effect and the latitude effect [*Dansgaard*, 1964; *Johnsen et al.*, 1989; *Vinther et al.*, 2009]. Cooling of air masses with elevation and latitude, result in condensation, reduction on moisture content and distillation, and essentially the elevation and latitude effect on $\delta^{18}O$ is a result of this. Thus it is not surprising that temperature and $\delta^{18}O$ can be described using the same geographical parameters. The spatial variations of $\delta^{18}O_{ann}$ is described for Greenland precipitation as

$$\delta^{18}O_{ann} = \mathbf{a} * elev_{site} + \mathbf{b} * lat_{site} + \mathbf{c} \qquad (2)$$

–10–

where $elev_s$ and lat_{site} describes respectively the elevation and latitude of the site of the measurement and the coefficients **a, b** and **c** determines the dependence of elevation and latitude. The coefficients of $\delta^{18}O$ are estimated using multiple linear regression, results of the regression for all data and for test of subsets of the data are shown in tab. 5.

–11–

$\delta^{18}O_{ann}$ **parameterization coefficients**
$\delta^{18}O_{ann} = a * elev_{site} + b * lat_{site} + c$

	a [‰ / m]	b [°C/°N]	c [°C]	R^2	# obs.	RMSE [‰]
Data sets						
Ice cores	-0.0059 ± 0.0003	-0.66 ± 0.02	30.43 ± 1.77	0.90	153	1.3
Ice cores + GNIP	-0.0058 ± 0.0004	-0.65 ± 0.03	29.90 ± 1.51	0.93	159	1.33
GNIP (NB: only coastal data)	-0.062 ± 0.034	-0.66 ± 0.1	33.08 ± 7.86	0.93	6	1.98
Latitude						
North (> 75°N)	-0.0057 ± 0.0004	-0.53 ± 0.15	20.12 ± 12.17	0.79	62	1.64
Central (75°N -69°N)	-0.0063 ± 0.0003	-1.26 ± 0.10	75.26 ± 6.98	0.94	44	1.01
South (< 69°N)	-0.0057 ± 0.0002	-0.40 ± 0.08	12.83 ± 4.74	0.97	53	.60
Longitude						
West (> 47°W)	-0.0042 ± 0.0003	-0.70 ± 0.05	31.85 ± 3.73	0.95	14	0.60
Central (47°W- 37°W)	-0.0053 ± 0.0003	-0.66 ± 0.02	29.12 ± 1.43	0.95	113	1.09
East (< 37°W)	-0.0070 ± 0.0003	-1.05 ± 0.07	61.48 ± 5.36	0.96	32	1.09
Elevation						
High (> 2300m)	-0.0052 ± 0.0007	-0.66 ± 0.04	29.84 ± 3.27	0.89	131	1.3
All non-coastal (> 1825m)	-0.0059 ± 0.0003	-0.66 ± 0.02	30.43 ± 1.77	0.90	153	1.3
All data (the coefficients used in this study)	**-0.0058 ± 0.0004**	**-0.65 ± 0.03**	**29.90 ± 1.51**	**0.93**	**159**	**1.33**

Table 5. $\delta^{18}O_{ann}$ parameterization coefficients for different subsets of the full dataset.

–12–

319   The results of the regression using only the GNIP data should be interpreted with cau-
320 tion because all 6 data points are coastal, with a range of elevation spanning only $12 - 77$
321 m.a.s.l. In contrast the main part the ice core data origins from the high interior GrIS. Nev-
322 ertheless, it is interesting to note that GNIP and ice core data is comparably sensitive to lat-
323 itude changes, $b_{GNIP} = -0.66 \pm 0.1$ ‰/°N and $b_{icecores} = -0.66 \pm 0.2$ ‰/°N.

324   In agreement with the findings from the temperature data, the $\delta^{18}O_{ann}$ does not show
325 a sensitivity to elevation that changes with latitude. Here all values of the elevation coefficient,
326 a, are within the range -0.0057 - -0.0063 ‰/m. Also in agreement with temperature data,
327 the longitude regions show that differences exist between the characteristics on the western
328 and eastern side of Greenland. The eastern side (here defined as longitude $< 37°$W) show
329 significantly higher sensitivity to elevation with $a_{east} = -0.0087$ °C/m than the western side
330 (here defined as longitude $> 47°$W)

331   For regression on the western region data (longitude $> 47°$W) the coefficients are found
332 to be $a_{west} = -0.0042 \pm 0.0003$ ‰/m, $b_{west} = -0.70 \pm 0.05$ ‰/°N, and $c_{west} = 31.85 \pm$
333 3.73 ‰ with $R^2 = 0.95$ and RMSE=0.60 ‰ for 14 observations.

334   For the eastern region (longitude $< 37°$W) the sensitivities to both elevation and lat-
335 itude are respectively 1.7 and 1.5 times larger. Thus $a_{east} = -0.0070 \pm 0.0003$ ‰/m, $b_{east} =$
336 -1.05 ± 0.05 ‰/°N, and $c_{east} = 61.48 \pm 5.36$ ‰ with $R^2 = 0.96$ and RMSE=1.09 ‰ for
337 32 observations. While the regression is based on a low number of observations, the results
338 still clearly indicate there exist east-west differences in the $\delta^{18}O_{ann}$ values over Greenland.

339   ### 3.3 Spatial characteristics of accumulation

340   The accumulation and precipitation data yield an overview of the spatial distribution of
341 GrIS accumulation and coastal precipitation (see fig. 1). For the GrIS, accumulation is high-
342 est in the south, and especially southeast, with the highest value of accumulation rate 1.11 w
343 eq. m/year at the southeastern slope. Northern GrIS is the driest region, and present the low-
344 est accumulation rates down to 0.09 w.eq. m/year. Coastal weather stations have precipitation
345 rates in the range $0.13 - 0.96$ w.eq. m/year. As expected, it was not found possible to param-
346 eterize the spatial distribution of annual accumulation for the entire Greenland region by means
347 of elevation and latitude. Similar to *Buchardt et al.* [2012], we find that the characteristics of
348 the accumulation rate vary greatly between the different regions of Greenland.

354   ## 4 Spatial maps

355   ### 4.1 Method

356   Spatial maps of surface temperature and $\delta^{18}O$ are created. The following sequence of
357 steps is used to create the spatial maps:

358   **Creation of parameterization-based spatial map**

359   First the spatial distribution is described using the linear parameterizations from this study
360 (e.g. $T_{ann} = a * elev_{site} + b * lat_{site} + c$).

361   A uniform parameterization is used to describe the entire Greenland. Only elevation and
362 latitude information is required to compute the spatial maps. Here the digital elevation model
363 (DEM) by *Bamber et al.* [2001] provides gridded information on elevation and latitude of Green-
364 land, here remapped from 5 km resolution to 0.1 ° resolution using bilinear mapping.

365   **Computation of residuals**

366   Hereafter the differences between each observation and the corresponding value of the
367 nearest-gridpoint location in the data-only spatial map are computed

–13–

Precipitation [w.eq. m/year]

0.1 0.2 0.3 0.4 0.6 1 1.5 2
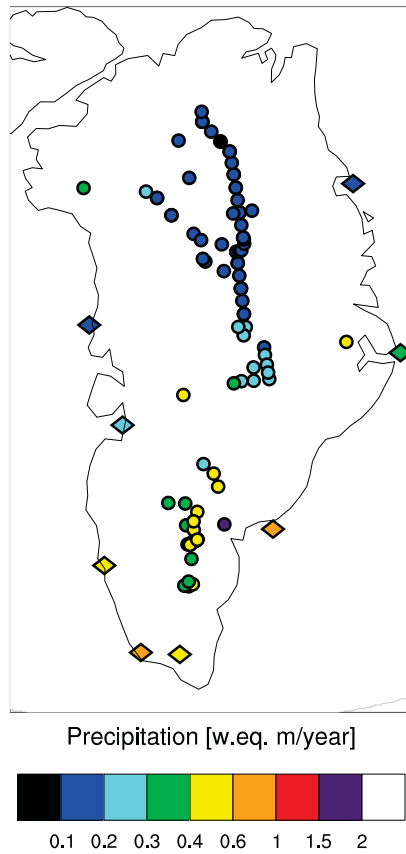
Figure 1.   *Accumulation and precipitation.*

This figure show the accumulation and precipitation data [w.eq m/year]. Here the symbols show the different data types. Circles represent ice core data, and diamonds represent DMI data. The colors of the symbols correspond to the annual mean value of the given observation. Note that the colorbar is not linear. See fig. 5 for a better overview of the spatial distribution of the data.

–14–

368   (e.g. $T_{res.} = T_{parm.} - T_{obs.}$).

369   **Elevation-correction of residuals**

370   An elevation-correction is applied to correct for the elevation differences between the
371   0.1 ° resolution DEM grid point elevation value and the true elevation of the each observa-
372   tional site. The elevation-correction is done using the empirical elevation dependencies found
373   in this study (e.g. for T_{ann}: $a = -0.0075°/m$ as in eq. 3).

374   **Creation of residual correction field**

375   A residual correction field is computed by fitting a surface, within the region

376     $58.5N - 84.5N$, $75W - 8W$, to the computed residual values. This is done using the
377   the algorithm "Surface Fitting using gridfit" by *D'Errico* [2005], MATLAB Central File Ex-
378   change, retrieved Dec 3, 2015.

379   **Creation of the residual-corrected spatial map**

380   The residual correction field is added to to the parameterization-based spatial map. This
381   yields a spatial map, based on a data-transparent and model-independent method, but corrected
382   for misfits data.

383   This method creates a gridded map, useful for model evaluation. Gridded fields are use-
384   ful to estimate variables in regions where observational data is scarce. While gridded data should
385   never be a replacement for the original data, the gridded data fields have many advantages in
386   terms of computing and visualizing model-data comparison. A gridded map of annual mean
387   data provides an overall spatial distribution of the annual means at the given region, but does
388   not represent any inter-annual or climate variations.

389   **4.2 Spatial map of surface temperature**

401   The spatial distribution of $T_{surface,ann}$ is described using multiple linear regression for
402   all available temperature data (200 locations). It is chosen to describe the temperatures for the
403   entire Greenland region using a uniform parameterization. Alternatively a different parame-
404   terization for different geographical subregions or different GrIS drainage basins (as in *Buchardt*
405   *et al.* [2012]) could have been used. However the small number of data per subgroup and the
406   varying representation of the full range of elevation within each subregion make the subregional
407   approach less favorable. Furthermore, combining the temperature parameterization of differ-
408   ent subregions into parameterization for the entire Greenland regions creates difficulties with
409   physical un-consistent discontinuities of values across borders. Results from this study show
410   that analysis of subregional parameterizations and datasets yield values of R^2 in the same range
411   as the regression value for all data, $R^2 = 0.98$. Therefore we argue that a more represen-
412   tative description of the spatial characteristics of Greenland temperature is achieved by span-
413   ning all data types and geographical subregions in the same parameterization.

    The resulting parameterization is given by

$$T_{surface,ann} = -0.0075 * elev_{site} - 0.78 * lat_{site} + 49.53 \qquad (3)$$

414   The standard error of the coefficients are $a = -0.0075 \pm 0.0001 \; °C/m$, $b = -0.78 \pm$
415     $0.02 \; °C/°N$, and $c = 49.53 \pm 1.53 \; °C$ with $R^2 = 0.98$ and RMSE=1.85 $°C$.

416   Using the linear relation between T_{ann} and elevation and latitude (eq. 3)

417   a parameterization-based spatial map of $T_{surface}$ is generated and shown in fig. 2 (a).
418   The residuals of the nearest-gridpoints values of the gridded maps ($T_{res.} = T_{parm.} - T_{obs.}$)
419   are shown fig. 2 (b). Coastal residual values are large for some observations, and the resid-
420   uals of nearby observations are not always similar in magnitude. There are two reasons for

–15–
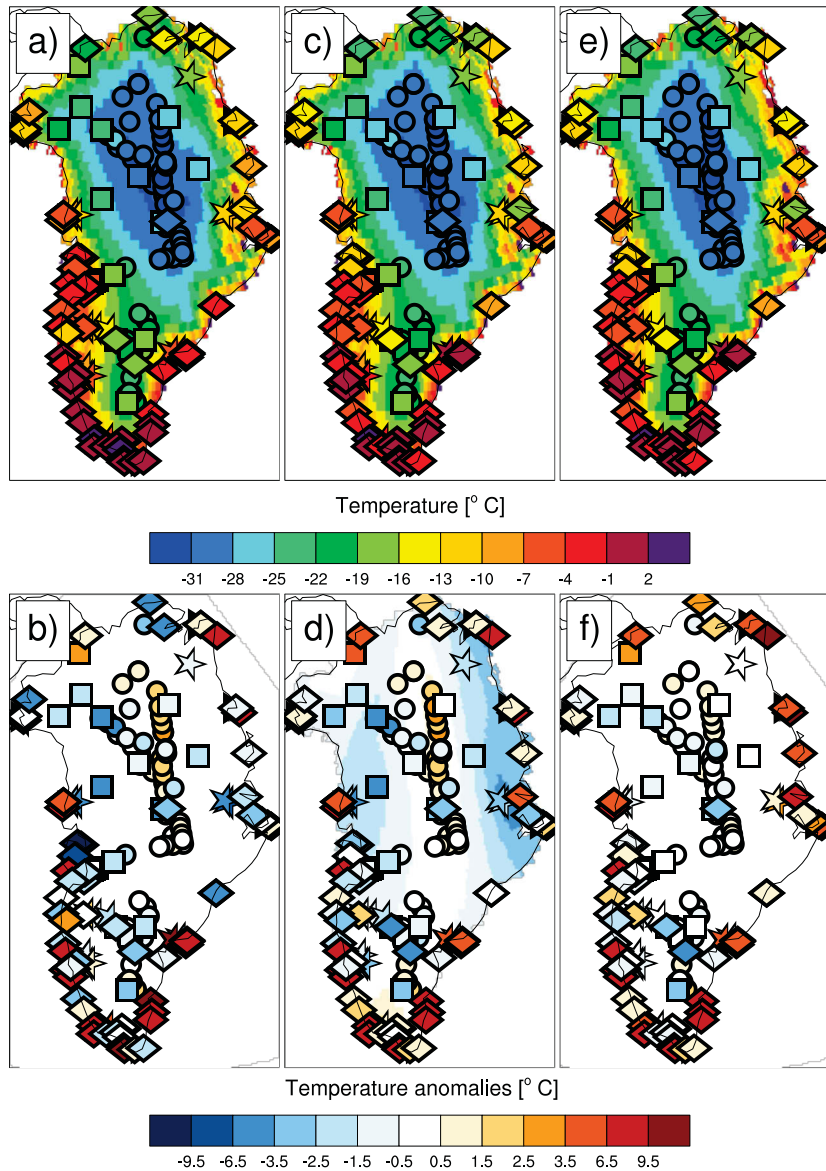
Figure 2. *Spatial maps of temperature for Greenland and residuals.*

This figure show the computed spatial map of $T_{surface}$ with and with out residual correction Residuals are for all plots calculated as $T_{res.} = T_{parm.} - T_{obs.}$. The symbols show the different data types. Circles represent ice core data, triangles represent GNIP data, squares represent GC-Net data, stars represent PROMICE data and diamonds represent data from DMI. The colors of the symbols correspond to the annual mean value of the given observation. a) Spatial map of temperature based on parameterization only. b) The residual values computed as shown as colors of the symbols. Blue (red) colors refer to points where the parameterization is too cold (warm) compared to observations. c) Spatial map $T_{surface}$ with elevation corrected observations. d) Residuals between map and elevation corrected observations. Contours show the computed residual correction field. e) Spatial map $T_{surface}$ with residual correction added f) Residuals of the corrected spatial map. Note that the colorbar is not linear. –16–

this. First, coastal temperature measurements of nearby sites might represent the regions in the local fjord system rather than the regional temperate, thus resulting in temperature differences with variations of 3-4 $°C$. Second, the values of elevations in the DEM can vary up to 500 m in nearby grid points thus resulting in temperature variations of nearby grid points of up to 3.75 $°C$.

All temperature observations (the values of the symbols) are elevation-corrected to match the nearest-gridpoint values of the DEM elevation using the empirical elevation dependency $a = -0.0075°/m$ from eq.3. These elevation-corrected temperatures are then compared to the spatial map based on the temperature parameterization (fig. 2 (c)). The elevation corrected residuals ($T_{res.,elev.corr.} = T_{parm.} - T_{obs.,elev.corr.}$) show the true range of the misfit between the generated spatial map and the observation. They range from -4.3 $°C$ to 9.8 $°C$.

A residual correction field is computed using the described "gridfit-algorithm". The "springs" regularization is used to improve the handling of neighbouring locations with alternating signs of temperature residuals. Elevation corrected residuals from coastal stations (the DMI and GNIP data) are not included in the residual correction field, due the non-systematic bias at the coast. The residuals are shown in fig. 2 (d). The contours of the residual correction field for temperature are also shown (note the reversed colors). The correction increases the temperature at the the lower elevation slopes of the GrIS and decreases the temperature at the high elevations, which in agreement with the spatial characteristics of temperature analysed for the sub-regions.

The spatial map is hereafter corrected for residuals by applying a the residual correction to the parameterization spatial map (fig. 2 (e))

Fig. 2 (f) show the remaining residuals after residual correction is applied to the spatial map

($T_{res.,corrected} = T_{parm.,corrected} - T_{obs.}$). It is seen that residual correction improves the fit of the map with observations over the GrIS, but the coastal locations are not improved. The range of all residuals are $-5.4°C$ to $12.3°C$. Overall, fig. 2 show that the spatial parameterization of T_{ann} over Greenland can be used to describe the spatial distribution of temperature for the GrIS at first order, however residuals remains.
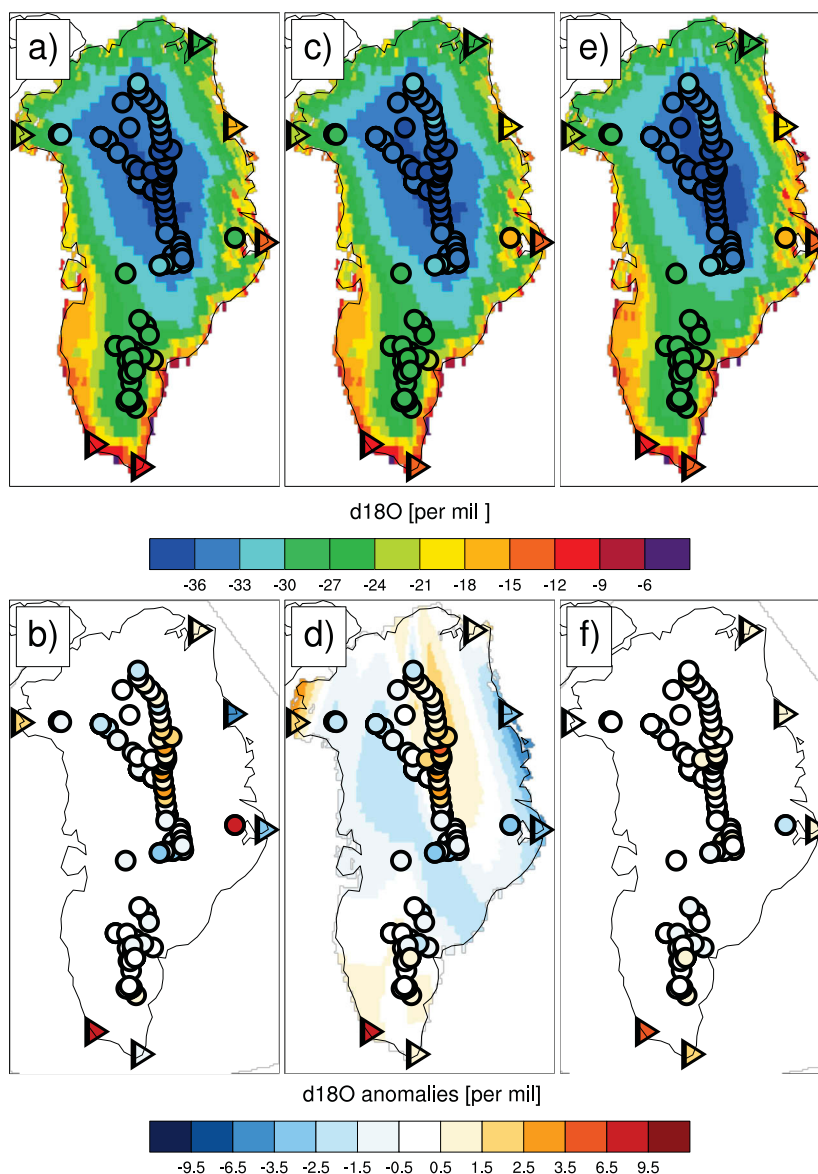
4.3 Spatial map of $\delta^{18}O_{ann}$

Techniques for creating global or regional gridded maps of isotopic distributions ("isoscapes") comprise spatial interpolation, objective mapping or clusters of regionalized climatic regression models [*Bowen and Revenaugh*, 2003; *Terzer et al.*, 2013]. For polar regions, $\delta^{18}O$ for Antarctica has been described using multiple linear regression[*Masson-Delmotte et al.*, 2008; *Wang et al.*, 2009] and Generalized Additive Modeling [*Wang et al.*, 2010]. Because of the different geographical configuration of Antarctica, distance to the coast and longitude was also included in these parameterizations. Because of the benefits of expressing the spatial distribution of $\delta^{18}O_{ann}$ using one parameterization describing the conditions for the entire Greenland region, the parameterization is thus created based on all data of $\delta^{18}O_{ann}$ and a given by

$$\delta^{18}O_{ann} = -0.0058 * elev_{site} - 0.65 * lat_{site} + 29.90 \tag{4}$$

where the standard error on the coefficients are $a = -0.0058 \pm 0.0004$ ‰/m, $b = -0.65 \pm 0.03$ ‰/°N, and $c = 29.90 \pm 1.51$ ‰ with $R^2 = 0.93$ and RMSE=1.33 ‰ for 159 observations

The gridded map of $\delta^{18}O_{ann}$ for Greenland, generated using eq. 4 is shown in fig. 3. The spatial map using only the parameterization is shown in fig. 3 (a). The residuals, for nearest non-missing grid point, is calculated as $\delta^{18}O_{res.} = \delta^{18}O_{parm.} - \delta^{18}O_{obs.}$. The residuals are within the range -3.55 ‰ to 7.56 ‰, these are shown in fig. 3 (b).

–17–

d18O [per mil]

-36 -33 -30 -27 -24 -21 -18 -15 -12 -9 -6

d18O anomalies [per mil]

-9.5 -6.5 -3.5 -2.5 -1.5 -0.5 0.5 1.5 2.5 3.5 6.5 9.5

Figure 3. *Spatial maps of $\delta^{18}O$ for Greenland and residuals.*

This figure show the computed spatial map of δ^{18}O with and with out residual correction. Residuals are for all plots calculated as $\delta^{18}O_{res.} = \delta^{18}O_{parm.} - \delta^{18}O_{obs.}$. The symbols show the different data types. Circles represent ice core data, triangles represent GNIP data. The colors of the symbols correspond to the annual mean value of the given observation. a) Spatial map of δ^{18}O based on parameterization only, b) The residual values are shown as colors of the symbols. Blue (red) colors refer to points where the parameterization is too negative (positive) compared to observations. c) Spatial map δ^{18}O with elevation corrected observations. d) Residuals between map and elevation corrected observations. Contours show the computed residual correction field. e) Spatial map δ^{18}O with residual correction added f) Residuals of the corrected spatial map. Note that the colorbar is not linear.

–18–

Elevation correction are applied to the values to match the values of the DEM elevation. Here the elevation dependency $a = -0.0058°/m$ from eq.4 is used. The elevation corrected values are shown in fig. 3 (c) and the residuals in fig. 3 (d). The effects of elevation correction is clearly seen for Renland at the east coast. This ice core is drilled on a small high plateau ice cap separated from the GrIS. The true elevation is much higher than described by the DEM. Due to the simplicity of the parameterizations not all observations ($\delta^{18}O_{obs}$) match the parameterized values ($\delta^{18}O_{parm.}$). The ice core residuals range from -3.2 ‰ to -4.4 ‰, and GNIP data from -2.7 ‰ to 7.0 ‰

The residual correction fields are applied to the spatial map of the parameterization (see fig. 3 (e)). As the regional biases are more systematic than for temperature, the "springs" regularizer is not applied in the gridfit routine in this case. Due to lack of near by eastern observations constraining the residual correction Renland was not included. As a control, the residuals of the corrected spatial map are computed. For ice core data they are within the range -2.2 ‰ to 2.4 ‰, and for GNIP data from 0.01 ‰ to 6.1 ‰. To conclude, fig. 3) show that the spatial distribution of $\delta^{18}O$ for Greenland can be described by means of elevation and latitude and remaining residuals are improved using the residual correction.

The plot of the residuals $\delta^{18}O_{res.}$ show an interesting structure in northern Greenland with east-west differences. West of the ice divide the $\delta^{18}O$ values of the ice cores are higher than suggested by the regression model and east of the ice divide the observed $\delta^{18}O$ values are lower than suggested by the regression, thus confirming the east-west differences found in the analysis of subsets of data in sec. 3.2. This suggest that other processes than depletion as a result of cooling with increasing latitude and elevation are important for $\delta^{18}O$ here.

5 Discussion

Based on data from a total of 326 locations at Greenland the spatial distribution of $T_{surface}$ and $\delta^{18}O$ are described by parameterizations. The uncertainty of the spatial regression are determined both by the uncertainty of the temporal mean of each observations and also by the uncertainty in the representation of the spatial distribution. In the following the data will be compared to other gridded products of temperature and precipitation. Here after the robustness of the parameterisations used for the generation of the spatial maps will be analysed and discussed.

5.1 Comparison to other gridded data and reanalysis products

5.1.1 4.6.1.1. Temperature

The gridded map of temperature is created using a combination of near surface and surface temperature. The resulting map is compared to commonly used gridded maps of temperature based on observations or reanalysis data (see fig. 4). These are the following: Observation-based gridded near-surface temperature map based on AWS data [*Fausto et al.*, 2009]. Reanalysis data of surface temperature (T_{skin}) and temperature at 2 meter height (T_{2m}) from ERA-interim (1979-2012) [*Dee et al.*, 2011]. A combination of reanalysis and regional model data for Greenland using RACMO (1957-2008) *Ettema et al.* [2009]. No elevation correction is applied.

Comparison with existing gridded fields of temperature show an overall agreement with observations and other gridded estimates, both in terms of spatial pattern and absolute values. The temperature data is a combination of surface-temperature (ice cores), near-surface temperature (PROMICE, GC-Net) and air temperature (the coastal stations; DMI and GNIP). This can explain why ice cores and AWS data from the ice sheet display different temperature even at location close to each other. Differences in temperatures due to atmospheric temperature inversion layers, length of time period and natural variability might also explain these dissimilarities.

–19–
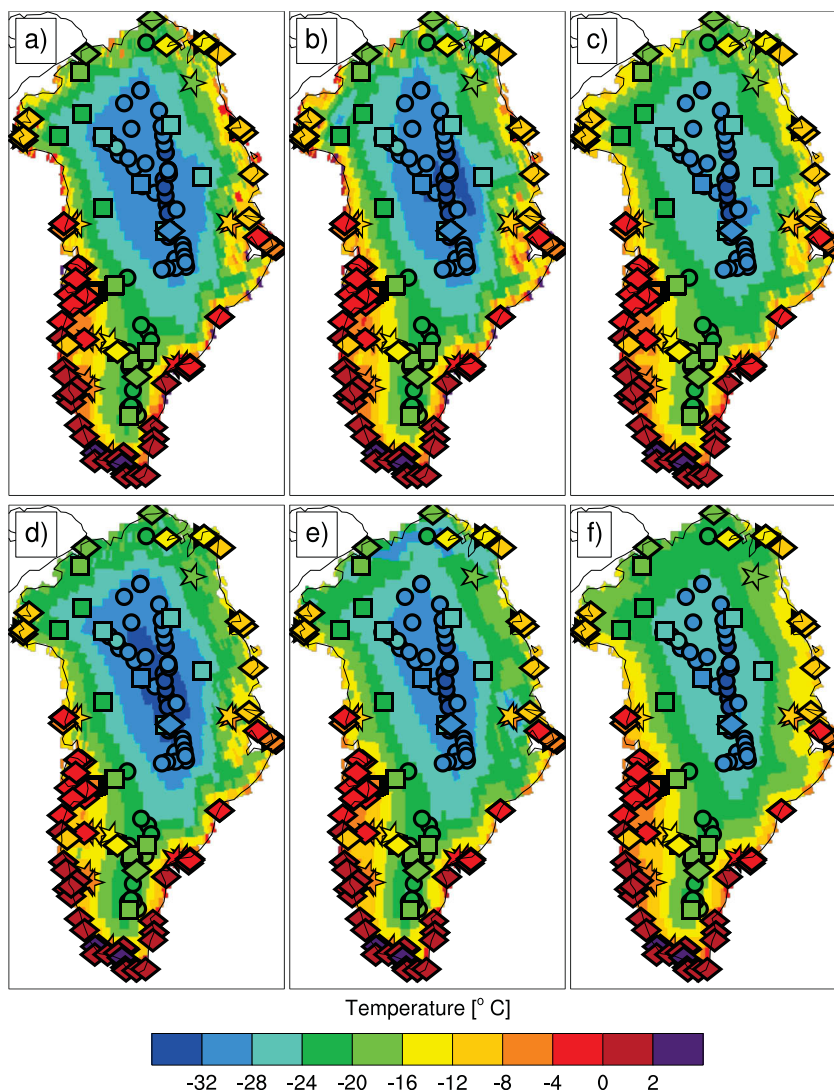
Figure 4. *Gridded temperature maps and data from this study compared to other gridded temperature estimates.*

This figure show annual mean temperature data from the observations compared to annual means of gridded data, reanalysis and regional model products. Here the symbols show the different data types. Circles represent ice core data, triangles represent GNIP data, squares represent GC-Net data, stars represent PROMICE data and diamonds represent data from DMI. The colors of the symbols correspond to the annual mean value of the given observation. a) The gridded annual mean near-surface temperature map from this study without residual correction, b) The gridded annual mean near-surface temperature map from this study with residual correction, c) Near surface annual mean temperature for present day from *Fausto et al.* [2009], d) Annual mean skin temperature from ERA-Interim (1979-2012). e) Annual mean T_{2m} from ERA-Interim (1979-2012). f) Annual mean skin temperature for RACMO (1957-2008) [*Ettema et al.*, 2009].

Interestingly the comparison of the point-data to the gridded temperature reveals that surface and near-surface temperature estimates for GrIS varies in a range of $2-4°$ C for high interior Greenland. The map of *Fausto et al.* [2009] T_{2m} is warmest. ERA-Interim $T_{surface}$ have very cold values at low elevation in the coastal northern tip of Greenland and colder than observations near mid-eastern area near Scoresbysund. This is not as clear in the T_{2m} fields. RACMO is in general the coldest at the interior of the ice sheet except for south dome at southern Greenland where ERA-interim is closer to the temperatures.

5.1.2 4.6.1.2. Accumulation and precipitation

Comparison between data from ice core accumulation, data from meteorological measurements of precipitation and gridded estimates of accumulation and precipitation requires considerations on the dissimilarities. Coastal data provide solid precipitation data not accumulation data and the relation between solid precipitation on the coast and accumulation from ice cores on the ice sheet is unknown. Steep coastal terrain, fjord systems and microclimatic differences might influence the precipitation for coastal stations. Wind drift and sastrugi formation might influence the accumulation records, and sublimation, melt and evaporation processes can influence comparison of accumulation records with re-analysis based precipitation estimates.

The accumulation data achieved from ice cores are compared to a selection of gridded maps of accumulation [*Burgess et al.*, 2010], precipitation (RACMO [*Ettema et al.*, 2009] and ERA-Interim [*Dee et al.*, 2011]), and "precipitation-evaporation" (P-E) (ERA-Interim [*Dee et al.*, 2011]). Results are shown in fig. 5. Results show that variations exist in the gridded estimates of accumulation, precipitation and P-E and their match with accumulation and precipitation data.

The accumulation map by *Burgess et al.* [2010] based on a calibration of PolarMM5 using a large selection of ice core and coastal data show, as expected accumulation values that match the ice cores (fig. 5 (a)). Both precipitation maps (fig. 5 (b and d)) have values lower than ice core accumulation for central northern Greenland. RACMO precipitation show good agreement with the accumulation ice core data near the southern part of the GrIS, but ERA-I precipitation is higher than accumulation from ice cores. However, as expected evaporation is more important in the warmer southern region and the P-E field for ERA-Interim (fig. 5 (c)) show a better match with accumulation data here. Melt of the ice sheet surface is more frequent and could potentially alter the accumulation rate. Due to the existing dry bias in precipitation for ERA-Interim, the northern regions become even drier when accumulation is compared to P-E.

Except for the calibrated map of *Burgess et al.* [2010], the coastal precipitation values do not match the gridded estimates. The coastal weather stations are often located in fjords and local conditions might be important here. However an inadequate representation of the steep Greenland topography might also explain the discrepancy.

5.2 Sensitivity to variability

The uncertainty of the spatial regressions are determined both by the uncertainty of the temporal mean of each observations and also by the uncertainty in the representation of the spatial distribution. Temporal variability of temperature and d18O will be discussed separately. Hereafter robustness testing of the parameterizations are conducted.

5.2.1 4.6.2.1 Variability of temperature

The parameterizations in this study uses temporal means for each observation. Each of these mean, span a subset of the full present-day time period 1890-2014. It is assumed that the mean values is representative of the full time period 1890-2014. However temperature ob-
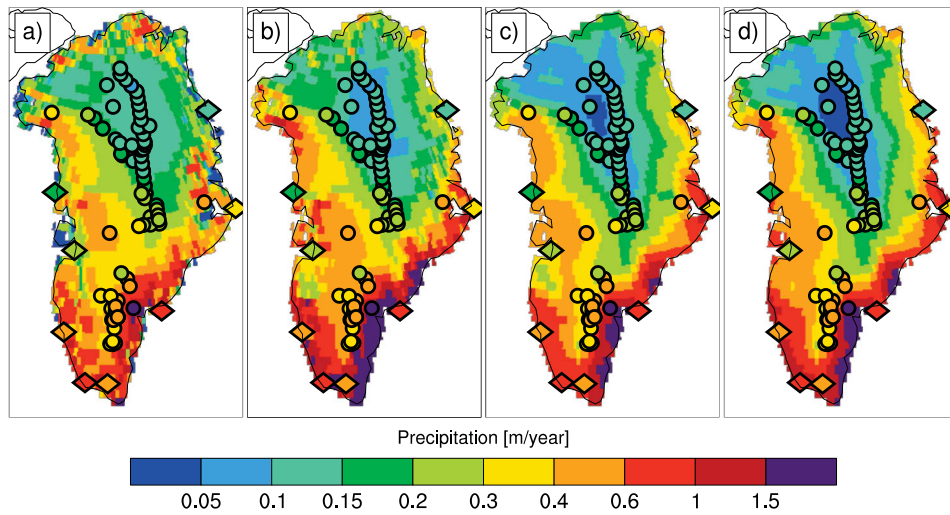
Figure 5. *Accumulation and precipitation observation compared to gridded maps.*
This figure show annual mean accumulation and precipitation data [w.eq m/year] from the observations
compared to annual means of gridded reanalysis and regional model products. Here the symbols show the dif-
ferent data types. Circles represent ice core accumulation data and diamonds represent precipitation data from
DMI. The colors of the symbols correspond to the annual mean value of the given observation. a) Annual
mean accumulation map based on ice cores from *Burgess et al.* [2010], b) Annual mean precipitation from
ERA-Interim (1979-2012), c) Annual mean P-E (precipitation - evaporation) from ERA-Interim (1979-2012),
d) Annual mean precipitation using RACMO (1957-2008) [*Ettema et al.*, 2009]. Note the range of the color
scale is selected to focus on GrIS conditions, and variations at the southeastern Greenland slopes are not well
represented using these color scale.

servation from GrIS are only short term measurements and might not represent the values of the mean present-day surface conditions at GrIS. This is especially relevant as most AWS-instruments on the GrIS are installed after year 2000, thus recording temperatures during a period with anomalously high near-surface temperatures [*Box et al.*, 2013]. Borehole temperatures are mainly measured during the colder time period 1975-1995, and are therefore providing an excellent supplement to the AWS temperature measurements.

The only long-term records are the coastal temperature measurements from DMI. Potentially these measurements could be used to correct for the warm bias recorded in the AWS measurements. Yet while a correlation between coastal temperatures and $\delta^{18}O$ variations from ice cores exist [*Vinther et al.*, 2006], it is unclear whether this relation is constant in time and whether the temperatures at the ice sheet respond to warming trends from sea surface conditions [*Noel et al.*, 2014].

The data types span different measurement types that are all used to represent the same variable. For temperature the data comprise coastal T_{2m}, near-surface T_{2m} from ice-sheet AWS, and borehole temperatures from ice cores. Coastal temperatures might be influenced by local conditions in the surrounding fjords. Surface melt of the GrIS can influence the 10 m depth temperature for boreholes located in regions with frequent melting/refreezing [*Reeh*, 2008]. Similarly melt can also control the AWS temperature observations in the ablation zone *Fausto et al.* [2009]. Melt is not a big concern here as dominant part of the ice cores are drilled in the high interior, yet melt might influence the southern region temperatures.

Warming trends of the GrIS can not be excluded to impact the results, yet we argue that the spatial regression of temperature data representing different time periods and data types of colder and warmer temperatures produce a mean $T_{surface}$ of GrIS that are representative of present day conditions. Comparison with other temperature maps for Greenland show that the resulting absolute values and spatial representations are comparable to regional models and re-analysis products.

5.2.2 4.6.2.2 Variability of $\delta^{18}O$

The existence of long-term records of $\delta^{18}O$ for Greenland allow an analysis of the importance of time span length to accurately predict the average of the entire data series for $\delta^{18}O$. Whether a longer time span is more likely than any short span to represent the mean values of $\delta^{18}O$ is analyzed for two long-term records:

NEEM ($77.44°N, 51.07°W, 2484$ m) (1890-2007).

South Dome ($63.53°N, 44.58°W, 2854$ m) (1890-1957 & 1958-2012).

The mean for the full data series is shown together with time period means of 5 year, 10 year and 25 year (see fig. 6). From the figure it can be seen that natural variability is present in both records and common trends in data are negligible until near year 2000.

–23–
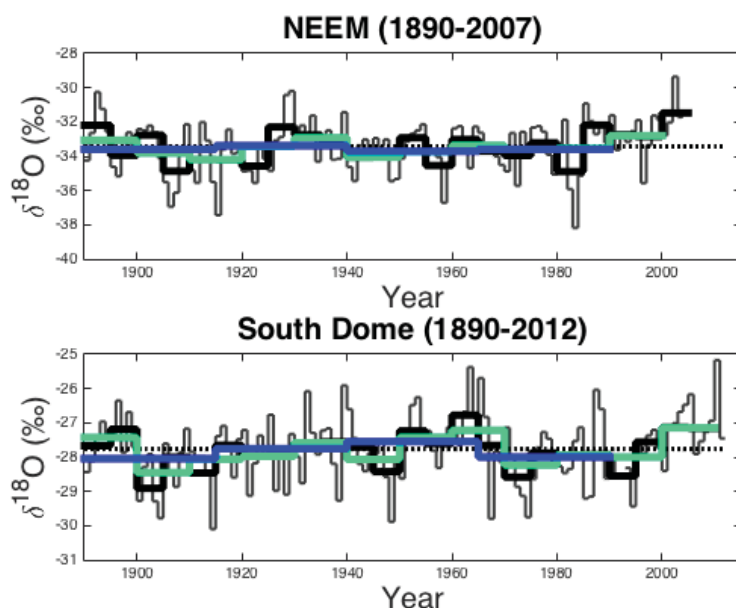
Figure 6. *The representativeness of different length of temporal means for records of $\delta^{18}O$ for NEEM and*
South Dome.
Two time series of $\delta^{18}O$ data. The grey line is the annual $\delta^{18}O$ values. The black line is the 5 year average.
The green line is the 10 year average. The blue line is the 25 year average and the dashed line is the mean for
the full period.

Similar to analysis of accumulation variability by *Cogley* [2004], we find that long-term
time series yield values that better resembles the mean values for the full period. Short term
data included in this study might thus be biased, but the range of the temporal variations are
comparable to the error of the regression, RMSE=1.33 ‰. Thus we conclude that this method
is robust to temporal varations in $\delta^{18}O$.

It was considered applying a uniform or regional time period correction to the mean val-
ues to account for time period biases. Yet this approach was rejected as the limited coverage
of long-term data for the entire time period 1890-2014 challenges possibilities for trend cor-
rections. Furthermore the regional differences in the variability of precipitation and temper-
ature [*Burgess et al.*, 2010; *Mernild et al.*, 2015; *Hanna et al.*, 2011] create an argument for
doing a regional-dependent correction of variability, but the limited spatial coverage does not
give adequate enough information to makes us able to do such a correction.

5.3 Robustness testing of the parameterizations

A robustness testing of the spatial parameterizations of $T_{surface}$ and $\delta^{18}O$ are conducted.
Both spatial representation and the importance of natural variability influencing the means are
tested.

–24–
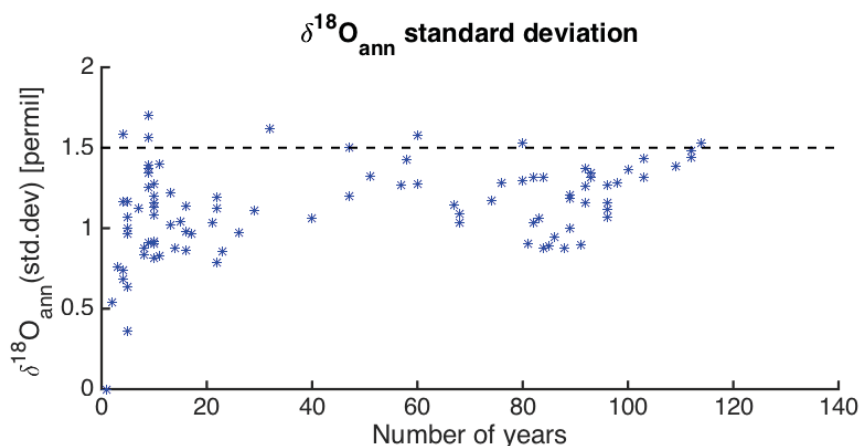
Figure 7. *Standard deviation of annual mean $\delta^{18}O$ for each station.*
Each value is displayed with blue markers and is plotted against the number of years of measurement for the same station. Standard deviation of the ice core data calculated on longer time periods than (1890-2014) are not include here. The dashed line $\delta^{18}O_{std.dev} = 1.5$ ‰ is the $\delta^{18}O_{\sigma,max}$ used in this study.

Analysis of time series of $\delta^{18}O$ and temperature records show the range of the natural variability of the data for each of the locations. The standard deviation of the data time series plotted against the number of years that the given time series span. From fig. 7 and fig. 8 it is clear that natural variability is present in the records of $\delta^{18}O$ and temperature. Based on the figure a rough estimate of the maximum of the range of the standard deviation ($\delta^{18}O_{\sigma,max}$) is set to $\delta^{18}O_{std.dev} = 1.5$ ‰ (dashed line). Similarly $T_{\sigma,max}$) is set to $T_{std.dev} = 3°$ C

The parameterization coefficients used to create the gridded maps are here tested for robustness to the spatial representation described by the selection of data points. This is done separately for temperature $T_{surface}$ and $\delta^{18}O$. A bootstrapping method is applied without re-placement.

A subset of 50 randomly selected data points out of a total of 200 data points for temperature and 159 for ice cores are selected for *N=1000 times*. The parameterization coefficients are determined using multiple linear regression on the subset of the data. For each selection, n, absolute values and differences between the parameterization values and the observed values (all borehole temperatures and ice core $\delta^{18}O$) are computed for selected locations, where both $T_{surface}$ and $\delta^{18}O$ is measured at the same location. The locations represent a wide range of latitude and elevation values at the higher elevation regions of the ice sheet. The result of this robustness test is shown as the grey bars in histogram fig. 9 and fig. 10 and table 6 and table 7 where the coordinates of the locations are also found.
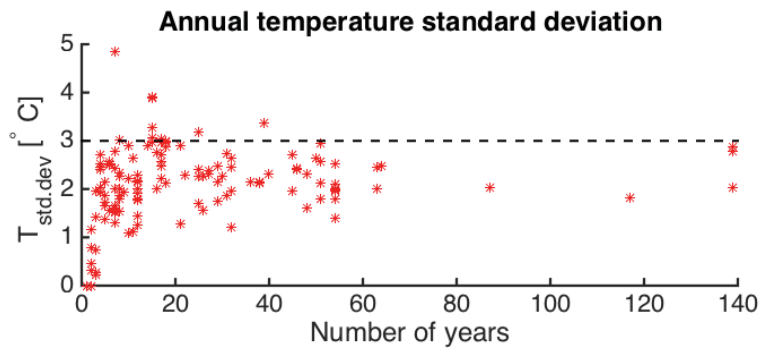
Figure 8. *Standard deviation of annual mean temperature for each station.*

This figure displays the standard deviation of annual mean temperature for each station. Each value is displayed with red markers and is plotted against the number of years of measurement for the same station. The dashed line $T_{std.dev} = 3°$ C is the selected $T_{\sigma,max}$ used in to denote the maximum of the range of standard deviation this study.

678   Analysis of the importance of time period means (fig. 6) shows that for mean values based
679 on 5 year averages the range of the mean values time period error is within the $\delta^{18}O_{std.dev} =$
680 1.5 found for the natural variability of the records. 72 % of the ice core $\delta^{18}O$ mean values
681 represent time periods of 5 years or longer. The importance of representing the right time pe-
682 riod is analyzed. For $N = 1000$ times a random error within the range $0 \pm \delta^{18}O_{\sigma,max}$ $\delta^{18}O_{\sigma,max} =$
683 1.5 is added to each of the data points. Hereafter the parameterization coefficients are deter-
684 mined for the full dataset with the random error and the differences between the parameter-
685 ization values and the observed values are computed. The same is conducted for temperature
686 with random errors in the range of $0 \pm T_{\sigma,max}$, where $T_{\sigma,max} = 3°$ C, as estimated from
687 the results of fig. 8.

688   The mean bias of the parameterizations is the same, subset sampling and random errors
689 produce the same bias compared to the temperature borehole observations. Only the standard
690 deviation varies, with fewer variations for the error testing than for the sampling testing. Largest
691 variations in temperature are found for "ongt19" in northern Greenland.

692   Regional parameterization might yield a better description of spatially anti-correlated sig-
693 nal from NAO on each side of the ice divide *Sodemann et al.* [2008a,b]; *Appenzeller* [1998];
694 *Vinther* [2003]; *Vinther et al.* [2010]. However it is found that divisions of data in subregions
695 of Greenland create challenges for regions where number off observations are limited and where
696 the range of elevation and latitude of observations within the subregion does not create a good
697 regression. Furthermore the combination of regional parameterization into a map for the en-
698 tire GrIS creates un-physical boundaries at the regional borders. Therefore it is chosen to de-
699 scribe all Greenland data using one parameterization.

700   While recent warming trends, overrepresentation of data from certain time periods and
701 mismatch between comparison of $T_{surface}$ and T_{2m} can however not be ruled out to influ-
702 ence the parameterization, based on the robustness testing it is clear that the variations are com-
703 parable to the RMSE errors of the regression on all data. Therefore we conclude that the pa-
704 rameterization can describe the spatial distribution within the range ± 1.5 ‰ and $\pm 3°$ C.

Temperature difference values for robustness test

Location	Coordinates	Elevation	Sampling		Variability	
			mean [$°C$]	std.dev [$°C$]	mean diff. [$°C$]	std.dev [$°C$]
NGRIP	$75.10°N, 42.32°W$	2918 m	0.73	0.40	0.71	0.21
South Dome	$63.53°N, 44.58°W$	2854 m	1.07	0.49	1.11	0.27
NEEM	$77.44°N, 51.08°W$	2484 m	-1.01	0.46	-1.04	0.20
Camp Century	$77.17°N, 61.10°W$	1880 m	-0.33	0.46	-0.36	0.18
GRIP	$72.57°N, 37.62°W$	3232 m	0.55	0.39	0.55	0.22
ongt19	$78.00°N, 36.40°W$	2234 m	2.99	0.49	2.96	0.20

714 **Table 6.**   Mean values and standard deviations of temperature differences

715 computed as $T_{diff,n} = T_{parm.,n} - T_{obs}$ for the given locations for each n of $N = 1000$ realizations for the

716 given locations for the robustness test.

–27–
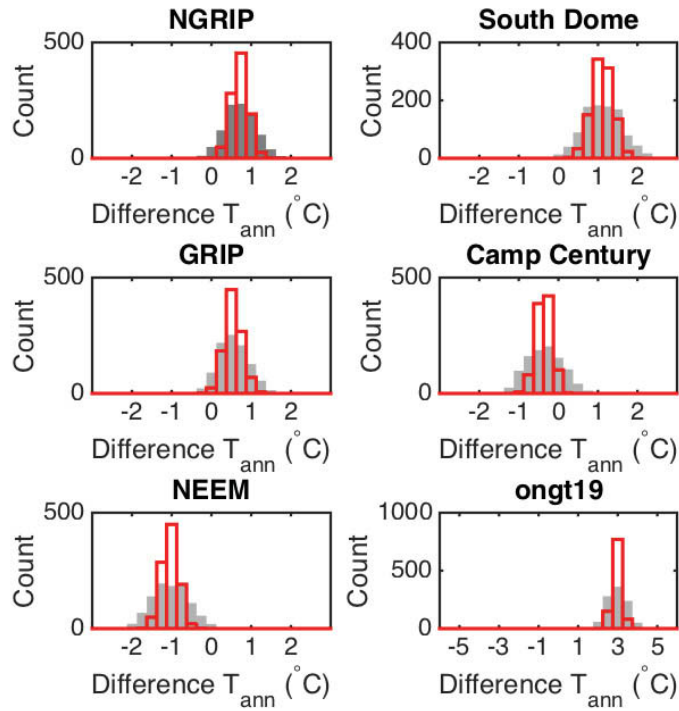
Figure 9. *Histogram from the temperature robustness test.*

706 This figure displays the results of the robustness test of the parameterization (see also table 6).

707 *The sampling sensitivity test:* The histogram with grey bars shows the values of difference between the

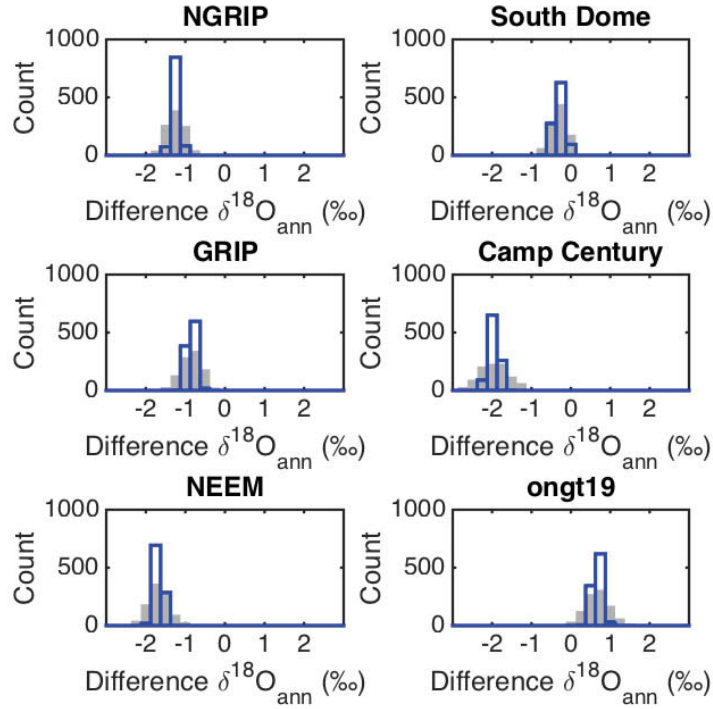708 observations and the parameterizations values computed as

709 $T_{diff,n} = T_{parm.,n} - T_{obs}$ for the given locations for each n of $N = 1000$ realizations.

710 *The error-sensitivity test:*The red line histogram show the results from the error-sensitivity test where regres-

711 sion is conducted for all data with a random error applied to each data point. The error has a random value

712 within the range of 0 to $\pm T_{\sigma,max}$, where $T_{\sigma,max}$ = 3° C, as estimated from the results of fig. 8. Note that

713 "ongt19" is plotted on a different temperature range.

Figure 10. *Histogram from $\delta^{18}O$ sampling sensitivity test.*

718 This figure displays the results of the bootstrapping sampling sensitivity test (see also table 7).

719 *The sampling sensitivity test:* The grey histogram show the values of difference between the observations and

720 the parameterizations values computed as $\delta^{18}O_{diff,n} = \delta^{18}O_{parm.,n} - \delta^{18}O_{obs}$ for the given locations for

721 each n of $N = 1000$ realizations for the given locations.

722 *The error-sensitivity test:* The blue line histogram show the results from the error-sensitivity test where re-

723 gression is conducted for all data with a random error applied to each data point. The error has a random

724 value within the range of 0 to $\pm\delta^{18}O_{\sigma,max}$, where $\delta^{18}O_{\sigma,max} = 1.5$ ‰, as estimated from the results of fig.

725 7.

6 Conclusion

730   This study presents a comprehensive database consisting of data from 326 ice core and

731 weather station observations during the period 1890-2014. The data comprise annual and sea-

732 sonal mean values of $\delta^{18}O$, δD and d-excess, accumulation and temperatures from ice core

733 boreholes, from near-ice-surface measurements and temperatures from air measurements for

734 Greenland. Data originates from ice core measurements, GNIP data and meteorological ob-

735 servations from the DMI and the projects PROMICE and GC-Net.

736   Based on multiple linear regression methods using the data from the database, the spa-

737 tial characteristics of $T_{surface}$ and $\delta^{18}O$ for Greenland are described. The resulting linear pa-

738 rameterizations describes, respectively $\delta^{18}O$ and temperature by means of latitude and eleva-

739 tion only. The multiple linear regression approach was also used to investigate differences in

740 the regression coefficients among different datasets used to form the database, and differences

741 in the regression coefficients for different geographical subregions. Differences in the west-

742 ern and eastern region response to changes with elevation are found for both $T_{surface}$ and $\delta^{18}O$.

δ^{18}O difference values for robustness test

Location	Coordinates	Elevation	Sampling		Variability	
			mean [$°C$]	std.dev [‰]	mean diff. [‰]	std.dev [‰]
NGRIP	$75.1°N, 42.32°W$	2918 m	-1.28	0.23	-1.25	0.09
South Dome	$63.53°N, 44.58°W$	2854 m	-0.29	0.22	-0.30	0.13
NEEM	$77.44°N, 51.07°W$	2484 m	-1.71	0.28	-1.69	0.10
Camp Century	$77.17°N, 61.1°W$	1880 m	-1.97	0.40	-1.97	0.12
GRIP	$72.57°N, 37.62°W$	3232 m	-0.87	0.27	-0.84	0.10
ongt19	$78.00°N, 36.40°W$	2234 m	0.65	0.33	0.66	0.11

Table 7. Mean values and standard deviations of δ^{18}O differences computed as $\delta^{18}O_{diff,n} = \delta^{18}O_{parm.,n} - \delta^{18}O_{obs}$ for the given locations for each n of $N = 1000$ realizations of the robustness test.

Furthermore the temperature decrease with higher elevation is more rapid in high-elevation regions than in coastal and mid-elevation regions.

For the first time an observational-based gridded map of δ^{18}O of precipitation is created for Greenland. This is done using the empirical parameterization for the annual mean δ^{18}O data from 185 ice cores and 6 coastal GNIP observations. The gridded maps are constructed in a sequence of steps. First, a parametrization-based spatial map is created using a DEM of Greenland. Here after the residuals between the map and observations are computed. An elevation-correction is applied to correct for differences between DEM grid point elevation and the true elevation of the each observational site. The fit of the map to data is hereafter improved by adding a residual-correction field using a surface fitting algorithm of the data. The residual correction field is added to to the parameterization-based spatial map. This yields a spatial map, based on a data-transparent and model-independent method, but corrected for misfits to data. Based on the robustness testing and the RMSE errors from the regression on all data we conclude that the parameterization can describe the spatial distribution within

the range ± 1.5 ‰.

A data-based gridded map is also created for Greenland annual mean $T_{surface}$, using the same approach. Here borehole data from ice cores are for the first time included together with AWS observations. A dominant part of the ice core borehole temperatures are measured in the years 1970-1995. This aid to constrain the spatial variation of GrIS $T_{surface}$ to conditions before the recent warming. Here robustness testing and RMSE error yield an error range of $\pm 3°$ C. The gridded maps of temperature also show values in the same range and a similar spatial distribution compared to other gridded temperature maps for Greenland. However recent warming trends, overrepresentation of data from certain time periods and mismatch between comparison of $T_{surface}$ and T_{2m} can not be ruled out to influence this parameterization. The database and gridded maps provide model-independent descriptions of the present-day spatial distribution of isotope-model relevant parameters at Greenland. We therefore suggest this dataset and gridded maps as a common tool for performance testing, inter-model comparison as well as future development and improvement of isotope models.

Acknowledgments

–30–

References

Appenzeller, C. (1998), North Atlantic Oscillation Dynamics Recorded in Greenland Ice Cores, *Science*, *282*(5388), 446–449, doi:10.1126/science.282.5388.446.

Bales, R. C., Q. Guo, D. Shen, J. R. McConnell, G. Du, J. F. Burkhart, V. B. Spikes, E. Hanna, and J. Cappelen (2009), Annual accumulation for Greenland updated using ice core data developed during 2000 to 2006 and analysis of daily coastal meteorological data, *Journal of Geophysical Research*, *114*(D6), D06,116, doi: 10.1029/2008JD011208.

Bamber, J. L., R. L. Layberry, and S. Gogineni (2001), A new ice thickness and bed data set for the greenland ice sheet: 1. measurement, data reduction, and errors, *Journal of Geophysical Research: Atmospheres*, *106*(D24), 33,773–33,780.

Blossey, P. N., Z. Kuang, and D. M. Romps (2010), Isotopic composition of water in the tropical tropopause layer in cloud-resolving simulations of an idealized tropical circulation, *Journal of Geophysical Research: Atmospheres*, *115*(D24).

Bonne, J.-L. L., V. Masson-Delmotte, O. Cattani, M. Delmotte, C. Risi, H. Sodemann, and H. C. Steen-Larsen (2014), The isotopic composition of water vapour and precipitation in Ivittuut, southern Greenland, *Atmospheric Chemistry and Physics*, *14*(9), 4419–4439, doi:10.5194/acp-14-4419-2014.

Bowen, G. J., and J. Revenaugh (2003), Interpolating the isotopic composition of modern meteoric precipitation, *Water Resources Research*, *39*(10).

Box, J. E., N. Cressie, D. H. Bromwich, J.-H. Jung, M. Van Den Broeke, J. Van Angelen, R. R. Forster, C. Miège, E. Mosley-Thompson, B. Vinther, et al. (2013), Greenland ice sheet mass balance reconstruction. part i: Net snow accumulation (1600-2009), *Journal of climate*, *26*(11), 3919–3934.

Buchardt, S. L., H. B. Clausen, B. M. Vinther, and D. Dahl-Jensen (2012), Investigating the past and recent $\delta^{18}O$-accumulation relationship seen in Greenland ice cores, *Climate of the Past*, *8*(6), 2053–2059, doi:10.5194/cp-8-2053-2012.

Burgess, E. W., R. R. Forster, J. E. Box, E. Mosley-Thompson, D. H. Bromwich, R. C. Bales, and L. C. Smith (2010), A spatially calibrated model of annual accumulation rate on the greenland ice sheet (1958–2007), *Journal of Geophysical Research: Earth Surface*, *115*(F2).

Calanca, P., H. Gilgen, S. Ekholm, and A. Ohmura (2000), Gridded temperature and accumulation distributions for greenland for use in cryospheric models, *Annals of Glaciology*, *31*(1), 118–120.

Cappelen, J., et al. (2013a), Greenland - dmi historical climate data collection 1873-2012, *Technical Report 13-04*.

Cappelen, J., et al. (2013b), Weather observations from greenland 1958–2012, *Technical Report 13-11*.

Cogley, J. G. (2004), Greenland accumulation: An error model, *Journal of Geophysical Research: Atmospheres*, *109*(D18).

Dahl-Jensen, D., K. Mosegaard, N. Gundestrup, G. D. Clow, S. J. Johnsen, A. W. Hansen, and N. Balling (1998), Past temperatures directly from the greenland ice sheet, *Science*, *282*(5387), 268–271.

Dansgaard, W. (1964), Stable Isotopes in Precipitation, *Tellus*, *16*(4), 436–468, doi: 10.1111/j.2153-3490.1964.tb00181.x.

Dansgaard, W., and S. Johnsen (1969), A flow model and a time scale for the ice core from camp century, greenland, *Journal of Glaciology*, *8*, 215–223.

–31–

828   Dee, D. P., S. M. Uppala, A. J. Simmons, P. Berrisford, P. Poli, S. Kobayashi, U. Andrae,
829   M. A. Balmaseda, G. Balsamo, P. Bauer, P. Bechtold, A. C. M. Beljaars, L. van de
830   Berg, J. Bidlot, N. Bormann, C. Delsol, R. Dragani, M. Fuentes, A. J. Geer, L. Haim-
831   berger, S. B. Healy, H. Hersbach, E. V. Holm, L. Isaksen, P. Kallberg, M. Koehler,
832   M. Matricardi, A. P. McNally, B. M. Monge-Sanz, J. J. Morcrette, B. K. Park,
833   C. Peubey, P. de Rosnay, C. Tavolato, J. N. Thepaut, and F. Vitart (2011), The ERA-
834   Interim reanalysis: configuration and performance of the data assimilation system,
835   *Quarterly Journal of The Royal Meteorological Society*, *137*(656, Part a), 553–597.

836   Dee, S., D. Noone, N. Buenning, J. Emile-Geay, and Y. Zhou (2015), Speedy-ier: A fast
837   atmospheric gcm with water isotope physics, *Journal of Geophysical Research: Atmo-*
838   *spheres*, *120*(1), 73–91.

839   D'Errico, J. (2005), Surface fitting using gridfit, *MATLAB central file exchange*, *643*.

840   Ettema, J., M. R. van den Broeke, E. van Meijgaard, W. J. van de Berg, J. L. Bamber,
841   J. E. Box, and R. C. Bales (2009), Higher surface mass balance of the greenland ice
842   sheet revealed by high-resolution climate modeling, *Geophysical Research Letters*,
843   *36*(12).

844   Fausto, R. S., A. P. Ahlstrø m, D. Van As, C. E. Bø ggild, and S. J. Johnsen (2009), A
845   new present-day temperature parameterization for Greenland, *Journal of Glaciology*,
846   *55*(189), 95–105, doi:10.3189/002214309788608985.

847   Hammer, C., H. Clausen, W. Dansgaard, N. Gundestrup, S. Johnsen, and N. Reeh (1978),
848   Dating of greenland ice cores by flow models, isotopes, volcanic debris, and continental
849   dust, *Journal of Glaciology*, *20*, 3–26.

850   Hanna, E., P. Huybrechts, J. Cappelen, K. Steffen, R. C. Bales, E. Burgess, J. R. Mc-
851   Connell, J. Peder Steffensen, M. Van den Broeke, L. Wake, G. Bigg, M. Griffiths, and
852   D. Savas (2011), Greenland Ice Sheet surface mass balance 1870 to 2010 based on
853   Twentieth Century Reanalysis, and links with global climate forcing, *Journal of Geo-*
854   *physical Research: Atmospheres*, *116*(D24), n/a–n/a, doi:10.1029/2011JD016387.

855   Herron, M. M., and C. C. Langway Jr (1980), Firn densification: an empirical model,
856   *Journal of Glaciology*, *25*, 373–385.

857   Hoffmann, G., M. Werner, and M. Heimann (1998), Water isotope module of the echam
858   atmospheric general circulation model: A study on timescales from days to several
859   years, *Journal of Geophysical Research: Atmospheres (1984–2012)*, *103*(D14), 16,871–
860   16,896.

861   IAEA, W., and W. WMO (2015), Global network of isotopes in precipitation, *The GNIP*
862   *database*.

863   Johnsen, S., H. B. Clausen, K. M. Cuffey, G. Hoffmann, J. Schwander, and T. Creyts
864   (2000), *Diffusion of stable isotopes in polar firn and ice: the isotope effect in firn diffu-*
865   *sion*, 121–140 pp., Sapporo.

866   Johnsen, S. J., W. Dansgaard, and J. W. C. White (1989), The origin of Arctic pre-
867   cipitation under present and glacial conditions, *Tellus B*, *41B*(4), 452–468, doi:
868   10.1111/j.1600-0889.1989.tb00321.x.

869   Jouzel, J., G. Russell, R. Suozzo, R. Koster, J. White, and W. Broecker (1987), Simula-
870   tions of the hdo and h2 18o atmospheric cycles using the nasa giss general circulation
871   model: The seasonal cycle for present-day conditions, *Journal of Geophysical Research:*
872   *Atmospheres (1984–2012)*, *92*(D12), 14,739–14,760.

873   Kurita, N., D. Noone, C. Risi, G. A. Schmidt, H. Yamada, and K. Yoneyama (2011), In-
874   traseasonal isotopic variation associated with the madden-julian oscillation, *Journal of*
875   *Geophysical Research: Atmospheres*, *116*(D24).

876   Lee, J.-E., I. Fung, D. J. DePaolo, and C. C. Henning (2007), Analysis of the global dis-
877   tribution of water isotopes using the NCAR atmospheric general circulation model,
878   *Journal of Geophysical Research*, *112*(D16), 1–14, doi:10.1029/2006JD007657.

879   Masson-Delmotte, V., S. Hou, A. Ekaykin, J. Jouzel, A. Aristarain, R. Bernardo,
880   D. Bromwich, O. Cattani, M. Delmotte, S. Falourd, et al. (2008), A review of antarctic
881   surface snow isotopic composition: observations, atmospheric circulation, and isotopic

modeling*, *Journal of Climate*, *21*(13), 3359–3387.

Mathieu, R., D. Pollard, J. E. Cole, J. W. White, R. S. Webb, and S. L. Thompson (2002), Simulation of stable water isotope variations by the genesis gcm for modern conditions, *Journal of Geophysical Research: Atmospheres (1984–2012)*, *107*(D4), ACL–2.

Mernild, S. H., E. Hanna, J. R. McConnell, M. Sigl, A. P. Beckerman, J. C. Yde, J. Cappelen, J. K. Malmros, and K. Steffen (2015), Greenland precipitation trends in a long-term instrumental climate context (1890–2012): evaluation of coastal and ice core records, *International Journal of Climatology*, *35*(2), 303–320.

Mosley-Thompson, E., J. McConnell, R. Bales, Z. Li, P.-N. Lin, K. Steffen, L. Thompson, R. Edwards, and D. Bathke (2001), Local to regional-scale variability of annual net accumulation on the greenland ice sheet from parca cores, *Journal of Geophysical Research: Atmospheres*, *106*(D24), 33,839–33,851.

Noel, B., X. Fettweis, W. Van De Berg, M. Van Den Broeke, and M. Erpicum (2014), Sensitivity of greenland ice sheet surface mass balance to perturbations in sea surface temperature and sea ice cover: a study with the regional climate model mar, *Cryosphere (The)*, *8*, 1871–1883.

Noone, D. (2003), Water isotopes in ccsm for studying water cycles in the climate system, *8th Annual CCSM workshop, Breckenridge, Colorado*.

Ohmura, A., and N. Reeh (1991), New precipitation and accumulation maps for greenland, *J. Glaciol*, *37*(125), 140–148.

Pfahl, S., H. Wernli, K. Yoshimura, and M. Dubey (2012), The isotopic composition of precipitation from a winter storm–a case study with the limited-area model cosmo iso., *Atmospheric Chemistry & Physics*, *12*(3).

Reeh, N. (2008), A nonsteady-state firn-densification model for the percolation zone of a glacier, *Journal of Geophysical Research: Earth Surface*, *113*(F3).

Risi, C., S. Bony, F. Vimeux, and J. Jouzel (2010), Water-stable isotopes in the LMDZ4 general circulation model: Model evaluation for present-day and past climates and applications to climatic interpretations of tropical isotopic records, *Journal of Geophysical Research: Atmospheres*, *115*, 1–27, doi:10.1029/2009JD013255.

Ritz, C., A. Fabre, and A. Letréguilly (1996), Sensitivity of a greenland ice sheet model to ice flow and ablation parameters: consequences for the evolution through the last climatic cycle, *Climate Dynamics*, *13*(1), 11–23.

Roche, D. (2013), δ 18 o water isotope in the iloveclim model (version 1.0)–part 1: Implementation and verification, *Geoscientific Model Development*, *6*(5), 1481–1491.

Schmidt, G. a., A. N. LeGrande, and G. Hoffmann (2007), Water isotope expressions of intrinsic and forced variability in a coupled ocean-atmosphere model, *Journal of Geophysical Research*, *112*(D10), 1–18.

Shen, D., Y. Liu, and S. Huang (2012), Annual accumulation over the greenland ice sheet interpolated from historical and newly compiled observation data, *Geografiska Annaler: Series A, Physical Geography*, *94*(3), 377–393.

Sodemann, H., C. Schwierz, and H. Wernli (2008a), Interannual variability of Greenland winter precipitation sources: Lagrangian moisture diagnostic and North Atlantic Oscillation influence, *Journal of Geophysical Research - Atmospheres*, *113*(D3), doi: 10.1029/2007JD008503.

Sodemann, H., V. Masson-Delmotte, C. Schwierz, B. M. Vinther, and H. Wernli (2008b), Interannual variability of Greenland winter precipitation sources: 2. Effects of North Atlantic Oscillation variability on stable isotopes in precipitation, *Journal of Geophysical Research-Atmospheres*, *113*(D12), 1–21, doi:10.1029/2007JD009416.

Steen-Larsen, H. C., V. Masson-Delmotte, J. Sjolte, S. J. Johnsen, B. M. Vinther, F.-M. Bréon, H. Clausen, D. Dahl-Jensen, S. Falourd, X. Fettweis, et al. (2011), Understanding the climatic signal in the water stable isotope records from the neem shallow firn/ice cores in northwest greenland, *Journal of Geophysical Research: Atmospheres*, *116*(D6).

–33–

Steffen, K., and J. Box (2001), Surface climatology of the greenland ice sheet: Greenland climate network 1995–1999, *Journal of Geophysical Research: Atmospheres*, *106*(D24), 33,951–33,964.

Steffen, K., J. Box, and W. Abdalati (1996), Greenland climate network: Gc-net, *US Army Cold Regions Reattach and Engineering (CRREL), CRREL Special Report*, pp. 98–103.

Sturm, K., G. Hoffmann, B. Langmann, and W. Stichler (2005), Simulation of δ18o in precipitation by the regional circulation model remoiso, *Hydrological Processes*, *19*(17), 3425–3444.

Terzer, S., L. Wassenaar, L. Araguás-Araguás, and P. Aggarwal (2013), Global isoscapes for δ 18 o and δ 2 h in precipitation: improved prediction using regionalized climatic regression models, *Hydrology and Earth System Sciences*, *17*(11), 4713–4728.

Tindall, J., P. Valdes, and L. C. Sime (2009), Stable water isotopes in hadcm3: Isotopic signature of el niño–southern oscillation and the tropical amount effect, *Journal of Geophysical Research: Atmospheres (1984–2012)*, *114*(D4).

van As, D., R. S. Fausto, A. Ahlstrøm, S. Andersen, M. Andersen, M. Citterio, K. Edelvang, P. Gravesen, H. Machguth, F. Nick, et al. (2011), Programme for monitoring of the greenland ice sheet (promice): first temperature and ablation record, *Geological Survey of Denmark and Greenland Bulletin*, *23*, 73–76.

Vinther, B. M. (2003), NAO signal recorded in the stable isotopes of Greenland ice cores, *Geophysical Research Letters*, *30*(7), 1–4, doi:10.1029/2002GL016193.

Vinther, B. M., K. K. Andersen, P. D. Jones, K. R. Briffa, and J. Cappelen (2006), Extending greenland temperature records into the late eighteenth century, *Journal of Geophysical Research: Atmospheres*, *111*(D11).

Vinther, B. M., S. L. Buchardt, H. B. Clausen, D. Dahl-Jensen, S. J. Johnsen, D. a. Fisher, R. M. Koerner, D. Raynaud, V. Lipenkov, K. K. Andersen, T. Blunier, S. O. Rasmussen, J. P. Steffensen, and a. M. Svensson (2009), Holocene thinning of the Greenland ice sheet., *Nature*, *461*(7262), 385–388, doi:10.1038/nature08355.

Vinther, B. M., P. D. Jones, K. R. Briffa, H. B. Clausen, K. K. Andersen, D. Dahl-Jensen, and S. J. Johnsen (2010), Climatic signals in multiple highly resolved stable isotope records from Greenland, *Quaternary Science Reviews*, *29*(3-4), 522–538, doi:10.1016/j.quascirev.2009.11.002.

Wang, Y., S. Hou, V. Masson-Delmotte, and J. Jouzel (2009), A new spatial distribution map of δ18o in antarctic surface snow, *Geophysical Research Letters*, *36*(6).

Wang, Y., S. Hou, V. Masson-Delmotte, and J. Jouzel (2010), A generalized additive model for the spatial distribution of stable isotopic composition in antarctic surface snow, *Chemical Geology*, *271*(3), 133–141.

Weissbach, S., A. Wegner, T. Opel, H. Oerter, B. Vinther, and S. Kipfstuhl (2016), Spatial and temporal oxygen isotope variability in northern greenland–implications for a new climate record over the past millennium, *Climate of the Past*, *12*, 171–188.

Werner, M., P. M. Langebroek, T. Carlsen, M. Herold, and G. Lohmann (2011), Stable water isotopes in the ECHAM5 general circulation model: Toward high-resolution isotope modeling on a global scale, *Journal of Geophysical Research*, *116*(D15), 1–14, doi:10.1029/2011JD015681.

Werner, M., B. Haese, X. Xu, X. Zhang, M. Butzin, and G. Lohmann (2016), Glacial–interglacial changes in h218o, hdo and deuterium excess–results from the fully coupled echam5/mpi-om earth system model, *Geoscientific Model Development*, *9*(2), 647–670.

Yoshimura, K., M. Kanamitsu, D. Noone, and T. Oki (2008), Historical isotope simulation using Reanalysis atmospheric data, *Journal of Geophysical Research*, *113*(D19), 1–15, doi:10.1029/2008JD010074.

Yoshimura, K., M. Kanamitsu, and M. Dettinger (2010), Regional downscaling for stable water isotopes: A case study of an atmospheric river event, *J. Geophys. Res*, *115*, D18,114.

7 Conclusion and outlook

Northern Greenland is a, until now, less studied area in the Arctic. However, it is considered as key area for understanding the relation of the observed changes in global mean temperature and precipitation. The Greenland Ice Sheet has a strong impact on the global sea level. A change in the mass balance of the ice sheet towards more melting contributes directly to sea level rise. Large meltwater injections would also affect the ocean circulation due to changes in the fresh water budget, as well as the global atmospheric heat transport. To monitor and evaluate recent changes in the overall mass balance of the Greenland Ice Sheet, detailed studies of local accumulation rates, which represent the positive term in the mass balance, and their temporal changes over the last millennium, are of great relevance. However, until recently few data sets have been available from northern Greenland.

Values of $\delta^{18}O$ in ice and snow are used as a proxy of air temperature. Thus, evaluation of the temporal distribution of $\delta^{18}O$ from northern Greenland ice cores has the potential to fill in the gap of temperature data in the Arctic. In order to derive a reliable temporal signal, a detailed study of the spatial $\delta^{18}O$ distribution is necessary as the $\delta^{18}O$-temperature relationship can be influenced by locally varying factors. Such a data set would contribute to a more representative global mean and provide the potential to assess the recent temperature values in the context of history to answer the question- is there a recent warming trend in northern Greenland?

In this thesis, for the first time the full data set of 13 NGT 93/95 ice cores were made available and provide the basis for detailed spatial distribution studies. The records of the completed high-resolution $\delta^{18}O$ data set were dated and annual means of accumulation rate and $\delta^{18}O$ calculated. The lowest mean values for $\delta^{18}O$ are found east of the main ice divide, revealing a strong topographic influence on the mean $\delta^{18}O$ values. The main ice divide separates northern Greenland in an eastern and a western part. Apart from these large-scale variations in the mean values, a high local variability in the $\delta^{18}O$ records became obvious, which disturbed the climate signal and delimits the interpretation of data from isolated cores. By stacking northern Greenland $\delta^{18}O$ ice core data to one record the signal-to-noise ratio could be improved and the spatial variability could be separated from the climate signal for the first time. The stack is representative for a large area and is more trustworthy than multiproxy stacks because of the direct linear relationship of $\delta^{18}O$ to temperature. The stacked $\delta^{18}O$ record allows to extract the climate history over the last millennium. Well-known global climate events (e.g. MCA, LIA and ETCW) as well as a new event around 1420 A.D., are observed in the stacked record. The stack is sensitive to decadal variability (e.g. ETCW), which is not temporally resolved in climate

models. It was possible to extend the NGT 93/95 stack to 2011 A.D. by adding the records of recently drilled NGT-update cores. The resulting stack covers the last millennium as well as the most recent years. Its high quality allows for the first time an unambiguous assessment of the recent warming trend, which includes anomalous values over the last millennium.

The full NGT 93/95 data set enables more detailed statements about the spatial accumulation rate distribution and the size and location of the area of lowest accumulation rates in Greenland. The lowest values are found in the precipitation shadow east of the main divide, which covers an area larger than expected. The ice sheet topography is confirmed as the dominant impact factor influencing the accumulation rate distribution. The new available data also provide an update for the old accumulation rate maps (e.g. Ohmura and Rhee, 1991).

To summarize, the improved data set of spatial distribution of accumulation rates in northern Greenland contributes essentially to accurate mass balance studies for a more precise sea level rise forecast. The separation of local effects and climate signal in the $\delta^{18}O$ proxy data closes a gap of knowledge about temperature variability in the Arctic, which is important for the calculation of a more representative global mean temperature. For the first time, the temperature evolution during the past 1000 years in this climatic key area can be studied unambiguously.

The data set can be easily extended in the future, as the $\delta^{18}O$-stacked record is a basis for further updates. The most recent values can be easily assessed that way and the future warming trend be studied. The coefficient to link $\delta^{18}O$ to temperature is varying spatially as well as temporally. Measuring the firn temperature at least in 2 different depths at several of the drill sites would allow for a more accurate translation of $\delta^{18}O$ to temperature and possibly also for an assessment of the effect of polar amplification in northern Greenland. More data, ideally including seasonal cycles, would enable annual layer counting also in the deeper core segments of NGT 93/95 records from the dry northeast. For example, concentrations of Ca^{2+} and particulate dust show distinct seasonal cycles in Greenland with maxima in spring. The use of NO_3^- as a distinct marker for forest fires would also improve the dating process. Measurements via CFA could provide the necessary data. A dating with higher resolution of all NGT 93/95 cores offers the possibility to study the temporal variability of accumulation rates and changes in their spatial distribution over the last millennium. This information can further improve the accuracy of mass balance studies in Greenland. Records of trace elements also contribute to a better understanding of the mechanisms behind the natural variability of temperature in northern Greenland like the influence of NAO and the occurrence of blocking situations. Learning about these mechanisms offers the possibility to improve the implementation of these processes into climate models with the aim to reproduce the natural variability and enable more precise forecasts.

References

Andersen, K. K., Ditlevsen, P. D., Rasmussen, S. O., Clausen, H. B., Vinther, B. M., Johnsen, S. J., and Steffensen, J. P.: Retrieving a common accumulation record from Greenland ice cores for the past 1800 years, J. Geophys. Res.-Atmos., 111, D15106, 2006a.

Andersen, K. K., Svensson, A., Johnsen, S. J., Rasmussen, S. O., Bigler, M., Röthlisberger, R., Ruth, U., Siggaard-Andersen, M.-L., Peder Steffensen, J., and Dahl-Jensen, D.: The Greenland Ice Core Chronology 2005, 15–42ka. Part 1: constructing the time scale, Quat. Sci. Rev., 25, 3246-3257, 2006b.

Bales, R. C., McConnell, J. R., Mosley-Thompson, E., and Csatho, B.: Accumulation over the GReenland ice sheet from historical and recent records, Journal of Geophsical Research, 106, 13, 2001.

Bamber, J. L., Griggs, J. A., Hurkmans, R. T. W. L., Dowdeswell, J. A., Gogineni, S. P., Howat, I., Mouginot, J., Paden, J., Palmer, S., Rignot, E., and Steinhage, D.: A new bed elevation dataset for Greenland, The Cryosphere, 7, 499-510, 2013.

Barlow, L. K.: Evaluation of Seasonal to Decadal Scale Deuterium and Deuterium Excess Signals, GISP2 Ice Core, Summit Greenland, A.D. 1270-1985, 1994. University of Colorado, 1994.

Benson, C. S.: Greenland snow pit and core stratigraphic data 1952, 1953, 1954, 1955, U.S. Army Corps of Engineers Snow Ice and Permafrost Res, 70, 182, 1962.

Bigler, M., Wagenbach, D., Fischer, H., Kipfstuhl, J., Miller, H., Sommer, S., and Stauffer, B.: Sulphate record from a northeast Greenland ice core over the last 1200 years based on continuous flow analysis. In: Annals of Glaciology, Vol 35, Wolff, E. W. (Ed.), Annals of Glaciology, Int Glaciological Soc, Cambridge, 2002.

Box, J. E., Cressie, N., Bromwich, D. H., Jung, J.-H., van den Broeke, M., van Angelen, J. H., Forster, R. R., Miège, C., Mosley-Thompson, E., Vinther, B., and McConnell, J. R.: Greenland Ice Sheet Mass Balance Reconstruction. Part I: Net Snow Accumulation (1600–2009), J. Clim., 26, 3919-3934, 2013.

Bull, C.: Snow accumulation in north Greenland, J. Glaciol., 3, 12, 1958.

Cappelen, J.: Greenland - DMI Historical Climate Data Collection 1784-2014, Danish Meteorological Institute, Copenhagen, 1-97, 2015.

Chen, Q. S., Bromwich, D. H., and Bai, L. S.: Precipitation over Greenland retrieved by a dynamic method and its relation to cyclonic activity, J. Clim., 10, 839-870, 1997.

Cogley, J. G.: Greenland accumulation: An error model, J. Geophys. Res.-Atmos., 109, 15, 2004.

Comiso, J. C., Parkinson, C. L., Gersten, R., and Stock, L.: Accelerated decline in the Arctic sea ice cover, Geophys. Res. Lett., 35, 6, 2008.

Cowtan, K. and Way, R. G.: Coverage bias in the HadCRUT4 temperature series and its impact on recent temperature trends, Quarterly Journal of the Royal Meteorological Society, 140, 1935-1944, 2014.

Craig, H.: Isotopic Variations in Meteoric Waters, Science, 133, 1702-1703, 1961.

Dansgaard, W.: The Abundance of O18 in Atmospheric Water and Water Vapour, Tellus, 5, 461-469, 1953.

Dansgaard, W.: Stable isotopes in precipitation, Tellus, 16, 33, 1964.

Dansgaard, W., Clausen, H. B., Gundestrup, N., Johnsen, S. J., and Rygner, C.: Dating and Climatic Interpretation of Two Deep Greenland Ice Cores. In: Greenland Ice Core: Geophysics, Geochemistry, and the Environment, American Geophysical Union, 1985.

Dansgaard, W., Johnsen, S., Clausen, H., and Gundestrup, N.: Stable isotope glaciology, Meddelelser om Grönland, 197, 3, 1-27, C. A. Reitzel, Copenhangen, 1973.

Dansgaard, W., Johnsen, S. J., Reeh, N., Gundestrup, N., Clausen, H. B., and Hammer, C. U.: Climatic changes, Norsemen and modern man, Nature, 255, 24-28, 1975.

Dansgaard, W. and Tauber, H.: Glacier Oxygen-18 Content and Pleistocene Ocean Temperatures, Science, 166, 499-502, 1969.

Delworth, T. L. and Knutson, T. R.: Simulation of Early 20th Century Global Warming, Science, 287, 2246-2250, 2000.

Fischer, H.: Räumliche Variabilität in Eiskernzeitreihen Nordostgrönlands: Rekonstruktion klimatischer und luftchemischer Langzeittrends seit 1500 A.D, 1997.doctoral thesis, Ruprecht-Karls-University, Heidelberg, Germany, 1997.

Fischer, H. and Mieding, B.: A 1,000-year ice core record of interannual to multidecadal variations in atmospheric circulation over the North Atlantic, Clim. Dyn., 25, 65-74, 2005.

Fischer, H., Wagenbach, D., and Kipfstuhl, J.: Sulfate and nitrate firn concentrations on the Greenland ice sheet: 1. Large-scale geographical deposition changes, J. Geophys. Res., 103, 8, 1998a.

Fischer, H., Wagenbach, D., and Kipfstuhl, J.: Sulfate and nitrate firn concentrations on the Greenland ice sheet: 2. Temporal anthropogenic deposition changes, J. Geophys. Res.-Atmos., 103, 21935-21942, 1998b.

Fischer, H., Werner, M., Wagenbach, D., Schwager, M., Thorsteinnson, T., Wilhelms, F., Kipfstuhl, J., and Sommer, S.: Little Ice Age clearly recorded in northern Greenland ice cores, Geophys. Res. Lett., 25, 1749-1752, 1998c.

Fisher, D. A., Reeh, N., and Clausen, H. B.: Stratigraphic noise in time series derived from ice cores, Ann. Glaciol, 7, 76-83, 1985.

Freitag, J., Wilhelms, F., and Kipfstuhl, S.: Microstructure-dependent densification of polar firn derived from X-ray microtomography, J. Glaciol., 50, 243-250, 2004.

Friedmann, A., Moore, J. C., Thorsteinnson, T., Kipfstuhl, J., and Fischer, H.: A 1200 year record of accumulation from northern Greenland, Ann. Glaciol, 21, 6, 1995.

Funder, S.: Quaternary Geology of Greenland. In: Quaternary Geology of Canada and Greenland, Fulton, R. J. (Ed.), Geological Survey of Canada, Ottawa, 1989.

Greenland Ice-core Project (GRIP) Members: Climate instability during the last interglacial period recorded in the GRIP ice core, Nature, 364, 203-207, 1993.

Hanna, E., Fettweis, X., Mernild, S. H., Cappelen, J., Ribergaard, M. H., Shuman, C. A., Steffen, K., Wood, L., and Mote, T. L.: Atmospheric and oceanic climate forcing of the exceptional Greenland ice sheet surface melt in summer 2012, Int. J. Climatol., 34, 1022-1037, 2014.

Hanna, E., McConnell, J., Das, S., Cappelen, J., and Stephens, A.: Observed and Modeled Greenland Ice Sheet Snow Accumulation, 1958–2003, and Links with Regional Climate Forcing, J. Clim., 19, 344-358, 2006.

Held, I. M.: Climate science: The cause of the pause, Nature, 501, 318-319, 2013.

Hörhold, M. W., Kipfstuhl, S., Wilhelms, F., Freitag, J., and Frenzel, A.: The densification of layered polar firn, J. Geophys. Res., 116, 15, 2011.

IPCC: Climate Change 2001: The Scientific Basis. Contribution of Working Group I to the third Assessment report of the Intergovernmental Panel on Climate Change [Houghton, J.T.,Y. Ding, D.J. Griggs, M. Noguer, P.J. van der Linden, X. Dai, K. Maskell, and C.A. Johnson (eds.)], Cambridge University Press, Cambridge, United Kingdom and New York, USA, 1-881, 2001.

IPCC: Climate Change 2007: Synthesis Report, Contribution of Working Groups I, II and III to the Fourth Assessment Report of the Intergovernmental Panel on Climate Change,[[Core Writing Team, Pachauri, R.K and Reisinger, A. (eds.)]. IPCC, Geneva, Switzerland, 1-104, 2007.

IPCC: Climate Change 2013: The Physical Science Basis. Contribution of Working Group I to the Fifth Assessment Report of the Intergovernmental Panel on Climate Change, [Stocker, T.F., D. Qin, G.-K. Plattner, M. Tignor, S.K. Allen, J. Boschung, A. Nauels, Y. Xia, V. Bex

and P.M. Midgley (eds.)], Cambridge University Press, Cambridge, United Kingdom and New York, NY, USA, 1-1535, 2013.

Johnsen, S. J., Clausen, H. B., Cuffey, K. M., Hoffmann, G., Schwander, J., and Creyts, T.: Diffusion of stable isotopes in polar firn and ice : the isotope effect in firn diffusion. In: Physics of Ice Core Records:, Hokkaido University, 2000.

Johnsen, S. J., Clausen, H. B., Dansgaard, W., Gundestrup, N. S., Hammer, C. U., Andersen, U., Andersen, K. K., Hvidberg, C. S., Dahl-Jensen, D., Steffensen, J. P., Shoji, H., Sveinbjörnsdóttir, Á. E., White, J., Jouzel, J., and Fisher, D.: The δ18O record along the Greenland Ice Core Project deep ice core and the problem of possible Eemian climatic instability, J. Geophys. Res. Oceans, 102, 26397-26410, 1997.

Johnsen, S. J., Dansgaard, W., and White, J. W. C.: The origin of Arctic precipitation under present and glacial conditions, Tellus Ser. B, 41B, 452-468, 1989.

Jung-Rothenhäusler, F.: Fernerkundungs- und GIS-Studien in Nordostgrönland, 1998.Doctoral thesis, Universität Bremen, 1-161, 1998.

Kanagaratnam, P., Gogineni, S. P., Gundestrup, N., and Larsen, L.: High-resolution radar mapping of internal layers at the North Greenland Ice Core Project, J. Geophys. Res.-Atmos., 106, 33799-33811, 2001.

Karl, T. R., Arguez, A., Huang, B., Lawrimore, J. H., McMahon, J. R., Menne, M. J., Peterson, T. C., Vose, R. S., and Zhang, H.-M.: Possible artifacts of data biases in the recent global surface warming hiatus, Science, 348, 1469-1472, 2015.

Khan, S. A., Kjaer, K. H., Bevis, M., Bamber, J. L., Wahr, J., Kjeldsen, K. K., Bjork, A. A., Korsgaard, N. J., Stearns, L. A., van den Broeke, M. R., Liu, L., Larsen, N. K., and Muresan, I. S.: Sustained mass loss of the northeast Greenland ice sheet triggered by regional warming, Nature Clim. Change, 4, 292-299, 2014.

Knutson, T. R., Delworth, T. L., Dixon, K. W., Held, I. M., Lu, J., Ramaswamy, V., Schwarzkopf, M. D., Stenchikov, G., and Stouffer, R. J.: Assessment of Twentieth-Century Regional Surface Temperature Trends Using the GFDL CM2 Coupled Models, J. Clim., 19, 1624-1651, 2006.

Koch, J. P. and Wegener, A.: Wissenschaftliche Ergebnisse der dänischen Expedition nach Dronning Louises-Land und quer über das Inlandeis von Nordgrönland 1912-13 untder der Leitung von HAuptmann J. P. Koch, Reitzel, Copenhagen, 1930.

Lawrimore, J. H., Menne, M. J., Gleason, B. E., Williams, C. N., Wuertz, D. B., Vose, R. S., and Rennie, J.: An overview of the Global Historical Climatology Network monthly mean temperature data set, version 3, J. Geophys. Res.-Atmos., 116, 18, 2011.

Mann, M. E., Zhang, Z., Rutherford, S., Bradley, R. S., Hughes, M. K., Shindell, D., Ammann, C., Faluvegi, G., and Ni, F.: Global Signatures and Dynamical Origins of the Little Ice Age and Medieval Climate Anomaly, Science, 326, 1256-1260, 2009.

Masson-Delmotte, V., Schulz, M., Abe-Ouchi, A., Beer, J., Ganopolski, A., González Rouco, J. F., Jansen, E., Lambeck, K., Luterbacher, J., Naish, T., Osborn, T., Otto-Bliesner, B., Quinn, T., Ramesh, R., Rojas, M., Shao, X., and Timmermann, A.: Information from Paleoclimate Archives. In: Climate Change 2013: The Physical Science Basis. Contribution of Working Group I to the Fifth Assessment Report of the Intergovernmental Panel on Climate Change, Stocker, T. F., Qin, D., Plattner, G.-K., Tignor, M., Allen, S. K., Boschung, J., Nauels, A., Xia, Y., Bex, V., and Midgley, P. M. (Eds.), Cambridge University Press, Cambridge, United Kingdom and New York, NY, USA, 2013.

Masson-Delmotte, V., Steen-Larsen, H. C., Ortega, P., Swingedouw, D., Popp, T., Vinther, B. M., Oerter, H., Sveinbjornsdottir, A. E., Gudlaugsdottir, H., Box, J. E., Falourd, S., Fettweis, X., Gallée, H., Garnier, E., Gkinis, V., Jouzel, J., Landais, A., Minster, B., Paradis, N., Orsi, A., Risi, C., Werner, M., and White, J. W. C.: Recent changes in north-west Greenland climate documented by NEEM shallow ice core data and simulations, and implications for past-temperature reconstructions, The Cryosphere, 9, 1481-1504, 2015.

Mayewski, P. A., Rohling, E. E., Curt Stager, J., Karlén, W., Maasch, K. A., David Meeker, L., Meyerson, E. A., Gasse, F., van Kreveld, S., Holmgren, K., Lee-Thorp, J., Rosqvist, G., Rack, F., Staubwasser, M., Schneider, R. R., and Steig, E. J.: Holocene climate variability, Quat. Res., 62, 243-255, 2004.

Meehl, G. A., Arblaster, J. M., Fasullo, J. T., Hu, A., and Trenberth, K. E.: Model-based evidence of deep-ocean heat uptake during surface-temperature hiatus periods, Nature Clim. Change, 1, 360-364, 2011.

Miller, G. H., Alley, R. B., Brigham-Grette, J., Fitzpatrick, J. J., Polyak, L., Serreze, M. C., and White, J. W. C.: Arctic amplification: can the past constrain the future?, Quat. Sci. Rev., 29, 1779-1790, 2010.

Mosley-Thompson, E., McConnell, J. R., Bales, R. C., Li, Z., Lin, P. N., Steffen, K., Thompson, L. G., Edwards, R., and Bathke, D.: Local to regional-scale variability of annual net accumulation on the Greenland ice sheet from PARCA cores, J. Geophys. Res.-Atmos., 106, 33839-33851, 2001.

North Greenland Ice Core Project members.: High-resolution record of Northern Hemisphere climate extending into the last interglacial period, Nature, 431, 147-151, 2004.

Nghiem, S. V., Hall, D. K., Mote, T. L., Tedesco, M., Albert, M. R., Keegan, K., Shuman, C. A., DiGirolamo, N. E., and Neumann, G.: The extreme melt across the Greenland ice sheet in 2012, Geophys. Res. Lett., 39, 17, 2012.

Ohmura, A.: New temperature distribution maps for Greenland, Zeitschrift für Gletscherkunde und Glazialgeologie, 35, 1-20, 1987.

Ohmura, A. and Reeh, N.: New precipitation and accumulation maps for Greenland, J. Glaciol., 37, 140-148, 1991.

Ortega, P., Swingedouw, D., Masson-Delmotte, V., Risi, C., Vinther, B., Yiou, P., Vautard, R., and Yoshimura, K.: Characterizing atmospheric circulation signals in Greenland ice cores: insights from a weather regime approach, Clim. Dyn., 43, 2585-2605, 2014.

Pages2k Consortium.: Continental-scale temperature variability during the past two millennia, Nature Geosci, 6, 339-346, 2013.

Petit, J. R., Jouzel, J., Raynaud, D., Barkov, N. I., Barnola, J. M., Basile, I., Bender, M., Chappellaz, J., Davis, M., Delaygue, G., Delmotte, M., Kotlyakov, V. M., Legrand, M., Lipenkov, V. Y., Lorius, C., Pepin, L., Ritz, C., Saltzman, E., and Stievenard, M.: Climate and atmospheric history of the past 420,000 years from the Vostok ice core, Antarctica, Nature, 399, 429-436, 1999.

Rasmussen, S. O., Seierstad, I. K., Andersen, K. K., Bigler, M., Dahl-Jensen, D., and Johnsen, S. J.: Synchronization of the NGRIP, GRIP, and GISP2 ice cores across MIS 2 and palaeoclimatic implications, Quat. Sci. Rev., 27, 18-28, 2008.

Rignot, E., Velicogna, I., van den Broeke, M. R., Monaghan, A., and Lenaerts, J. T. M.: Acceleration of the contribution of the Greenland and Antarctic ice sheets to sea level rise, Geophys. Res. Lett., 38, 5, 2011.

Rimbu, N., Lohmann, G., and Grosfeld, K.: Northern Hemisphere atmospheric blocking in ice core accumulation records from northern Greenland, Geophys. Res. Lett., 34, 5, 2007.

Schaller, C. F., Freitag, J., Kipfstuhl, S., Laepple, T., Steen-Larsen, H. C., and Eisen, O.: A representative density profile for the North Greenland snowpack, The Cryosphere Discuss., 2016, 1-20, 2016.

Schwager, M.: Ice core analysis on the spatial and temporal variability of temperature and precipitation during the late Holocene in North Greenland, Alfred Wegener Institute for Polar and Marine Research, Bremen, 2000.

Serreze, M. C., Holland, M. M., and Stroeve, J.: Perspectives on the Arctic's Shrinking Sea-Ice Cover, Science, 315, 1533-1536, 2007.

Shepherd, A., Ivins, E. R., A, G., Barletta, V. R., Bentley, M. J., Bettadpur, S., Briggs, K. H., Bromwich, D. H., Forsberg, R., Galin, N., Horwath, M., Jacobs, S., Joughin, I., King, M. A., Lenaerts, J. T. M., Li, J., Ligtenberg, S. R. M., Luckman, A., Luthcke, S. B., McMillan,

M., Meister, R., Milne, G., Mouginot, J., Muir, A., Nicolas, J. P., Paden, J., Payne, A. J., Pritchard, H., Rignot, E., Rott, H., Sørensen, L. S., Scambos, T. A., Scheuchl, B., Schrama, E. J. O., Smith, B., Sundal, A. V., van Angelen, J. H., van de Berg, W. J., van den Broeke, M. R., Vaughan, D. G., Velicogna, I., Wahr, J., Whitehouse, P. L., Wingham, D. J., Yi, D., Young, D., and Zwally, H. J.: A Reconciled Estimate of Ice-Sheet Mass Balance, Science, 338, 1183-1189, 2012.

Shuman, C. A., Steffen, K., Box, J. E., and Stearns, C. R.: A Dozen Years of Temperature Observations at the Summit: Central Greenland Automatic Weather Stations 1987–99, Journal of Applied Meteorology, 40, 741-752, 2001.

Sigl, M., McConnell, J. R., Layman, L., Maselli, O., McGwire, K., Pasteris, D., Dahl-Jensen, D., Steffensen, J. P., Vinther, B., Edwards, R., Mulvaney, R., and Kipfstuhl, S.: A new bipolar ice core record of volcanism from WAIS Divide and NEEM and implications for climate forcing of the last 2000 years, J. Geophys. Res.-Atmos., 118, 1151-1169, 2013.

Sommer, S.: Hochauflösende Spurenstoffuntersuchungen an Eisbohrkernen aus Nord-Grönland, 1996. M. sc. thesis, Pysical Institute, University of Bern, Bern, Switzerland, 1996.

Taylor, K. C., Hammer, C. U., Alley, R. B., Clausen, H. B., Dahl-Jensen, D., Gow, A. J., Gundestrup, N. S., Kipfstuhl, J., Moore, J. C., and Waddington, E. D.: Elecrical conductivity measurements from the GISP2 and GRIP Greenland ice cores, Nature, 366, 549-552, 1993.

Tedesco, M., Fettweis, X., Mote, T., Wahr, J., Alexander, P., Box, J. E., and Wouters, B.: Evidence and analysis of 2012 Greenland records from spaceborne observations, a regional climate model and reanalysis data, The Cryosphere, 7, 615-630, 2013.

Vallelonga, P., Christianson, K., Alley, R. B., Anandakrishnan, S., Christian, J. E. M., Dahl-Jensen, D., Gkinis, V., Holme, C., Jacobel, R. W., Karlsson, N. B., Keisling, B. A., Kipfstuhl, S., Kjær, H. A., Kristensen, M. E. L., Muto, A., Peters, L. E., Popp, T., Riverman, K. L., Svensson, A. M., Tibuleac, C., Vinther, B. M., Weng, Y., and Winstrup, M.: Initial results from geophysical surveys and shallow coring of the Northeast Greenland Ice Stream (NEGIS), The Cryosphere, 8, 1275-1287, 2014.

van Geldern, R. and Barth, J. A. C.: Optimization of instrument setup and post-run corrections for oxygen and hydrogen stable isotope measurements of water by isotope ratio infrared spectroscopy (IRIS), Limnol. Oceanogr. Methods, 10, 13, 2012.

Vinther, B. M., Clausen, H. B., Johnsen, S. J., Rasmussen, S. O., Andersen, K. K., Buchardt, S. L., Dahl-Jensen, D., Seierstad, I. K., Siggaard-Andersen, M. L., Steffensen, J. P., Svensson, A., Olsen, J., and Heinemeier, J.: A synchronized dating of three Greenland ice cores throughout the Holocene, J. Geophys. Res.-Atmos., 111, D13102, 2006.

Vinther, B. M., Jones, P. D., Briffa, K. R., Clausen, H. B., Andersen, K. K., Dahl-Jensen, D., and Johnsen, S. J.: Climatic signals in multiple highly resolved stable isotope records from Greenland, Quat. Sci. Rev., 29, 522-538, 2010.

Weißbach, S., Wegner, A., and Kipfstuhl, S.: Snow Accumulation in North Greenland over the Last Millennium. In: Towards an Interdisciplinary Approach in Earth System Science: Advances of a Helmholtz Graduate Research School, Lohmann, G., Meggers, H., Unnithan, V., Wolf-Gladrow, D., Notholt, J., and Bracher, A. (Eds.), Springer International Publishing, Cham, 2015.

Weißbach, S., Wegner, A., Opel, T., Oerter, H., Vinther, B. M., and Kipfstuhl, S.: Spatial and temporal oxygen isotope variability in northern Greenland – implications for a new climate record over the past millennium, Clim. Past, 12, 171-188, 2016.

Werner, M.: Vergleichende Studie ueber die Verteilung vulkanogener Spurenstoffdepositionen in Nord-Ost-Groenland, Diplomarbeit, Institut fuer Umweltphysik, Heidelberg, 1-85, 1995.

White, J. W. C., Barlow, L. K., Fisher, D., Grootes, P., Jouzel, J., Johnsen, S. J., Stuiver, M., and Clausen, H.: The climate signal in the stable isotopes of snow from Summit, Greenland: Results of comparisons with modern climate observations, J. Geophys. Res. Oceans, 102, 26425-26439, 1997.

Wilhelms, F.: Leitfähigkeits- und Dichtemessung an Eisbohrkernen, Alfred Wegener Institute for Polar and Marine Research, Bremerhaven, 1996.

Zielinski, G. A.: Use of paleo-records in determining variability within the volcanism–climate system, Quat. Sci. Rev., 19, 417-438, 2000.